Density Model for Common Bottlenose Dolphin (*Tursiops truncatus*) for the U.S. East Coast: Supplementary Report

Model Version 6.1

Duke University Marine Geospatial Ecology Laboratory*

2023-05-27

Citation

When citing our methodology or results generally, please cite Roberts et al. (2016, 2023). The complete references appear at the end of this document. We are preparing a new article for a peer-reviewed journal that will eventually replace those. Until that is published, those are the best general citations.

When citing this model specifically, please use this reference:

Roberts JJ, Yack TM, Cañadas A, Fujioka E, Halpin PN, Barco SG, Boisseau O, Chavez-Rosales S, Cole TVN, Cotter MP, Cummings EW, Davis GE, DiGiovanni Jr. RA, Garrison LP, Gowan TA, Jackson KA, Kenney RD, Khan CB, Lockhart GG, Lomac-MacNair KS, McAlarney RJ, McLellan WA, Mullin KD, Nowacek DP, O'Brien O, Pabst DA, Palka DL, Quintana-Rizzo E, Redfern JV, Rickard ME, White M, Whitt AD, Zoidis AM (2022) Density Model for Common Bottlenose Dolphin (*Tursiops truncatus*) for the U.S. East Coast, Version 6.1, 2023-05-27, and Supplementary Report. Marine Geospatial Ecology Laboratory, Duke University, Durham, North Carolina.

Copyright and License

This document and the accompanying results are © 2023 by the Duke University Marine Geospatial Ecology Laboratory and are licensed under a Creative Commons Attribution 4.0 International License.

Model Version History

Version	Date	Description
1	2014-10-21	Initial version.
2	2014-11-13	Reconfigured detection hierarchy and adjusted NARWSS detection functions based on additional information from Tim Cole. Updated documentation.
3	2014-11-19	Removed CumVGPM180 predictor and refitted models.
4	2014-12-05	Fixed bug that applied the wrong detection function to segments NE_narwss_1999_widgeon_hapo dataset. Refitted model. Updated documentation.
4.1	2015-03-06	Updated the documentation. No changes to the model.
4.2	2015-05-14	Updated calculation of CVs. Switched density rasters to logarithmic breaks. No changes to the model.
4.3	2015-10-07	Updated the documentation. No changes to the model.

*For questions or to offer feedback please contact Jason Roberts (jason.roberts@duke.edu) and Tina Yack (tina.yack@duke.edu)

(continued)

Version	Date	Description
4.4	2016-04-21	Switched calculation of monthly 5% and 95% confidence interval rasters to the method used to produce the year-round rasters. (We intended this to happen in version 4.2 but I did not implement it properly.) No changes to the other rasters or the model itself. Model files released as supplementary information to Roberts et al. (2016).
5	2018-04-14	Began update to Roberts et al. (2015) model. Introduced new surveys from AMAPPS, NARWSS, UNCW, VAMSC, and the SEUS NARW teams. Updated modeling methodology. Refitted detection functions and spatial models from scratch using new and reprocessed covariates. Model released as part of a scheduled update to the U.S. Navy Marine Species Density Database (NMSDD).
6	2022-06-20	This model is a major update over the prior version, with substantial additional data, improved statistical methods, and an increased spatial resolution. It was released as part of the final delivery of the U.S. Navy Marine Species Density Database (NMSDD) for the Atlantic Fleet Testing and Training (AFTT) Phase IV Environmental Impact Statement. Several new collaborators joined and contributed survey data: New York State Department of Environmental Conservation, TetraTech, HDR, and Marine Conservation Research. We incorporated additional surveys from all continuing and new collaborators through the end of 2020. (Because some environmental covariates were only available through 2019, certain models only extend through 2019.) We increased the spatial resolution to 5 km and, at NOAA's request, we extended the model further inshore from New York through Maine. We reformulated and refitted all detection functions and spatial models. We updated all enviromental covariates to newer products, when available, and added several covariates to the set of candidates. For models that incorporated dynamic covariates, we estimated model uncertainty using a new method that accounts for both model parameter error and temporal variability.
6.1	2023-05-27	Completed the supplementary report documenting the details of this model. The model itself was not changed.

1 Survey Data

We built this model from data collected between 1998-2019 (Table 1, Figure 1). We excluded surveys that did not target small cetaceans or were otherwise problematic for modeling them. In keeping with our primary strategy for the 2022 modeling cycle, we excluded data prior to 1998 in order to utilize biological covariates derived from satellite ocean color observations, which were only available for a few months before 1998. We excluded data after 2019 in order to utilize zooplankton and micronekton biomass estimates from SEAPODYM (Lehodey et al. 2008), which preliminary modeling indicated were were effective spatial covariates but were only available through 2019. We restricted the model to aerial survey transects with sea states of Beaufort 4 or less (for a few surveys we used Beaufort 3 or less) and shipboard transects with Beaufort 5 or less (for a few we used Beaufort 4 or less). We also excluded transects with poor weather or visibility for surveys that reported those conditions.

Table 1: Survey effort and observations considered for this model. Effort is tallied as the cumulative length of on-effort transects. Observations are the number of groups and individuals encountered while on effort. Off effort observations and those lacking an estimate of group size or distance to the group were excluded.

			Effort	Observations		
Institution	Program	Period	1000s km	Groups	Individuals	Mean Group Size
Aerial Surveys						
HDR	Navy Norfolk Canyon	2018-2019	10	120	2,151	17.9
NEFSC	AMAPPS	2010-2019	83	105	902	8.6
NEFSC	NARWSS	2003-2016	380	56	500	8.9
NEFSC	Pre-AMAPPS	1999-2008	45	46	258	5.6
SEFSC	AMAPPS	2010-2019	110	1,202	12,043	10.0
SEFSC	MATS	2002-2005	27	574	7,831	13.6
UNCW	MidA Bottlenose	2002-2002	15	343	1,831	5.3
UNCW	Navy Cape Hatteras	2011-2017	34	283	5,538	19.6
UNCW	Navy Jacksonville	2009-2017	92	421	3,514	8.3
UNCW	Navy Norfolk Canyon	2015-2017	14	67	1,593	23.8
UNCW	Navy Onslow Bay	2007-2011	49	143	2,553	17.9
UNCW	SEUS NARW EWS	2005-2008	106	1,786	12,518	7.0
VAMSC	MD DNR WEA	2013-2015	15	278	2,277	8.2
VAMSC	Navy VACAPES	2016-2017	18	129	1,252	9.7
VAMSC	VA CZM WEA	2012-2015	19	140	1,196	8.5
		Total	**1,017**	**5,693**	**55,957**	**9.8**
Shipboard Surveys						
MCR	SOTW Visual	2012-2019	9	29	272	9.4
NEFSC	AMAPPS	2011-2016	15	265	3,037	11.5
NEFSC	Pre-AMAPPS	1998-2007	13	122	1,773	14.5
NJDEP	NJEBS	2008-2009	14	156	2,369	15.2
SEFSC	AMAPPS	2011-2016	16	171	3,212	18.8
SEFSC	Pre-AMAPPS	1998-2006	30	410	7,142	17.4
		Total	**96**	**1,153**	**17,805**	**15.4**
		Grand Total	**1,113**	**6,846**	**73,762**	**10.8**

Table 2: Institutions that contributed surveys used in this model.

Institution	Full Name
HDR	HDR, Inc.
MCR	Marine Conservation Research
NEFSC	NOAA Northeast Fisheries Science Center
NJDEP	New Jersey Department of Environmental Protection
SEFSC	NOAA Southeast Fisheries Science Center
UNCW	University of North Carolina Wilmington
VAMSC	Virginia Aquarium & Marine Science Center

Table 3: Descriptions and references for survey programs used in this model.

Program	Description	References
AMAPPS	Atlantic Marine Assessment Program for Protected Species	Palka et al. (2017), Palka et al. (2021)
MATS	Mid-Atlantic Tursiops Surveys	
MD DNR WEA	Aerial Surveys of the Maryland Wind Energy Area	Barco et al. (2015)
MidA Bottlenose	Mid-Atlantic Onshore/Offshore Bottlenose Dolphin Surveys	Torres et al. (2005)
NARWSS	North Atlantic Right Whale Sighting Surveys	Cole et al. (2007)
Navy Cape Hatteras	Aerial Surveys of the Navy's Cape Hatteras Study Area	McLellan et al. (2018)
Navy Jacksonville	Aerial Surveys of the Navy's Jacksonville Study Area	Foley et al. (2019)
Navy Norfolk Canyon	Aerial Surveys of the Navy's Norfolk Canyon Study Area	Cotter (2019), McAlarney et al. (2018)
Navy Onslow Bay	Aerial Surveys of the Navy's Onslow Bay Study Area	Read et al. (2014)
Navy VACAPES	Aerial Survey Baseline Monitoring in the Continental Shelf Region of the VACAPES OPAREA	Mallette et al. (2017)
NJEBS	New Jersey Ecological Baseline Study	Geo-Marine, Inc. (2010), Whitt et al. (2015)
Pre-AMAPPS	Pre-AMAPPS Marine Mammal Abundance Surveys	Mullin and Fulling (2003), Garrison et al. (2010), Palka (2006)
SEUS NARW EWS	Southeast U.S. Right Whale Early Warning System Surveys	
SOTW Visual	R/V Song of the Whale Visual Surveys	Ryan et al. (2013)
VA CZM WEA	Virginia CZM Wind Energy Area Surveys	Mallette et al. (2014), Mallette et al. (2015)

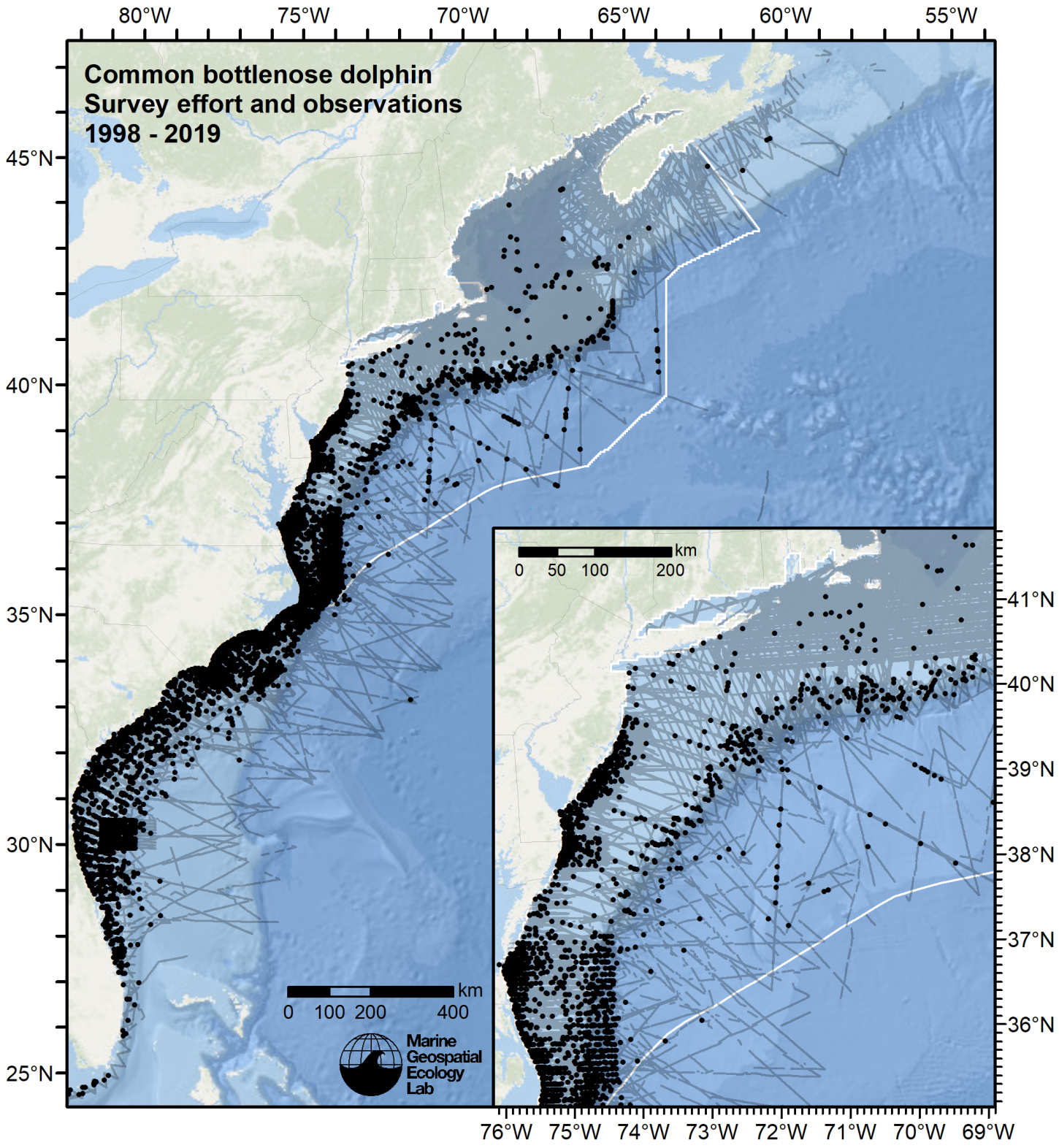

Figure 1: Survey effort and common bottlenose dolphin observations available for density modeling, after detection functions were applied, and excluded segments and truncated observations were removed.

2 Classification of Ambiguous Sightings

Observers occasionally experience difficulty identifying species, due to poor sighting conditions or phenotypic similarities between the possible choices. For example, observers may not always be able to distinguish fin whales from sei whales due their similiar size and shape. When this happens, observers will report an ambiguous identification, such as "fin or sei whale". In our density models, we handled ambiguous identifications in three ways:

1. For sightings with very generic identifications such as "large whale", we discarded the sightings. These sightings represented a clear minority when compared to those with definitive species identifications, but they are uncounted animals and our density models may therefore underestimate density to some degree.
2. For sightings of certain taxa in which a large majority of identifications were ambiguous (e.g. "unidentified pilot whale") rather than specific (e.g. "short-finned pilot whale" or "long-finned pilot whale"), it was not tractable to model the individual species so we modeled the generic taxon instead.
3. For sightings that reported an ambiguous identification of two species (e.g. "fin or sei whale") that are known to exhibit different habitat preferences or typically occur in different group sizes, and for which we had sufficient number of definitive sightings of both species, we first fitted a predictive model that classified the ambiguous sightings into one species or the other and then included the resulting classified sightings in the density models for each of the two species.

This section describes how we classified the third category of ambiguous sightings reported as "Atlantic spotted or bottlenose dolphin" into one species or the other.

For the predictive model, we used the cforest classifier (Hothorn et al. 2006), an elaboration of the classic random forest classifier (Breiman 2001). First, we trained a binary classifier using the sightings that reported definitive species identifications ("Atlantic spotted dolphin" and "bottlenose dolphin"). To increase the range of sampling of the classification model's covariates, the training data may have included additional surveys not considered for the density model, as well as transects from outside the spatial and temporal extents of the density model. Only on-effort sightings were used. We used the species ID as the response variable and environmental variables as covariates.

We used receiver operating characteristic (ROC) curve analysis to select a threshold for classifying the probabilistic predictions of species identifications made by the model into a binary result of one species or another. For the classification threshold, we selected the value that maximized the Youden index (Perkins and Schisterman 2006). Then, for all sightings reporting the ambiguous identification, we classified each as either one species or the other by processing the covariate values observed for it through the fitted model. We then included the classified sightings in the detection functions and density models. The sightings reported elsewhere in this document incorporate both the definitive sightings and the classified sightings, unless otherwise noted.

2.1 Classification Model

```
MODEL SUMMARY:
==============

Random Forest using Conditional Inference Trees

Number of trees: 100

Response: factor(OriginalScientificName)
Inputs: ClimChl, ClimDistToAEddy, ClimMnkEpi, ClimSST_CMC, ClimTKE, ClimZoo_SEAPODYM, Depth,
DistTo125m, DistTo300m, DistToShore, Slope
Number of observations: 10000

Number of variables tried at each split: 5

Estimated predictor variable importance (conditional = FALSE):

Importance
ClimZoo_SEAPODYM 0.02315
ClimChl 0.02170
DistToShore 0.01957
```

```
Slope 0.01445
ClimMnkEpi 0.01376
ClimTKE 0.01314
ClimSST_CMC 0.01227
ClimDistToAEddy 0.01017
Depth 0.00925
DistTo125m 0.00750
DistTo300m 0.00624

MODEL PERFORMANCE SUMMARY:
==========================

Statistics calculated from the training data.

Area under the ROC curve (auc)           = 0.977
Mean cross-entropy (mxe)                 = NA
Precision-recall break-even point (prbe) = 0.964
Root-mean square error (rmse)            = 0.224

User-specified cutoff = 0.560

Confusion matrix for that cutoff:

                            Actual Tursiops truncatus  Actual Stenella frontalis  Total
Predicted Tursiops truncatus                      8229                        303   8532
Predicted Stenella frontalis                       304                       1164   1468
Total                                             8533                       1467  10000

Model performance statistics for that cutoff:

Accuracy (acc)                               = 0.939
Error rate (err)                             = 0.061
Rate of positive predictions (rpp)           = 0.853
Rate of negative predictions (rnp)           = 0.147

True positive rate (tpr, or sensitivity)     = 0.964
False positive rate (fpr, or fallout)        = 0.207
True negative rate (tnr, or specificity)     = 0.793
False negative rate (fnr, or miss)           = 0.036

Positive prediction value (ppv, or precision) = 0.964
Negative prediction value (npv)              = 0.793
Prediction-conditioned fallout (pcfall)      = 0.036
Prediction-conditioned miss (pcmiss)         = 0.207

Matthews correlation coefficient (mcc)       = 0.758
Odds ratio (odds)                            = 103.988
SAR                                          = 0.713

Cohen's kappa (K)                            = 0.758
```

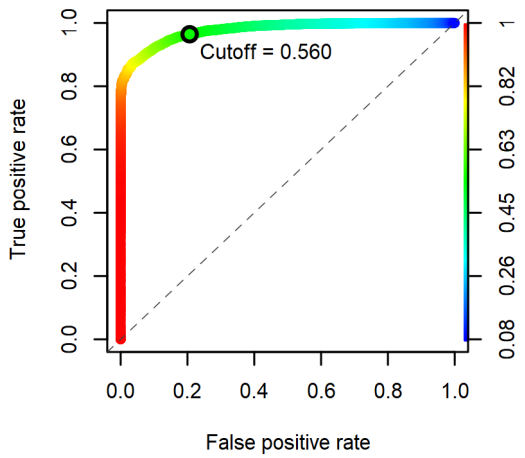

Figure 2: Receiver operating characteristic (ROC) curve summarizing the predictive performance of the ambiguous sighting classification model.

Table 4: Covariates used in the ambiguous sighting classification model.

Covariate	Description
ClimChl	Climatological monthly mean chlorophyll a concentration (mg m^{-3}) from Copernicus GlobColour (Garnesson et al. (2019)), provided by E.U. Copernicus Marine Service (product OCEANCOLOUR_GLO_CHL_L4_REP_OBSERVATIONS_009_082)
ClimDistToAEddy	Climatological monthly mean distance (km) to the edge of the closest anticyclonic mesoscale eddy of any age, derived with MGET (Roberts et al. (2010)) from the Aviso Mesoscale Eddy Trajectories Atlas (META2.0), produced by SSALTO/DUACS and distributed by AVISO+ (https://aviso.altimetry.fr) with support from CNES, in collaboration with Oregon State University with support from NASA, using the method of Schlax and Chelton (2016), based on Chelton et al. (2011)
ClimMnkEpi	Climatological monthly mean micronekton biomass available in the epipelagic zone, expressed as wet weight (g m^{-2}), from SEAPODYM (Lehodey et al. (2008); Lehodey et al. (2015)), provided by E.U. Copernicus Marine Service. doi: 10.48670/moi-00020. Computed as the sum of the SEAPODYM mnkc_epi, mnkc_mumeso, and mnkc_hmlmeso variables.
ClimSST_CMC	Climatological monthly mean sea surface temperature (°C) from GHRSST Level 4 CMC0.2deg and CMC0.1deg (Brasnett (2008); Canada Meteorological Center (2012); Meissner et al. (2016); Canada Meteorological Center (2016))
ClimTKE	Climatological monthly mean total kinetic energy (m^2 s^{-2}) derived from Aviso Ssalto/Duacs global gridded L4 reprocessed geostrophic currents, produced and distributed by E.U. Copernicus Marine Service. doi: 10.48670/moi-00148
ClimZoo_SEAPODYM	Climatological monthly mean zooplankton biomass expressed in carbon (g C m^{-2}) from SEAPODYM (Lehodey et al. (2008); Lehodey et al. (2015)), provided by E.U. Copernicus Marine Service. doi: 10.48670/moi-00020
Depth	Depth (m) of the seafloor, from SRTM30_PLUS (Becker et al. (2009))
DistTo125m	Distance (km) to the 125m isobath, derived from SRTM30_PLUS (Becker et al. (2009))
DistTo300m	Distance (km) to the 300m isobath, derived from SRTM30_PLUS (Becker et al. (2009))
DistToShore	Distance (km) to shore excluding Bermuda and Sable Island, derived from SRTM30_PLUS (Becker et al. (2009))
Slope	Slope (percent rise) of the seafloor, derived from SRTM30_PLUS (Becker et al. (2009))

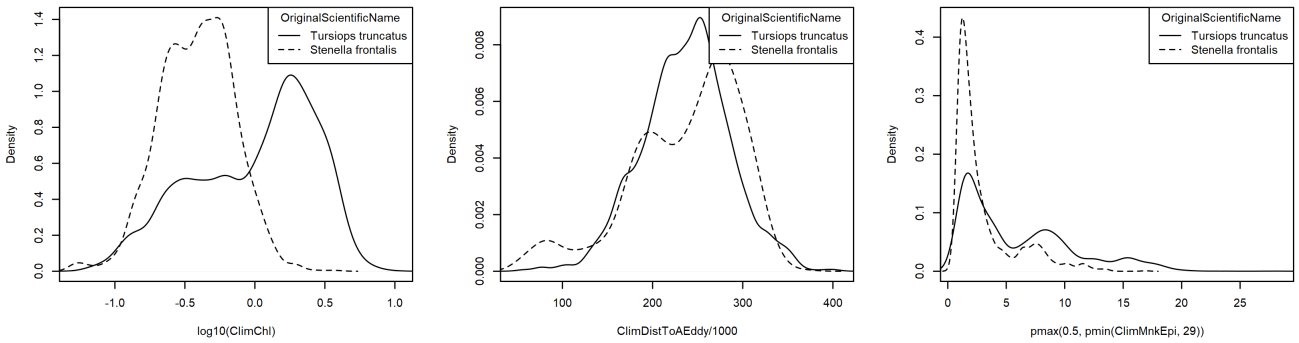

(a) Chlorophyll a concentration (mg m^{-3}) (b) Climatological distance to anticyclonic eddy (km) (c) Climatological epipelagic micronekton biomass (g m^{-2})

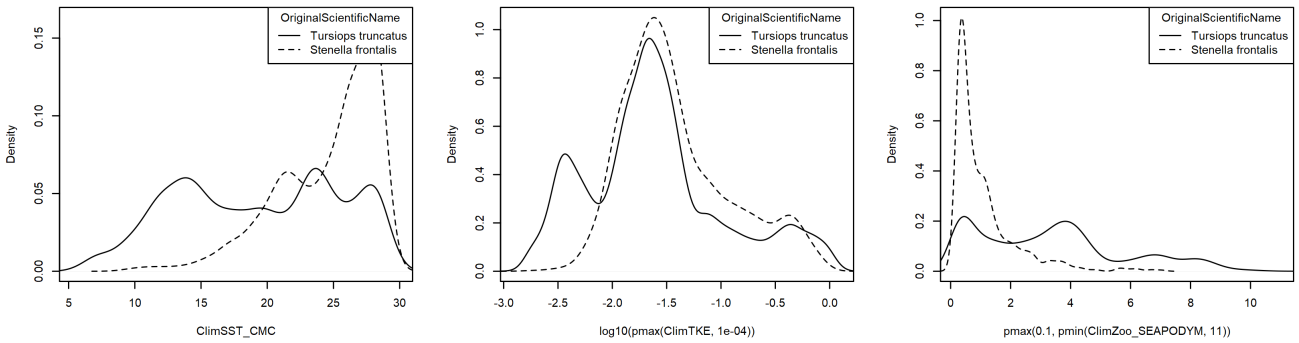

(d) Climatological sea surface temperature (°C) (e) Climatological total kinetic energy (m^2 s^{-2}) (f) Climatological zooplankton biomass (g C m^{-2})

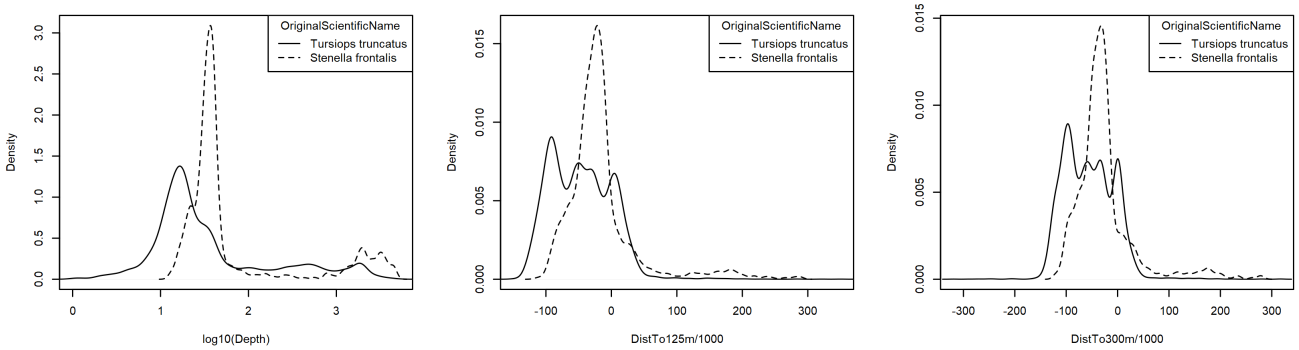

(g) Seafloor depth (m) (h) Distance to 125m isobath (km) (i) Distance to 300m isobath (km)

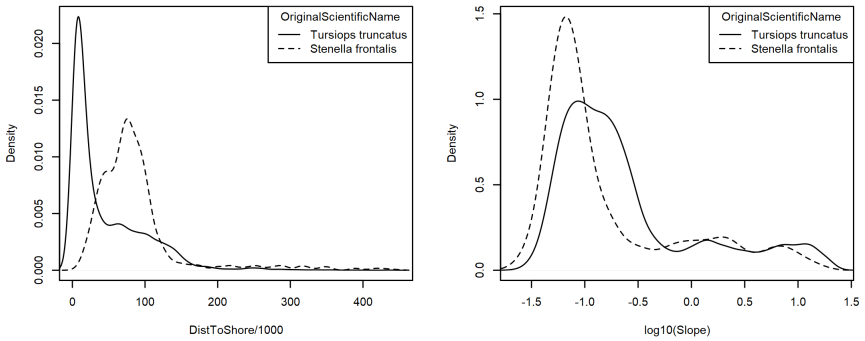

(j) Distance to shore (km) (k) Seafloor slope (percent rise)

Figure 3: Density histograms showing the per-species distribution of each covariate in the ambiguous sighting classification model. When a covariate exhibits a substantially different distribution for each species, it is a good candidate for differentiating the species. Transforms and other treatments are indicated in axis labels. *log10* indicates the covariate was $\log_{10}$ transformed. *pmax* and *pmin* indicate the covariate's minimum and maximum values, respectively, were Winsorized to the values shown. */1000* indicates meters were transformed to kilometers for interpretation convenience.

2.2 Classifications Performed

Table 5: Summary of the definitive sightings used to train the classification model, the ambiguous sightings to which the model was applied, and their resulting classifications. To increase the range of sampling of the classification model's covariates, the training data may have included additional surveys not considered for the density model, as well as transects from outside the spatial and temporal extents of the density model. Only on-effort sightings were used.

		Definitive			Classified	
Institution	Program	S. frontalis	T. truncatus	Ambiguous	S. frontalis	T. truncatus
Aerial Surveys						
HDR	Navy Norfolk Canyon	31	214	0	0	0
NEAq	CNM	2	16	0	0	0
NEAq	MMS-WEA	0	25	0	0	0
NEAq	NLPSC	0	24	0	0	0
NEFSC	AMAPPS	0	112	0	0	0
NEFSC	NARWSS	0	70	0	0	0
NEFSC	Pre-AMAPPS	1	99	0	0	0
NJDEP	NJEBS	0	91	0	0	0
NYS-DEC/TT	NYBWM	0	35	0	0	0
SEFSC	AMAPPS	288	1,865	115	42	73
SEFSC	MATS	100	679	20	8	12
SEFSC	SECAS	10	185	34	7	27
UNCW	MidA Bottlenose	1	348	0	0	0
UNCW	Navy Cape Hatteras	50	297	0	0	0
UNCW	Navy Jacksonville	343	428	0	0	0
UNCW	Navy Norfolk Canyon	37	69	0	0	0
UNCW	Navy Onslow Bay	65	148	0	0	0
UNCW	SEUS NARW EWS	5	1,784	0	0	0
VAMSC	MD DNR WEA	2	556	0	0	0
VAMSC	Navy VACAPES	2	135	0	0	0
VAMSC	VA CZM WEA	3	150	0	0	0
	Total	**940**	**7,330**	**169**	**57**	**112**
Shipboard Surveys						
MCR	SOTW Visual	5	21	0	0	0
NEFSC	AMAPPS	54	272	0	0	0
NEFSC	Pre-AMAPPS	16	177	0	0	0
NJDEP	NJEBS	0	160	0	0	0
SEFSC	AMAPPS	82	158	12	3	9
SEFSC	Pre-AMAPPS	370	415	35	12	23
	Total	**527**	**1,203**	**47**	**15**	**32**
	Grand Total	**1,467**	**8,533**	**216**	**72**	**144**

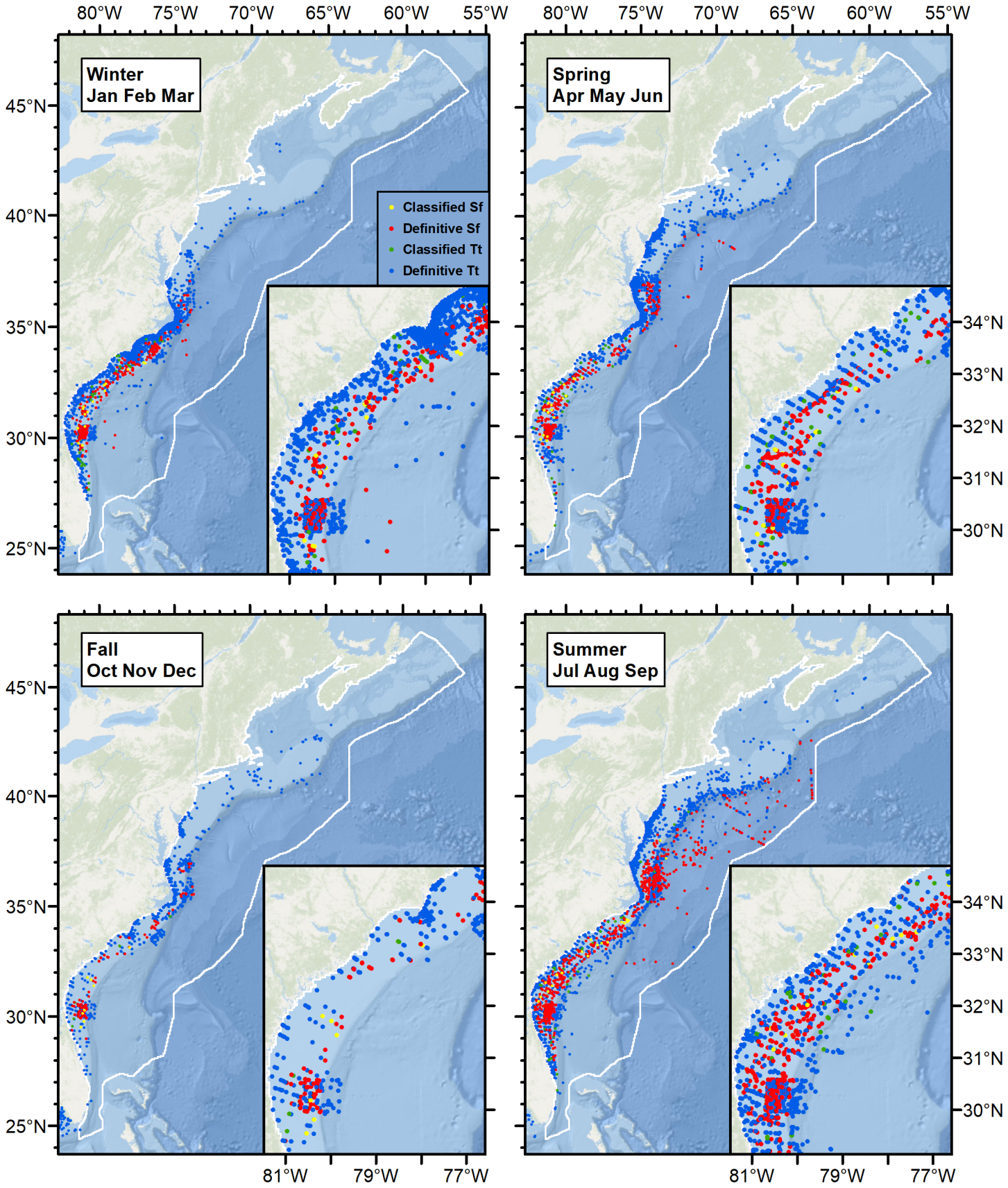

Figure 4: Definitive sightings used to train the model and ambiguous sightings classified by the model.

3 Detection Functions

3.1 With a Taxonomic Covariate

We fitted the detection functions in this section to pools of species with similar detectability characteristics and used the taxonomic identification as a covariate (ScientificName) to account for differences between them. We consulted the literature and observer teams to determine appropriate poolings. We usually employed this approach to boost the counts of observations in the detection functions, which increased the chance that other covariates such as Beaufort sea state could be used to account for differences in observing conditions. When defining the taxonomic covariate, we sometimes had too few observations of species to allocate each of them their own level of the covariate and had to group them together, again consulting the literature and observers for advice on species similarity. Also, when species were observed frequently enough to be allocated their own levels but statistical tests indicated no significant difference between the levels, we usually grouped them together into a single level.

3.1.1 Aerial Surveys

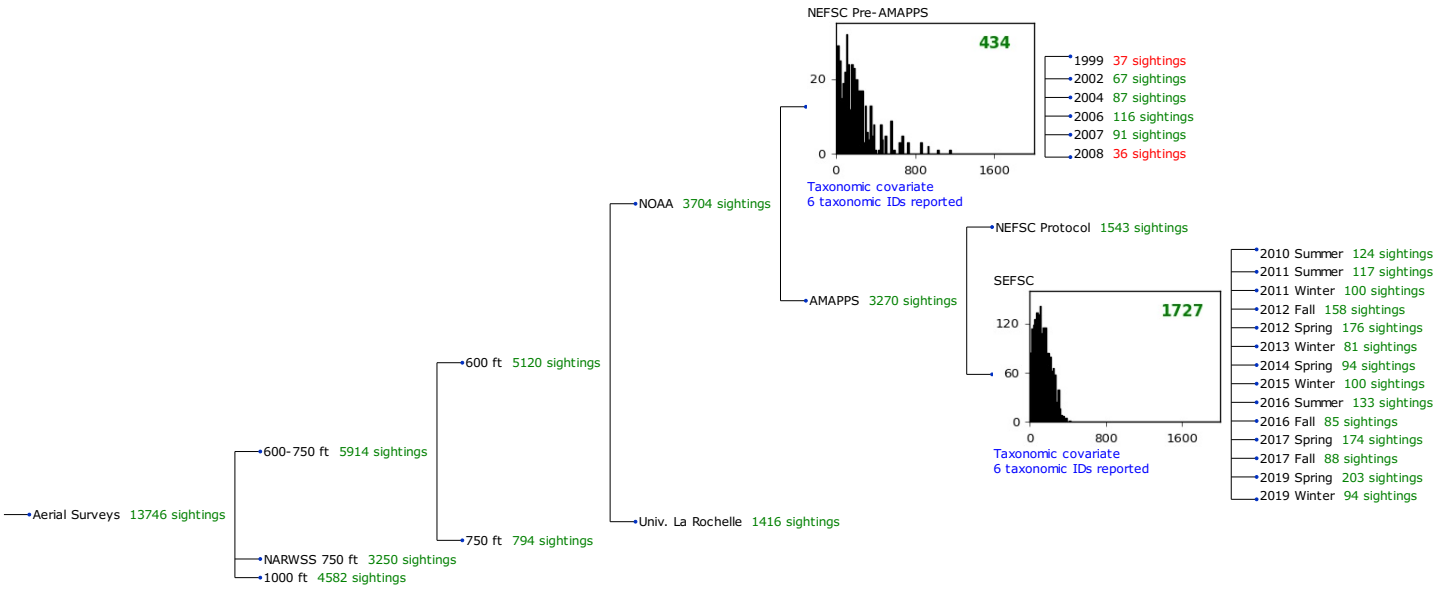

Figure 5: Detection hierarchy for aerial surveys, showing how they were pooled during detectability modeling, for detection functions that pooled multiple taxa and used used a taxonomic covariate to account for differences between them. Each histogram represents a detection function and summarizes the perpendicular distances of observations that were pooled to fit it, prior to truncation. Observation counts, also prior to truncation, are shown in green when they met the recommendation of Buckland et al. (2001) that detection functions utilize at least 60 sightings, and red otherwise. For rare taxa, it was not always possible to meet this recommendation, yielding higher statistical uncertainty. During the spatial modeling stage of the analysis, effective strip widths were computed for each survey using the closest detection function above it in the hierarchy (i.e. moving from right to left in the figure). Surveys that do not have a detection function above them in this figure were either addressed by a detection function presented in a different section of this report, or were omitted from the analysis.

3.1.1.1 NEFSC Pre-AMAPPS

After right-truncating observations greater than 600 m, we fitted the detection function to the 413 observations that remained (Table 6). The selected detection function (Figure 6) used a hazard rate key function with Beaufort (Figure 7) and ScientificName (Figure 8) as covariates.

Table 6: Observations used to fit the NEFSC Pre-AMAPPS detection function.

ScientificName	n
Delphinus, Lagenodelphis, Stenella	239
Lagenorhynchus	128
Tursiops, Steno	46
Total	**413**

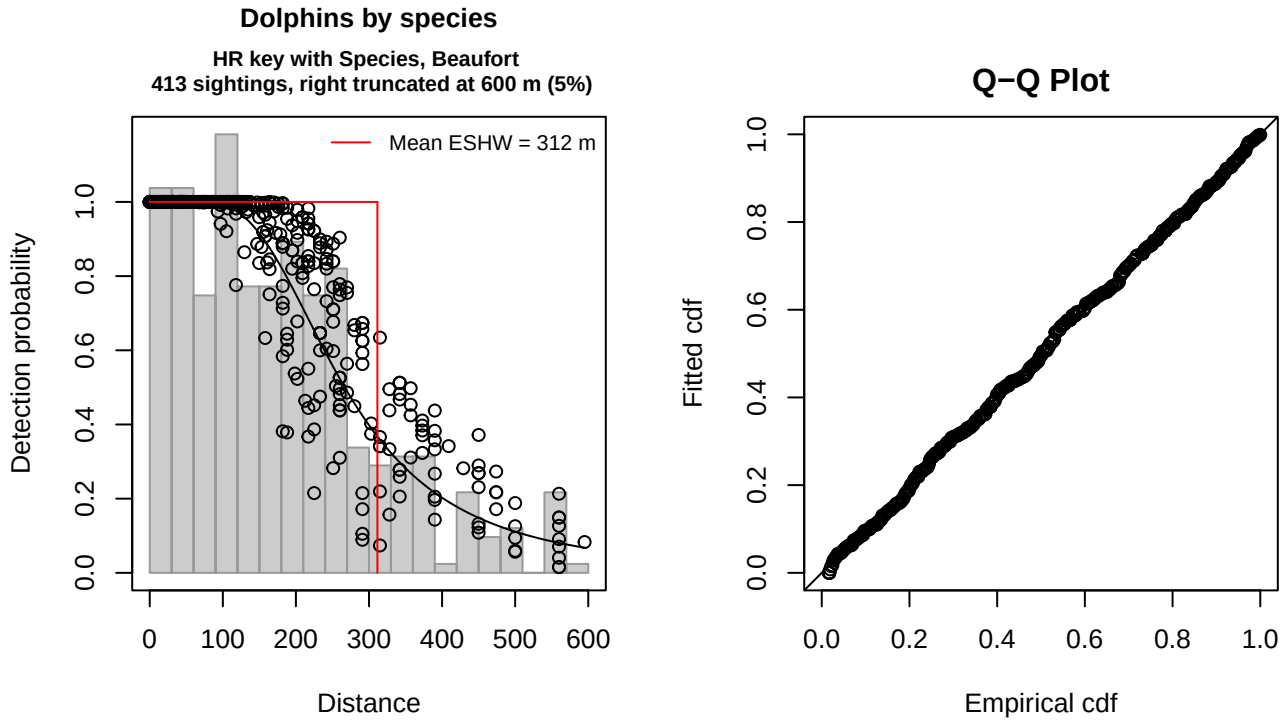

Figure 6: NEFSC Pre-AMAPPS detection function and Q-Q plot showing its goodness of fit.

Statistical output for this detection function:

```
Summary for ds object
Number of observations :  413
Distance range         :  0  -  600
AIC                    :  5043.994

Detection function:
 Hazard-rate key function

Detection function parameters
Scale coefficient(s):
                               estimate         se
(Intercept)                   5.3188665 0.15126469
ScientificNameLagenorhynchus  -0.1872175 0.11165678
ScientificNameTursiops, Steno -0.5457529 0.14785313
Beaufort                       0.1451869 0.05844944

Shape coefficient(s):
            estimate        se
(Intercept) 1.107015 0.1176733

                     Estimate          SE         CV
```

```
Average p             0.4982478  0.02373666 0.04764026
N in covered region 828.9047438 49.28440455 0.05945726

Distance sampling Cramer-von Mises test (unweighted)
Test statistic = 0.023324  p = 0.992716
```

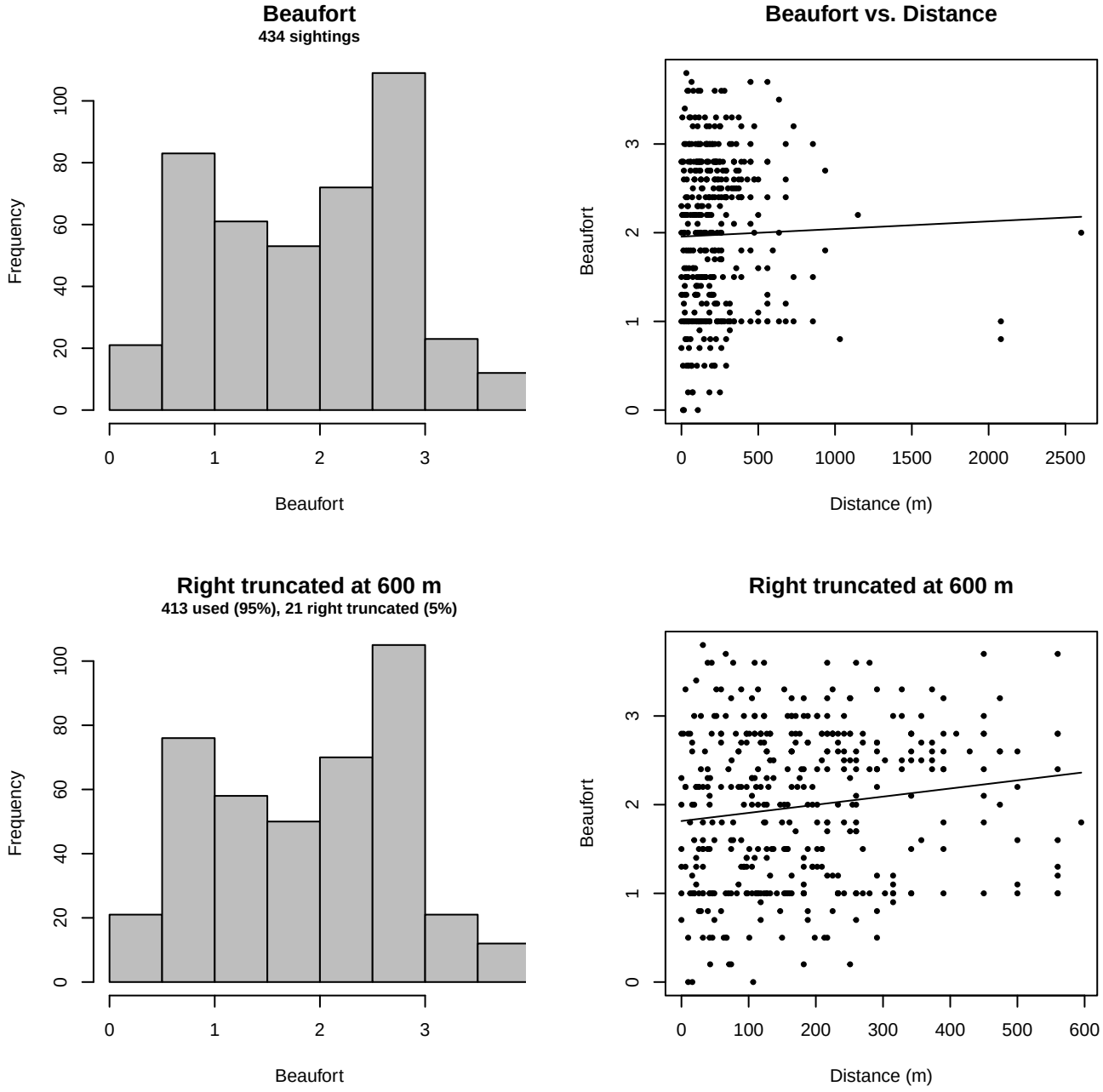

Figure 7: Distribution of the Beaufort covariate before (top row) and after (bottom row) observations were truncated to fit the NEFSC Pre-AMAPPS detection function.

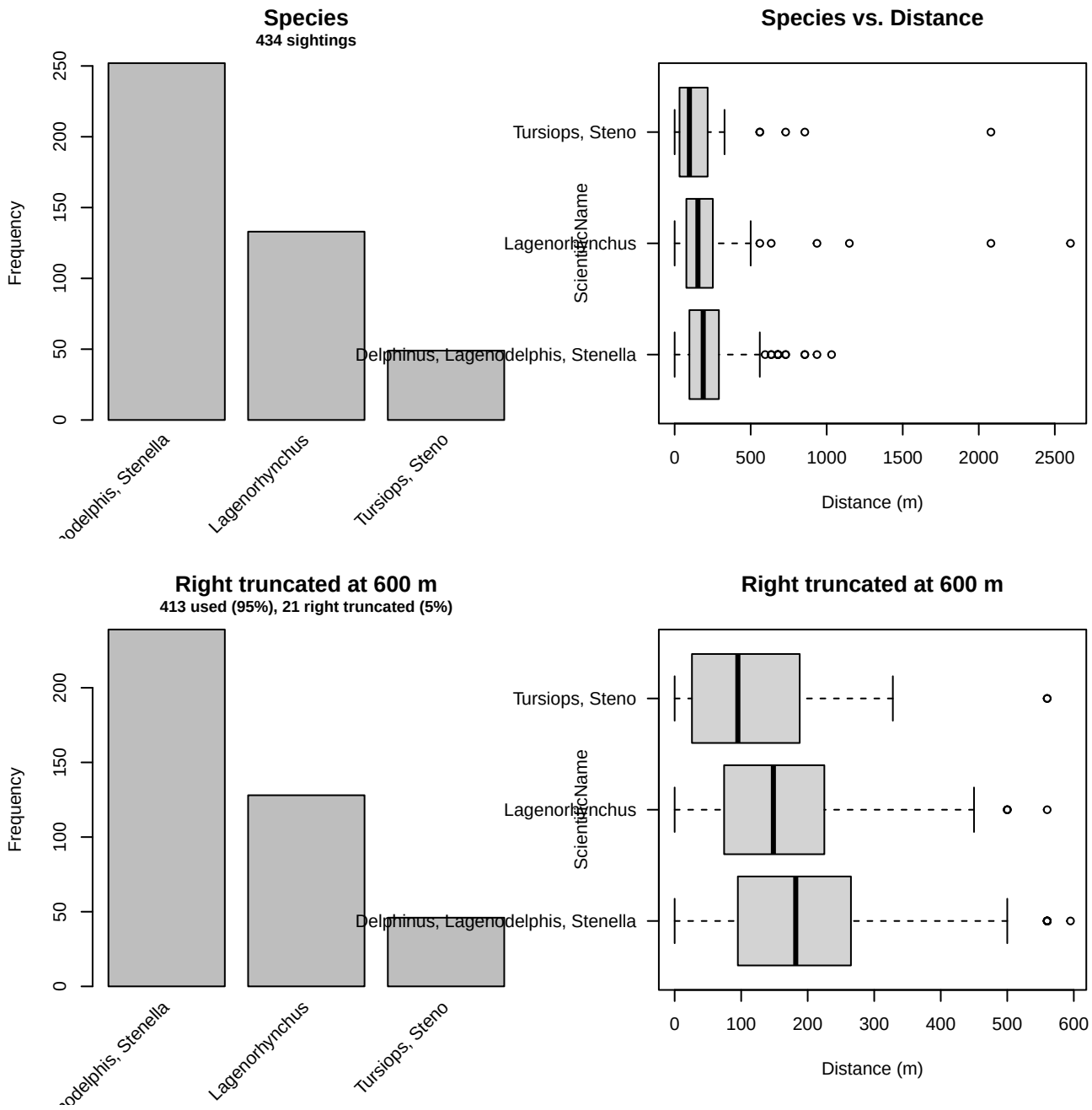

Figure 8: Distribution of the ScientificName covariate before (top row) and after (bottom row) observations were truncated to fit the NEFSC Pre-AMAPPS detection function.

3.1.1.2 SEFSC AMAPPS

After right-truncating observations greater than 325 m and left-truncating observations less than 15 m (Figure 10), we fitted the detection function to the 1628 observations that remained (Table 7). The selected detection function (Figure 9) used a hazard rate key function with Beaufort (Figure 11), ScientificName (Figure 12) and Season (Figure 13) as covariates.

Table 7: Observations used to fit the SEFSC AMAPPS detection function.

ScientificName	n
Delphinus, Tursiops, Lagenorhynchus, Steno	1422
Stenella, Lagenodelphis	206
Total	**1628**

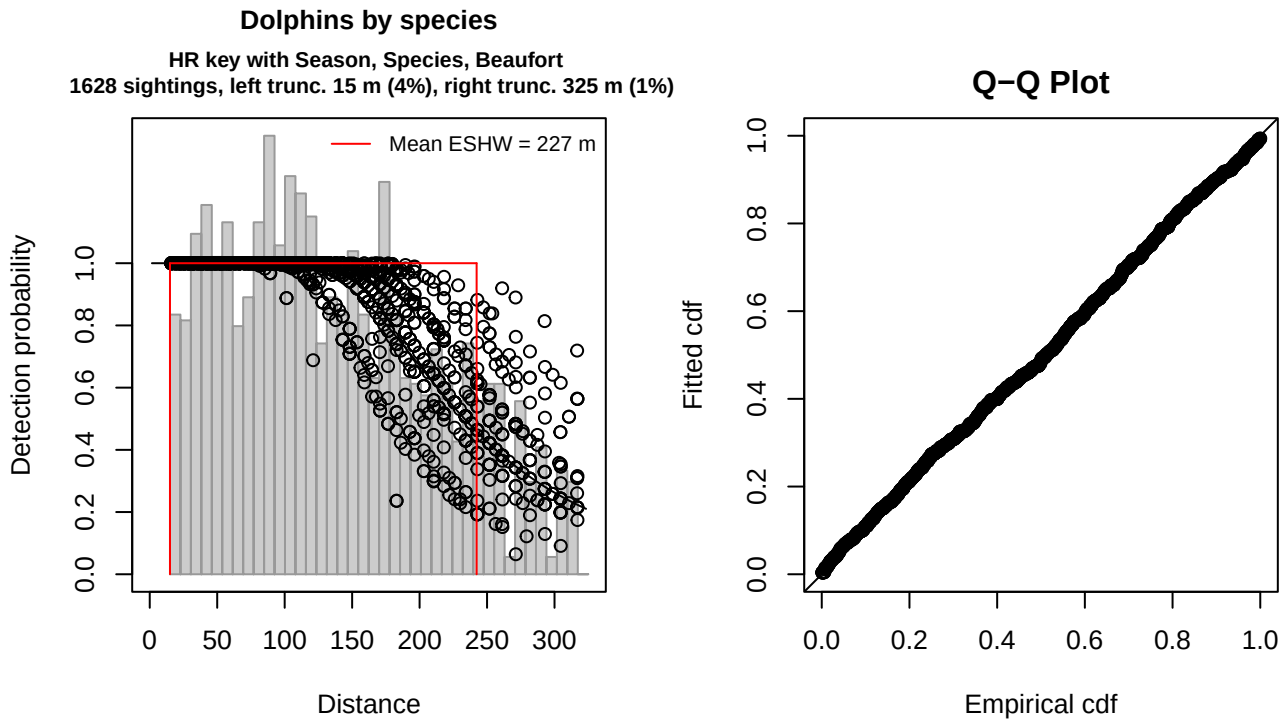

Figure 9: SEFSC AMAPPS detection function and Q-Q plot showing its goodness of fit.

Statistical output for this detection function:

```
Summary for ds object
Number of observations :  1628
Distance range         :  15  -  325
AIC                    :  18351.39

Detection function:
 Hazard-rate key function

Detection function parameters
Scale coefficient(s):
                                      estimate         se
(Intercept)                          5.4780735 0.08251975
SeasonSummer                         0.1269645 0.06172358
SeasonWinter                        -0.2356803 0.06102237
ScientificNameStenella, Lagenodelphis  0.2204074 0.08699872
Beaufort2                           -0.1192230 0.08713320
Beaufort3                           -0.1846083 0.08971655
Beaufort4                           -0.4027356 0.12330363

Shape coefficient(s):
            estimate        se
(Intercept) 1.266688 0.1150367

                       Estimate          SE         CV
Average p              0.720161  0.01522909 0.02114679
N in covered region 2260.605761 56.60731047 0.02504077

Distance sampling Cramer-von Mises test (unweighted)
Test statistic = 0.138923  p = 0.425167
```

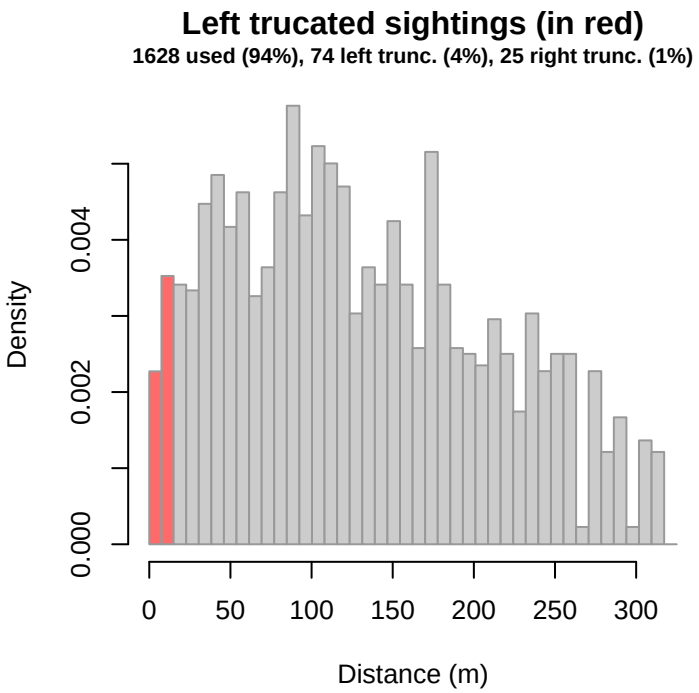

Figure 10: Density histogram of observations used to fit the SEFSC AMAPPS detection function, with the left-most bar showing observations at distances less than 15 m, which were left-truncated and excluded from the analysis [Buckland et al. (2001)]. (This bar may be very short if there were very few left-truncated sightings, or very narrow if the left truncation distance was very small; in either case it may not appear red.)

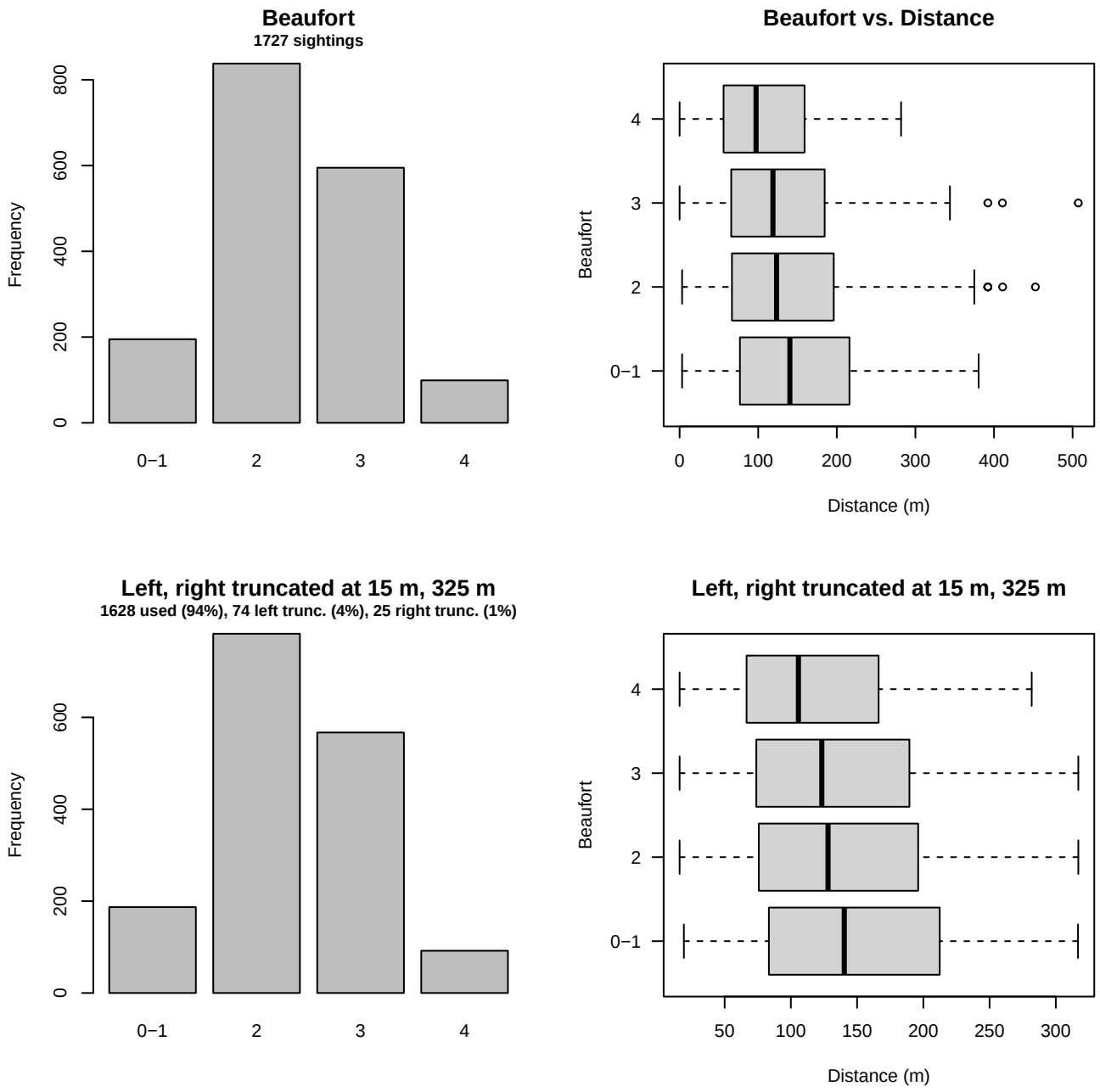

Figure 11: Distribution of the Beaufort covariate before (top row) and after (bottom row) observations were truncated to fit the SEFSC AMAPPS detection function.

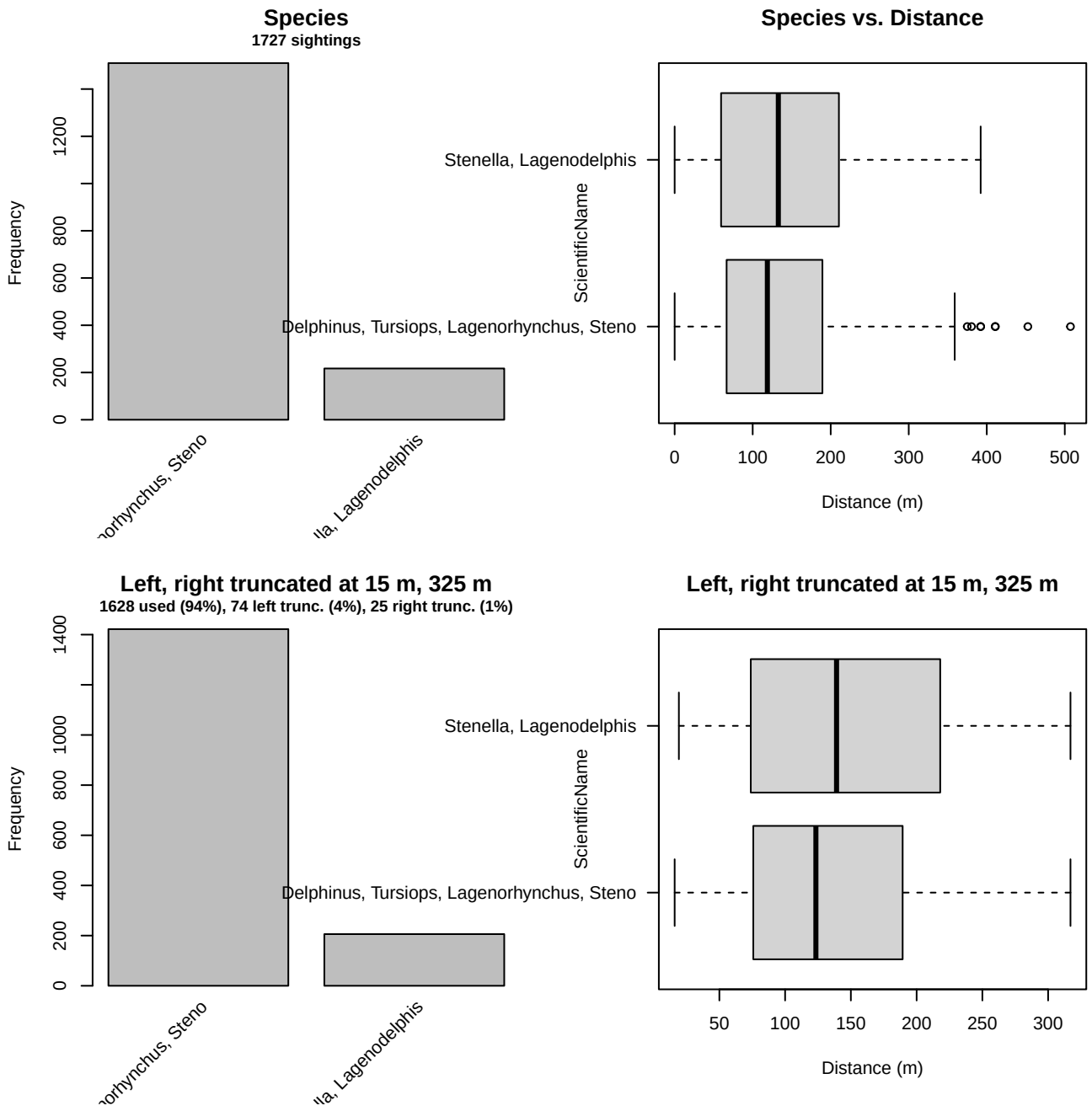

Figure 12: Distribution of the ScientificName covariate before (top row) and after (bottom row) observations were truncated to fit the SEFSC AMAPPS detection function.

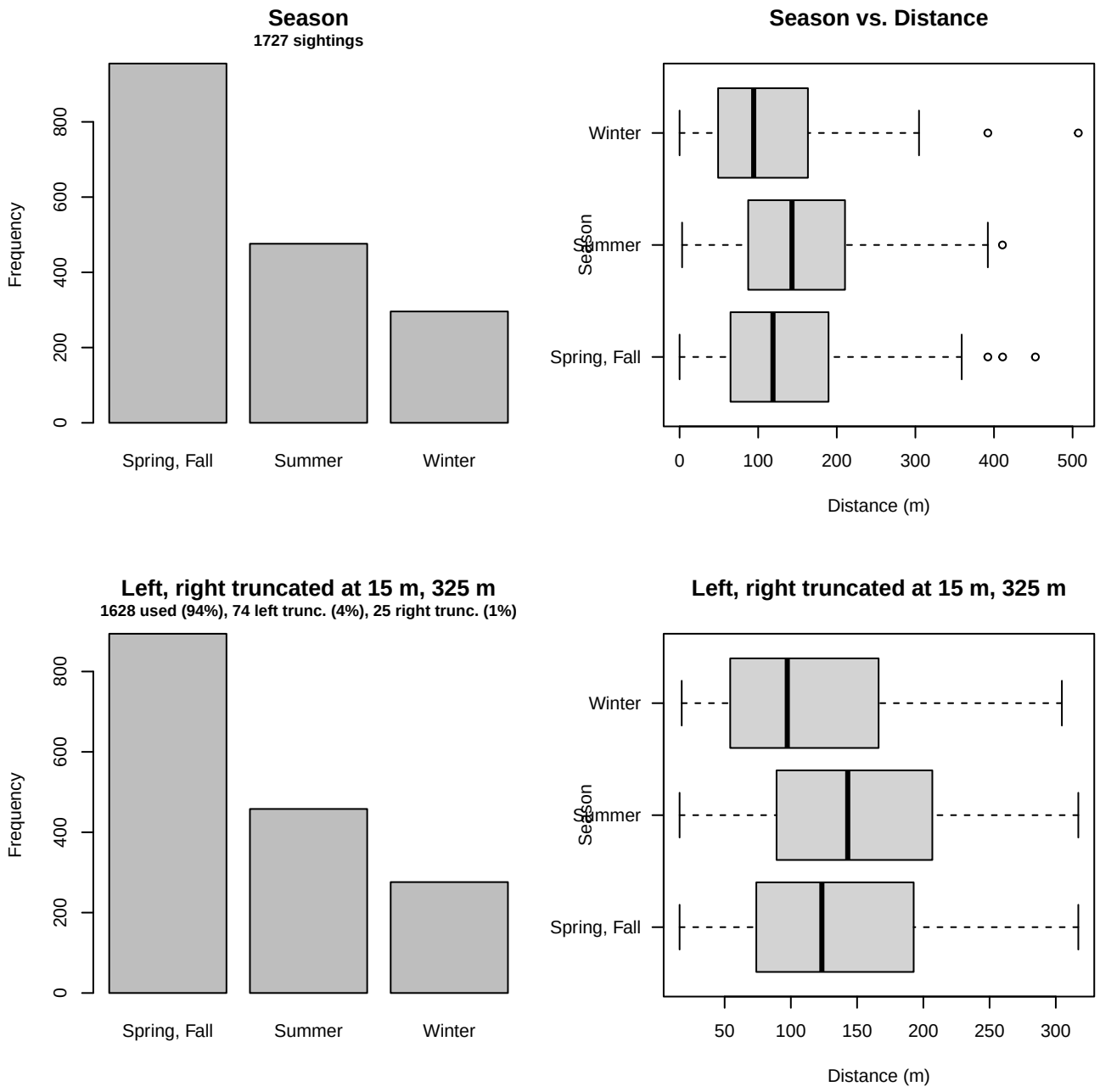

Figure 13: Distribution of the Season covariate before (top row) and after (bottom row) observations were truncated to fit the SEFSC AMAPPS detection function.

3.1.2 Shipboard Surveys

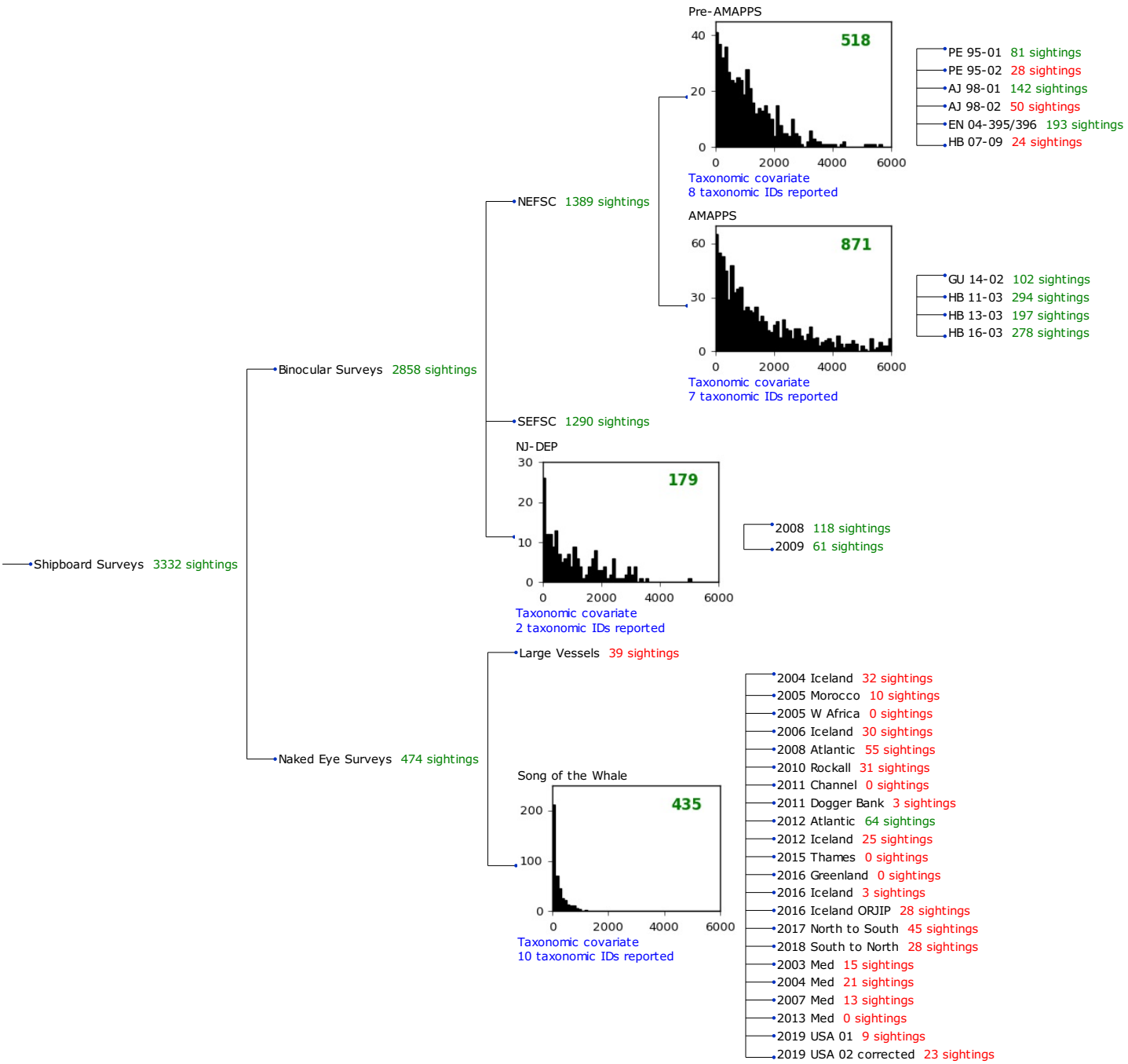

Figure 14: Detection hierarchy for shipboard surveys, showing how they were pooled during detectability modeling, for detection functions that pooled multiple taxa and used used a taxonomic covariate to account for differences between them. Each histogram represents a detection function and summarizes the perpendicular distances of observations that were pooled to fit it, prior to truncation. Observation counts, also prior to truncation, are shown in green when they met the recommendation of Buckland et al. (2001) that detection functions utilize at least 60 sightings, and red otherwise. For rare taxa, it was not always possible to meet this recommendation, yielding higher statistical uncertainty. During the spatial modeling stage of the analysis, effective strip widths were computed for each survey using the closest detection function above it in the hierarchy (i.e. moving from right to left in the figure). Surveys that do not have a detection function above them in this figure were either addressed by a detection function presented in a different section of this report, or were omitted from the analysis.

3.1.2.1 NEFSC Pre-AMAPPS

After right-truncating observations greater than 4000 m, we fitted the detection function to the 508 observations that remained (Table 8). The selected detection function (Figure 15) used a hazard rate key function with Beaufort (Figure 16), ScientificName (Figure 17) and VesselName (Figure 18) as covariates.

Table 8: Observations used to fit the NEFSC Pre-AMAPPS detection function.

ScientificName	n
Delphinus, Lagenorhynchus, Tursiops, Steno	365
Other Stenella, Lagenodelphis	130
Stenella frontalis	13
Total	**508**

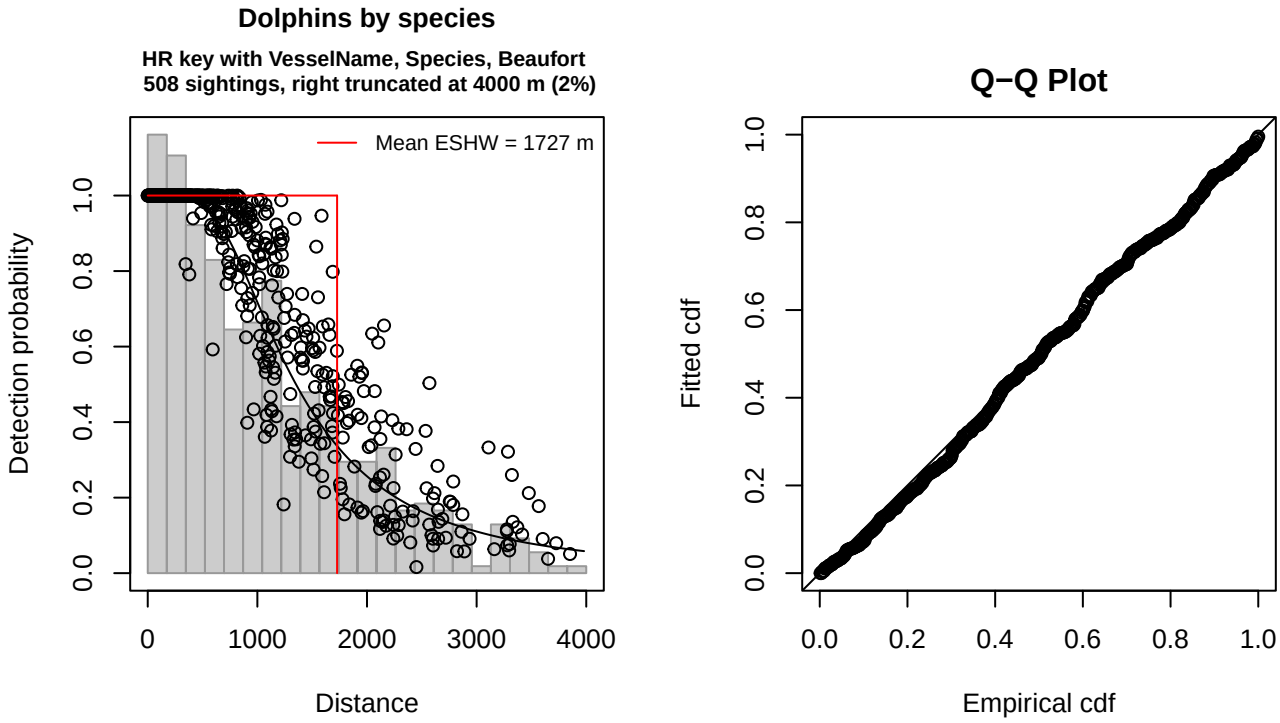

Figure 15: NEFSC Pre-AMAPPS detection function and Q-Q plot showing its goodness of fit.

Statistical output for this detection function:

```
Summary for ds object
Number of observations :  508
Distance range         :  0  -  4000
AIC                    :  8058.614

Detection function:
 Hazard-rate key function

Detection function parameters
Scale coefficient(s):
                                          estimate        se
(Intercept)                              7.3979634 0.1986065
VesselNameEndeavor, Bigelow              0.2529041 0.1095209
ScientificNameOther Stenella, Lagenodelphis  0.3555978 0.1258179
ScientificNameStenella frontalis        -0.8556981 0.3078540
```

```
Beaufort                                  -0.1897812 0.0694737

Shape coefficient(s):
             estimate        se
(Intercept) 0.8752144 0.1006522

                          Estimate          SE         CV
Average p                0.4071518  0.02118698 0.05203705
N in covered region 1247.6919609 78.15195776 0.06263722

Distance sampling Cramer-von Mises test (unweighted)
Test statistic = 0.120847  p = 0.492001
```

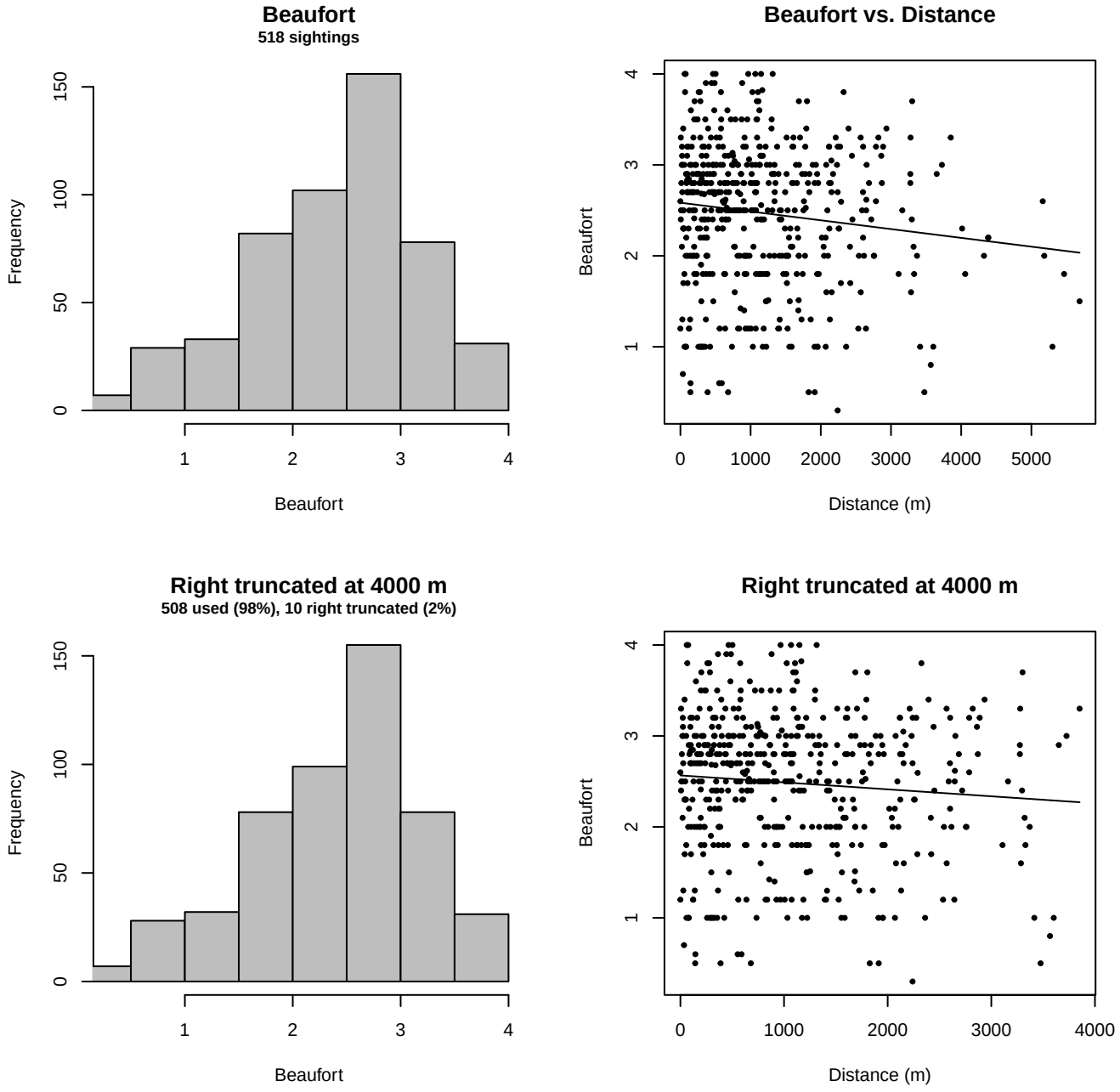

Figure 16: Distribution of the Beaufort covariate before (top row) and after (bottom row) observations were truncated to fit the NEFSC Pre-AMAPPS detection function.

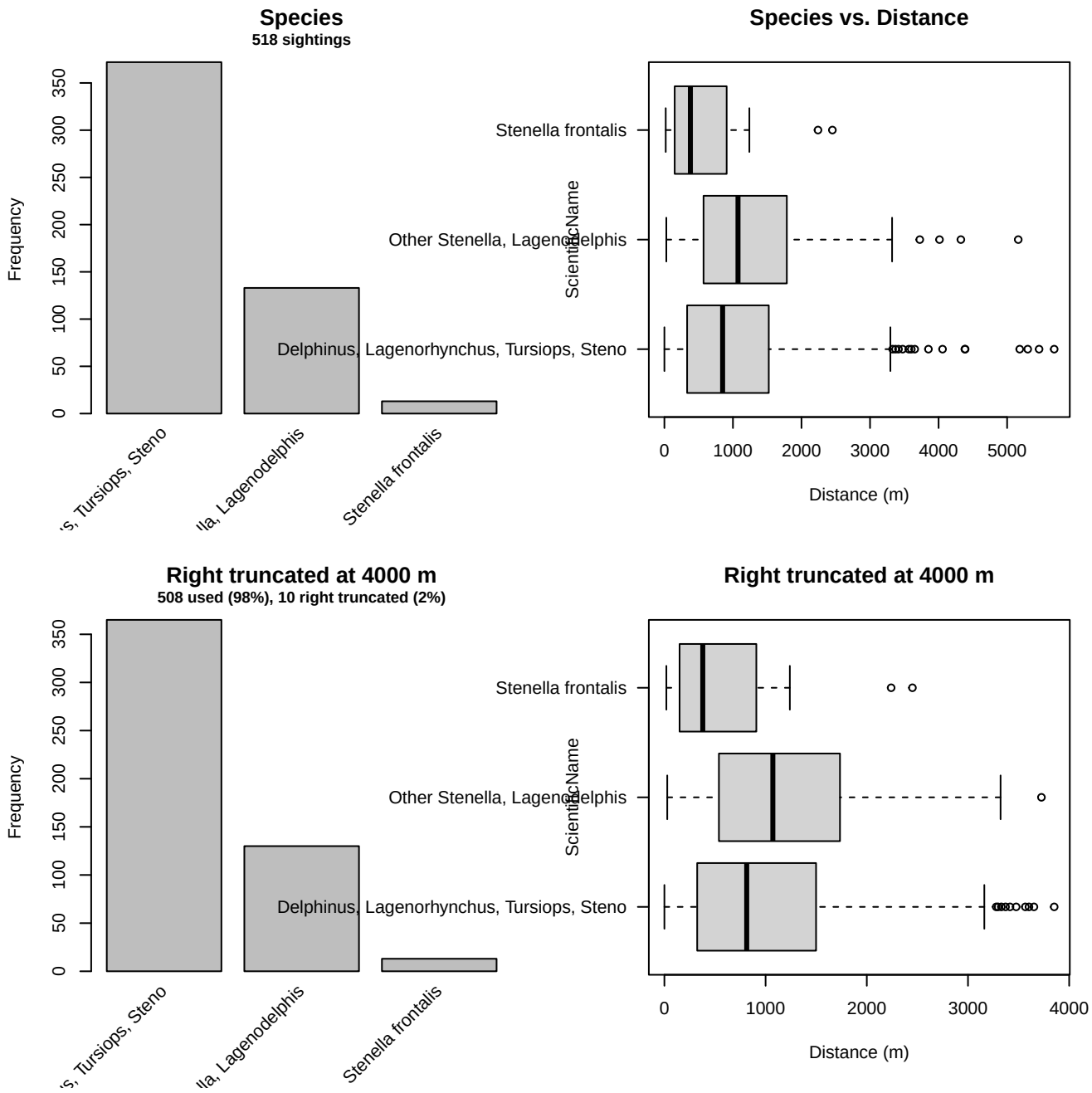

Figure 17: Distribution of the ScientificName covariate before (top row) and after (bottom row) observations were truncated to fit the NEFSC Pre-AMAPPS detection function.

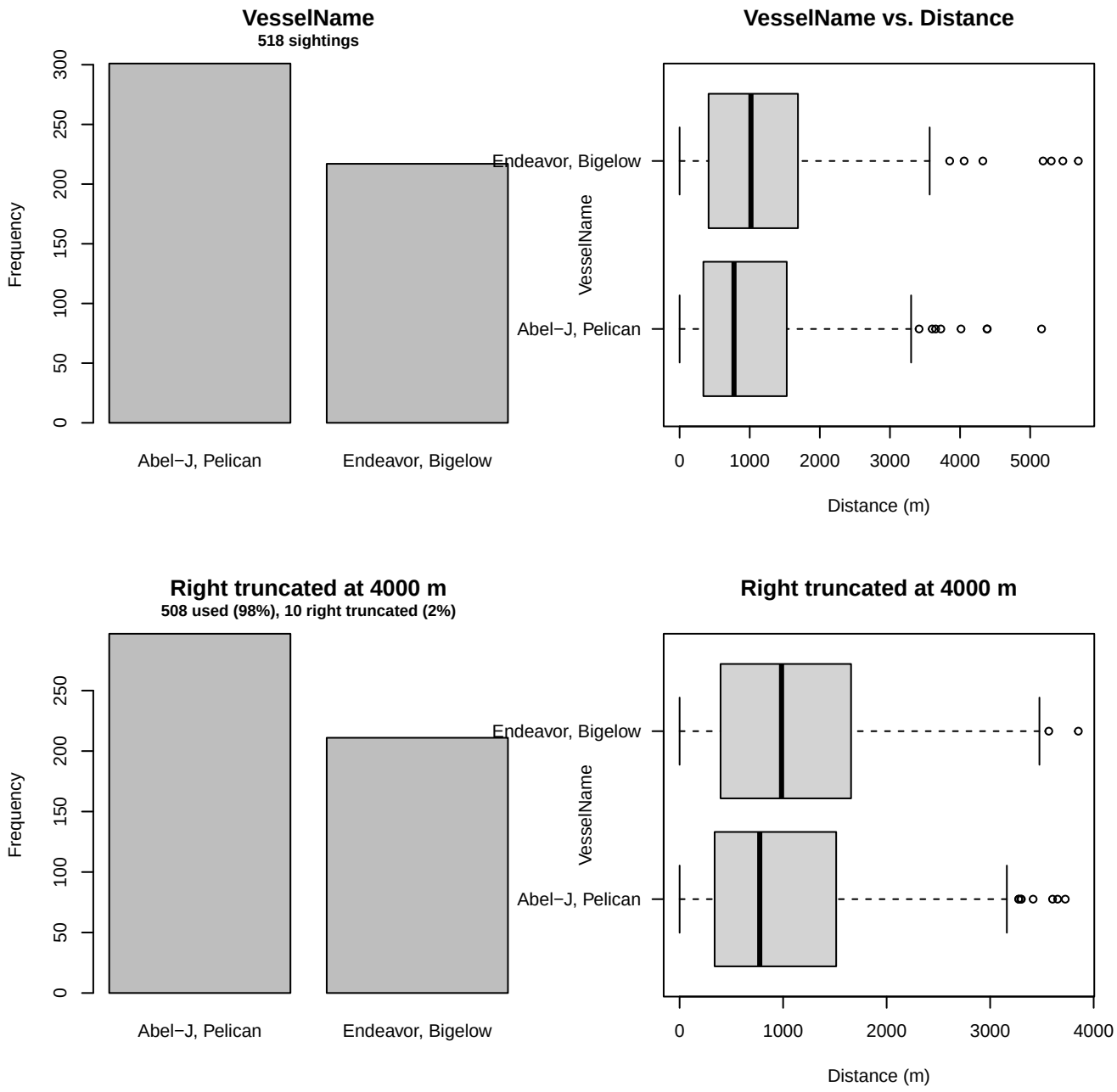

Figure 18: Distribution of the VesselName covariate before (top row) and after (bottom row) observations were truncated to fit the NEFSC Pre-AMAPPS detection function.

3.1.2.2 NEFSC AMAPPS

After right-truncating observations greater than 6000 m, we fitted the detection function to the 857 observations that remained (Table 9). The selected detection function (Figure 19) used a hazard rate key function with Beaufort (Figure 20) and ScientificName (Figure 21) as covariates.

Table 9: Observations used to fit the NEFSC AMAPPS detection function.

ScientificName	n
Delphinus, Lagenorhynchus	358
Other Stenella, Lagenodelphis	175
Stenella frontalis	53
Tursiops, Steno	271
Total	**857**

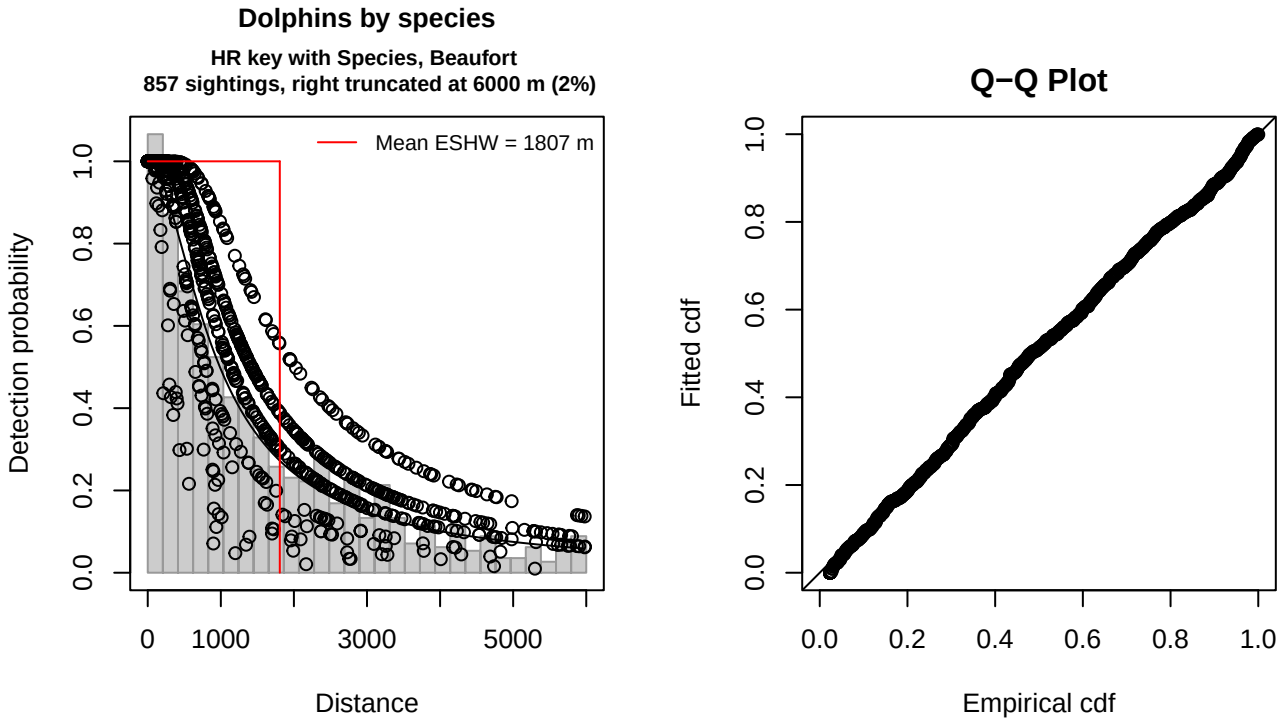

Figure 19: NEFSC AMAPPS detection function and Q-Q plot showing its goodness of fit.

Statistical output for this detection function:

```
Summary for ds object
Number of observations :  857
Distance range         :  0  -  6000
AIC                    :  14222.66

Detection function:
 Hazard-rate key function

Detection function parameters
Scale coefficient(s):
                                           estimate        se
(Intercept)                               7.0022801 0.1342692
ScientificNameOther Stenella, Lagenodelphis  0.3515378 0.1854896
ScientificNameStenella frontalis           -0.5910499 0.3033455
ScientificNameTursiops, Steno              -0.2176361 0.1602756
Beaufort3-4                                -0.5842019 0.1839783
Beaufort4-5                                -1.4374209 0.2667762

Shape coefficient(s):
            estimate        se
```

```
(Intercept) 0.356339 0.0663051

                         Estimate           SE         CV
Average p                0.2624967   0.01868208 0.07117073
N in covered region 3264.8026106 252.27662296 0.07727163

Distance sampling Cramer-von Mises test (unweighted)
Test statistic = 0.089267  p = 0.640081
```

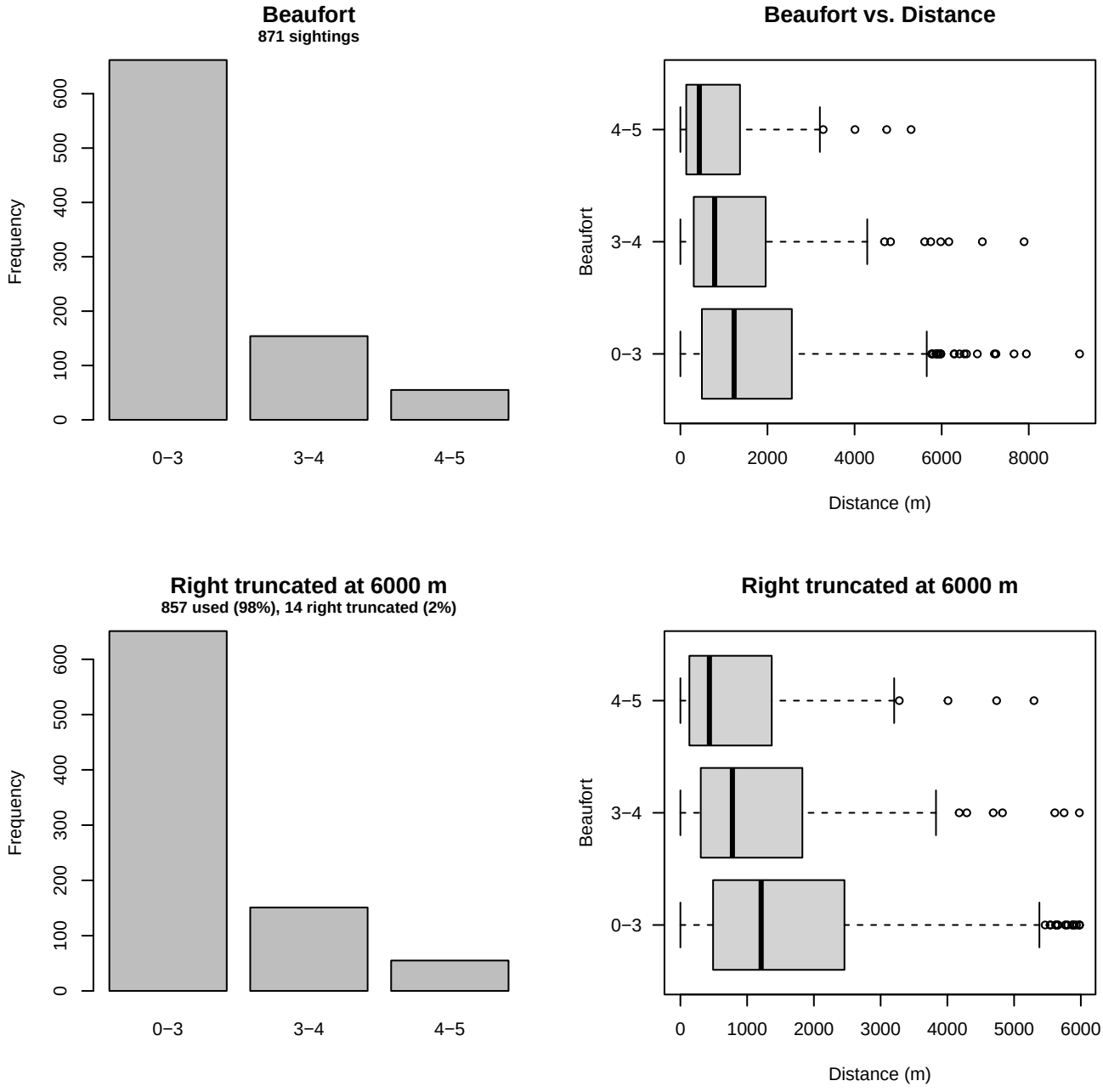

Figure 20: Distribution of the Beaufort covariate before (top row) and after (bottom row) observations were truncated to fit the NEFSC AMAPPS detection function.

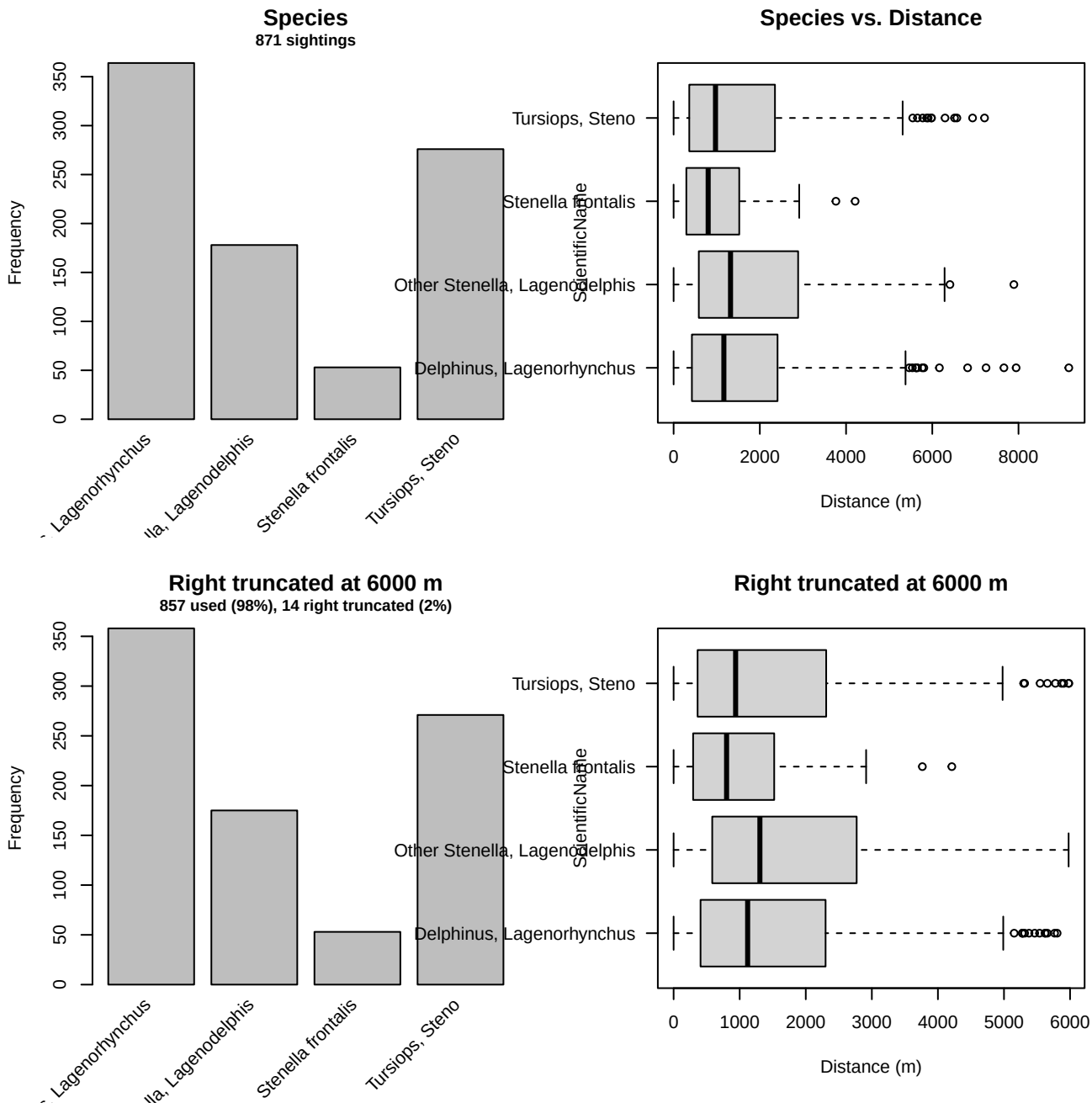

Figure 21: Distribution of the ScientificName covariate before (top row) and after (bottom row) observations were truncated to fit the NEFSC AMAPPS detection function.

3.1.2.3 NJ-DEP

After right-truncating observations greater than 3200 m, we fitted the detection function to the 175 observations that remained (Table 10). The selected detection function (Figure 22) used a hazard rate key function with ScientificName (Figure 23) as a covariate.

Table 10: Observations used to fit the NJ-DEP detection function.

ScientificName	n
Delphinus delphis	19
Tursiops truncatus	156
Total	**175**

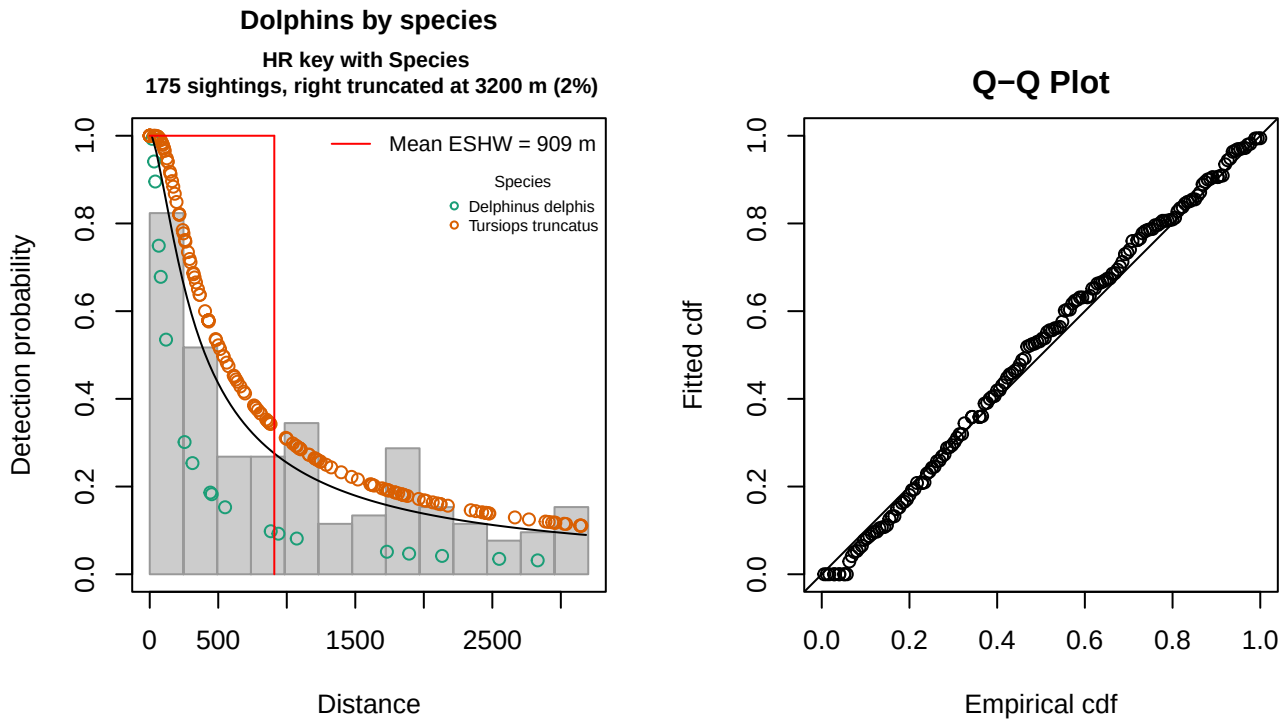

Figure 22: NJ-DEP detection function and Q-Q plot showing its goodness of fit.

Statistical output for this detection function:

```
Summary for ds object
Number of observations :  175
Distance range         :  0  -  3200
AIC                    :  2750.465

Detection function:
 Hazard-rate key function

Detection function parameters
Scale coefficient(s):
                                estimate        se
(Intercept)                     4.512698 0.9620506
ScientificNameTursiops truncatus 1.400338 0.8543953

Shape coefficient(s):
            estimate        se
(Intercept)        0 0.1617129

                       Estimate          SE        CV
Average p             0.2578318   0.05821781 0.2257976
N in covered region 678.7370004 159.72027878 0.2353198

Distance sampling Cramer-von Mises test (unweighted)
Test statistic = 0.132198  p = 0.448683
```

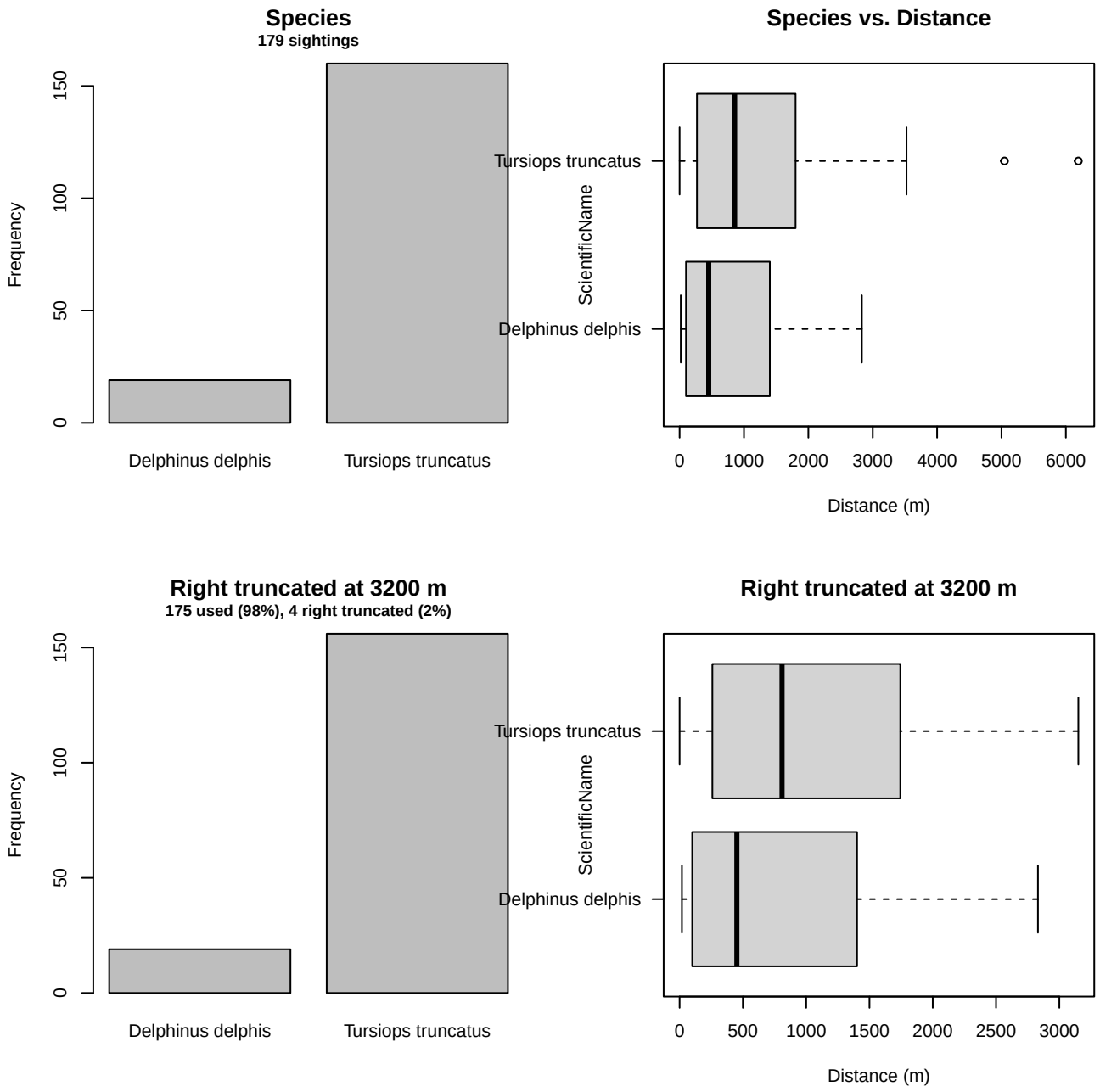

Figure 23: Distribution of the ScientificName covariate before (top row) and after (bottom row) observations were truncated to fit the NJ-DEP detection function.

3.1.2.4 Song of the Whale

After right-truncating observations greater than 700 m and left-truncating observations less than 1 m (Figure 25), we fitted the detection function to the 360 observations that remained (Table 11). The selected detection function (Figure 24) used a hazard rate key function with Beaufort (Figure 26), ScientificName (Figure 27) and Visibility (Figure 28) as covariates.

Table 11: Observations used to fit the Song of the Whale detection function.

ScientificName	n
All others	211
Delphinus	149
Total	**360**

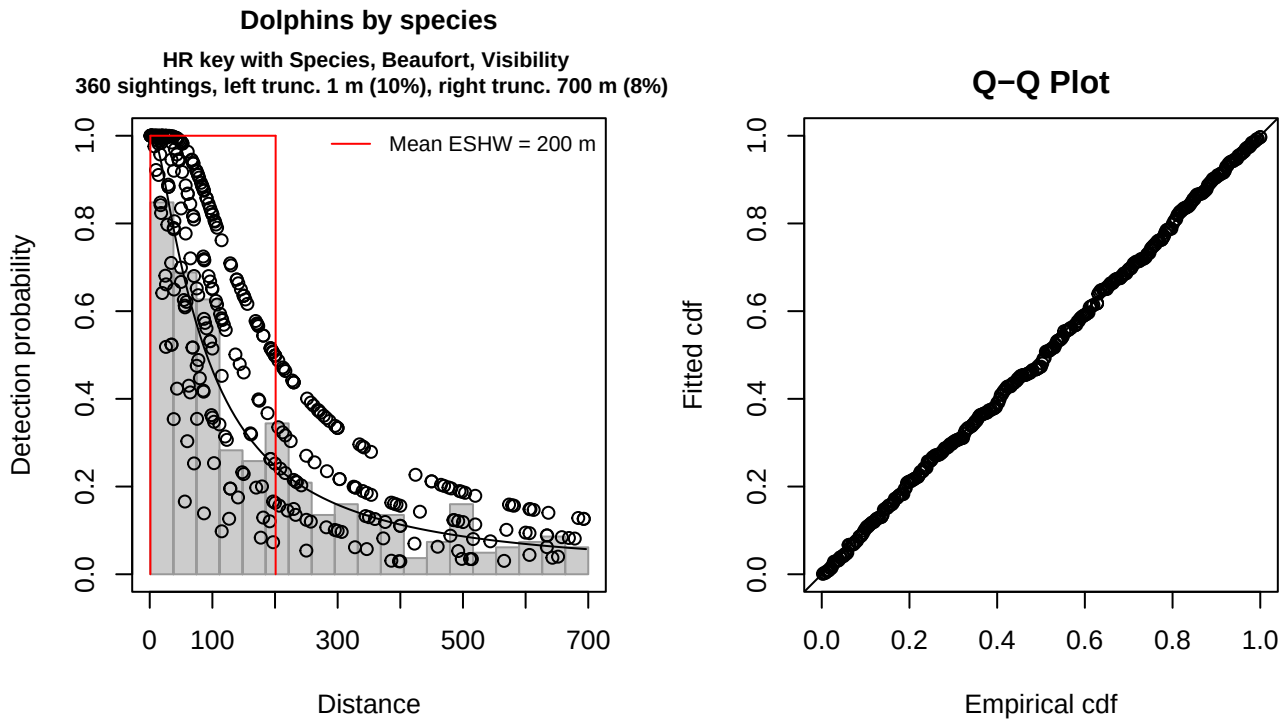

Figure 24: Song of the Whale detection function and Q-Q plot showing its goodness of fit.

Statistical output for this detection function:

```
Summary for ds object
Number of observations :  360
Distance range         :  1  -  700
AIC                    :  4434.06

Detection function:
 Hazard-rate key function

Detection function parameters
Scale coefficient(s):
                             estimate        se
(Intercept)                 5.0168382 0.2118228
ScientificNameDelphinus    -0.3746003 0.2526245
Beaufort3                  -0.6586604 0.2922112
Beaufort3.5-4              -1.3223280 0.3841776
VisibilityModerate (2-5nmi) -0.9687696 0.4363084

Shape coefficient(s):
             estimate         se
(Intercept) 0.2728327 0.09542948

                       Estimate           SE        CV
Average p              0.232512   0.02944422 0.1266352
N in covered region 1548.306965 209.54903632 0.1353408

Distance sampling Cramer-von Mises test (unweighted)
Test statistic = 0.019198  p = 0.997687
```

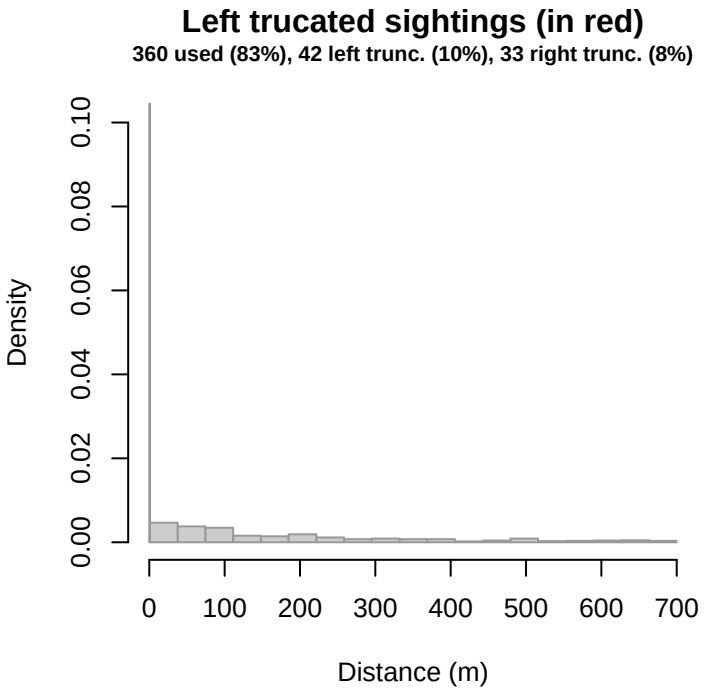

Figure 25: Density histogram of observations used to fit the Song of the Whale detection function, with the left-most bar showing observations at distances less than 1 m, which were left-truncated and not used to fit the detection function. (This bar may be very short if there were very few left-truncated sightings, or very narrow if the left truncation distance was very small; in either case it may not appear red.) These were excluded because they formed a problematic "spike" in detections close to the trackline, suggesting that animals approached the vessel (e.g. to bow-ride) prior to being detected. To address this, we fitted the detection function to the observations beyond the spike and assumed that within it, detection probability was 1, effectively treating it like a strip transect. We then added the left-truncated observations back into the analysis as if they occurred in this strip. This treatment may have resulted in an underestimation of detection probability.

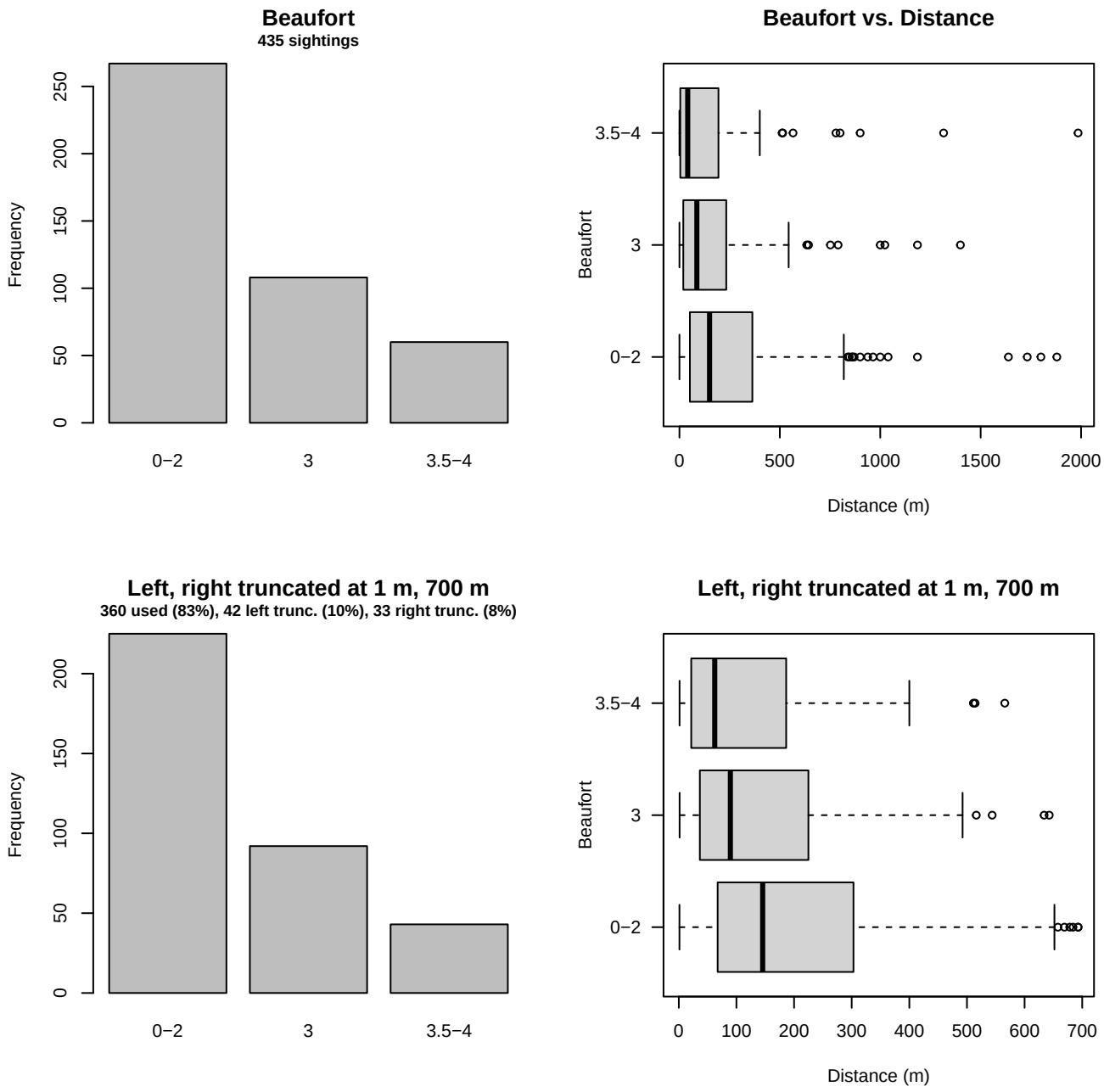

Figure 26: Distribution of the Beaufort covariate before (top row) and after (bottom row) observations were truncated to fit the Song of the Whale detection function.

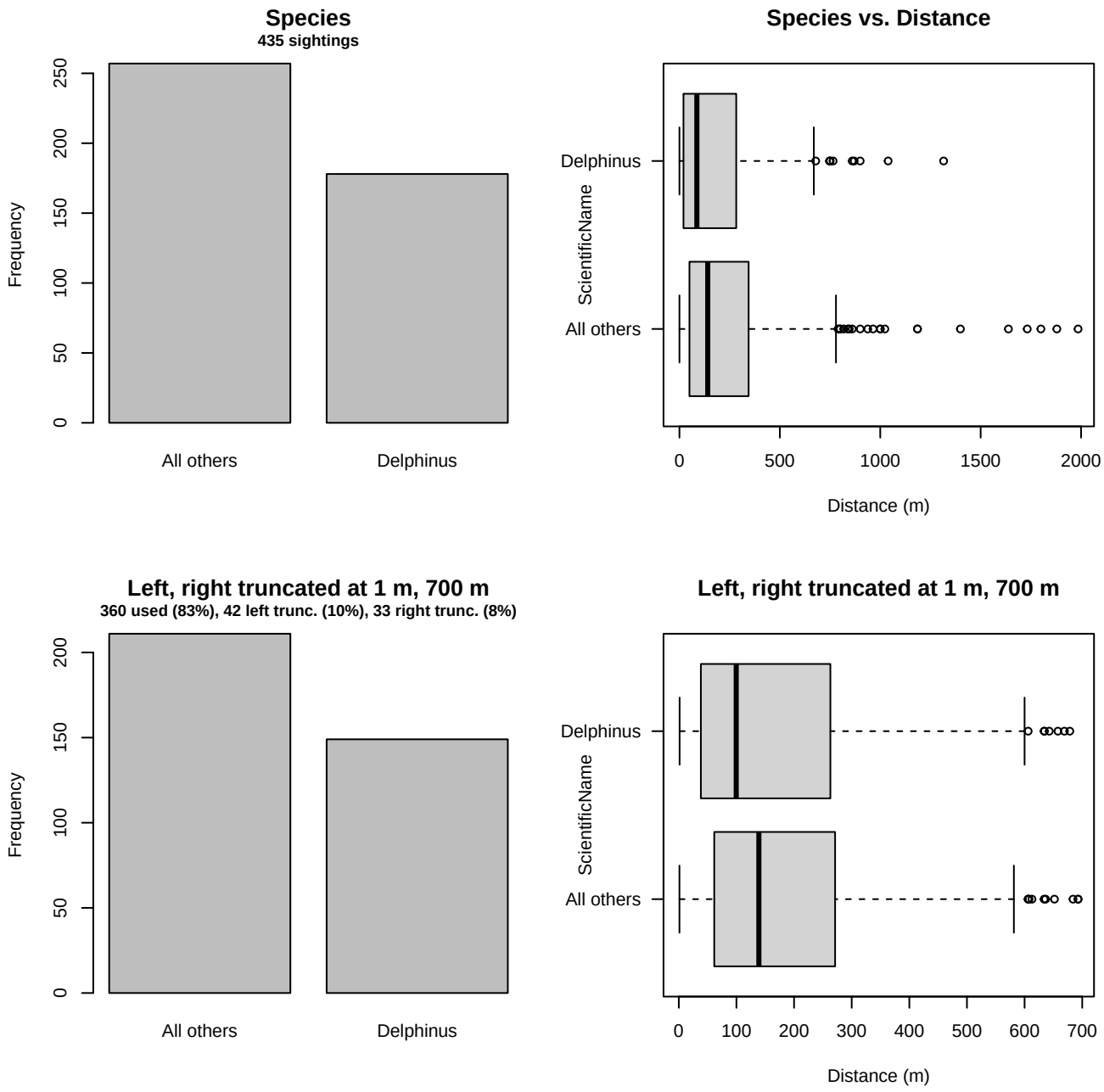

Figure 27: Distribution of the ScientificName covariate before (top row) and after (bottom row) observations were truncated to fit the Song of the Whale detection function.

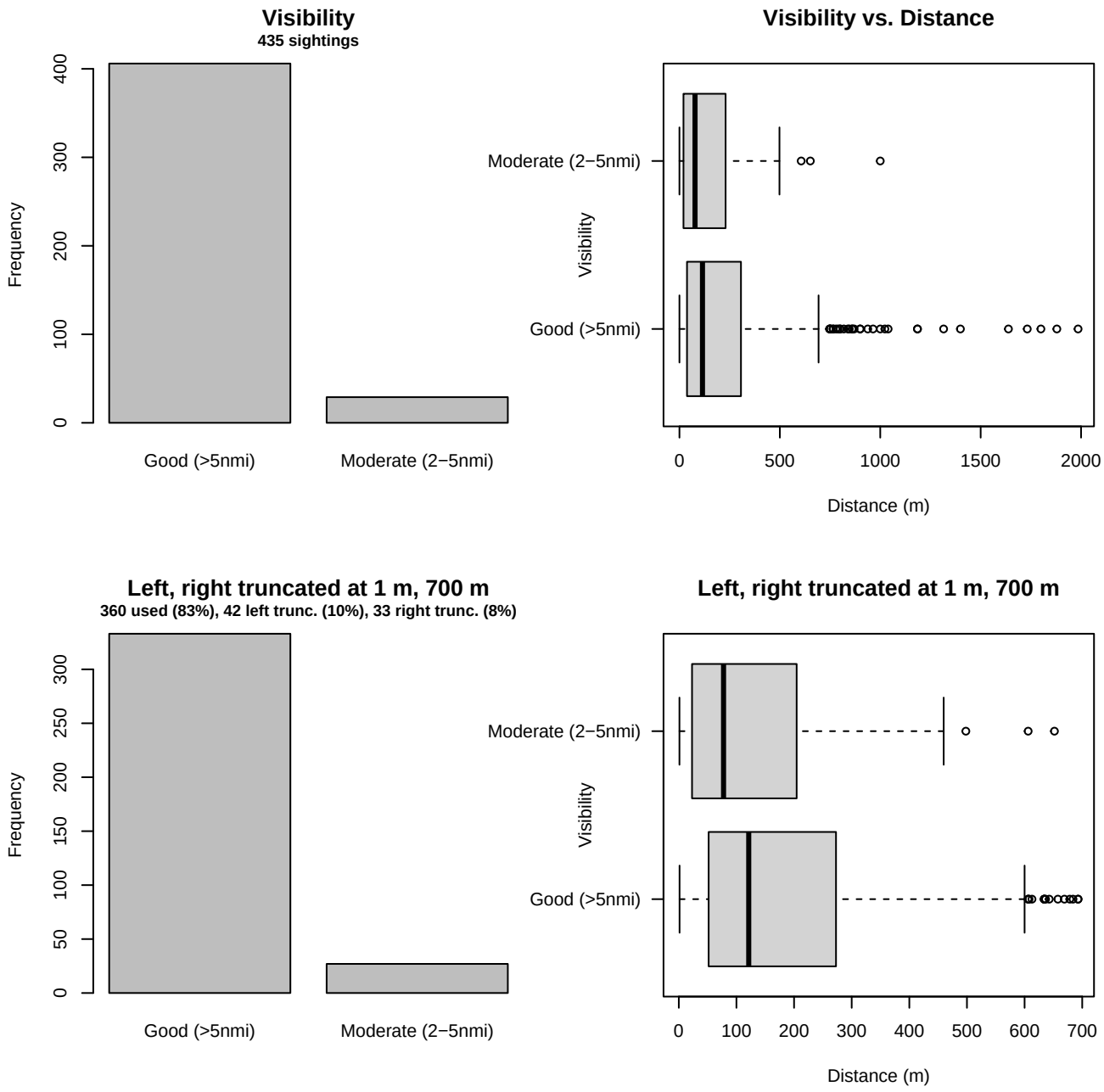

Figure 28: Distribution of the Visibility covariate before (top row) and after (bottom row) observations were truncated to fit the Song of the Whale detection function.

3.2 Without a Taxonomic Covariate

We fitted the detection functions in this section to pools of species with similar detectability characteristics but could not use a taxonomic identification as a covariate to account for differences between them. We usually took this approach after trying the taxonomic covariate and finding it had insufficient statistical power to be retained. We also resorted to it when the focal taxon being modeled had too few observations to be allocated its own taxonomic covariate level and was too poorly known for us to confidently determine which other taxa we could group it with.

3.2.1 Aerial Surveys

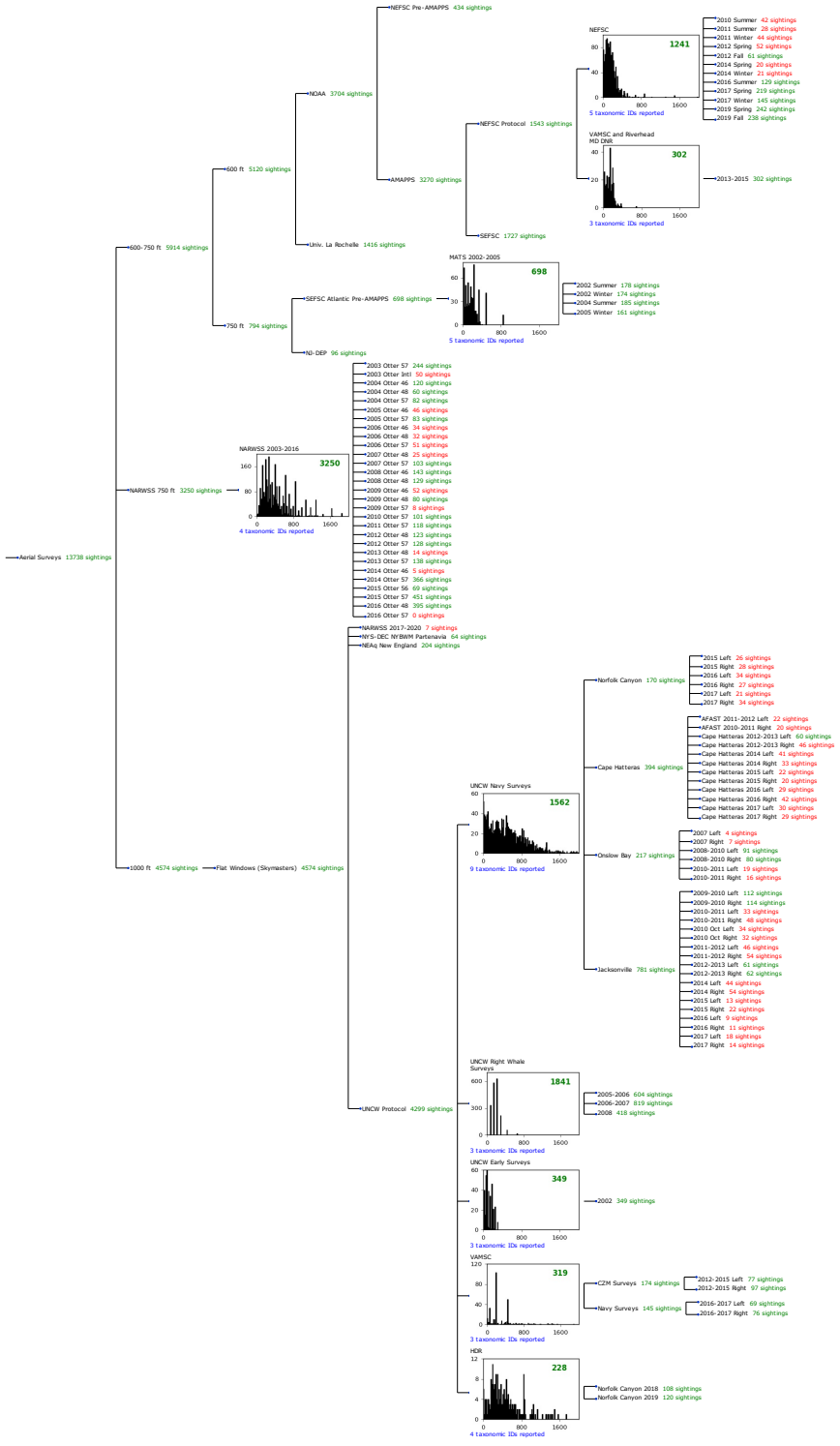

Figure 29: Detection hierarchy for aerial surveys, showing how they were pooled during detectability modeling, for detection functions that pooled multiple taxa but could not use a taxonomic covariate to account for differences between them. Each histogram represents a detection function and summarizes the perpendicular distances of observations that were pooled to fit it, prior to truncation. Observation counts, also prior to truncation, are shown in green when they met the recommendation of Buckland et al. (2001) that detection functions utilize at least 60 sightings, and red otherwise. For rare taxa, it was not always possible to meet this recommendation, yielding higher statistical uncertainty. During the spatial modeling stage of the analysis, effective strip widths were computed for each survey using the closest detection function above it in the hierarchy (i.e. moving from right to left in the figure). Surveys that do not have a detection function above them in this figure were either addressed by a detection function presented in a different section of this report, or were omitted from the analysis.

3.2.1.1 NEFSC AMAPPS

After right-truncating observations greater than 600 m, we fitted the detection function to the 1218 observations that remained (Table 12). The selected detection function (Figure 30) used a hazard rate key function with Season (Figure 31) as a covariate.

Table 12: Observations used to fit the NEFSC AMAPPS detection function.

ScientificName	n
Delphinus delphis	817
Lagenorhynchus acutus	280
Lagenorhynchus albirostris	3
Stenella coeruleoalba	13
Tursiops truncatus	105
Total	**1218**

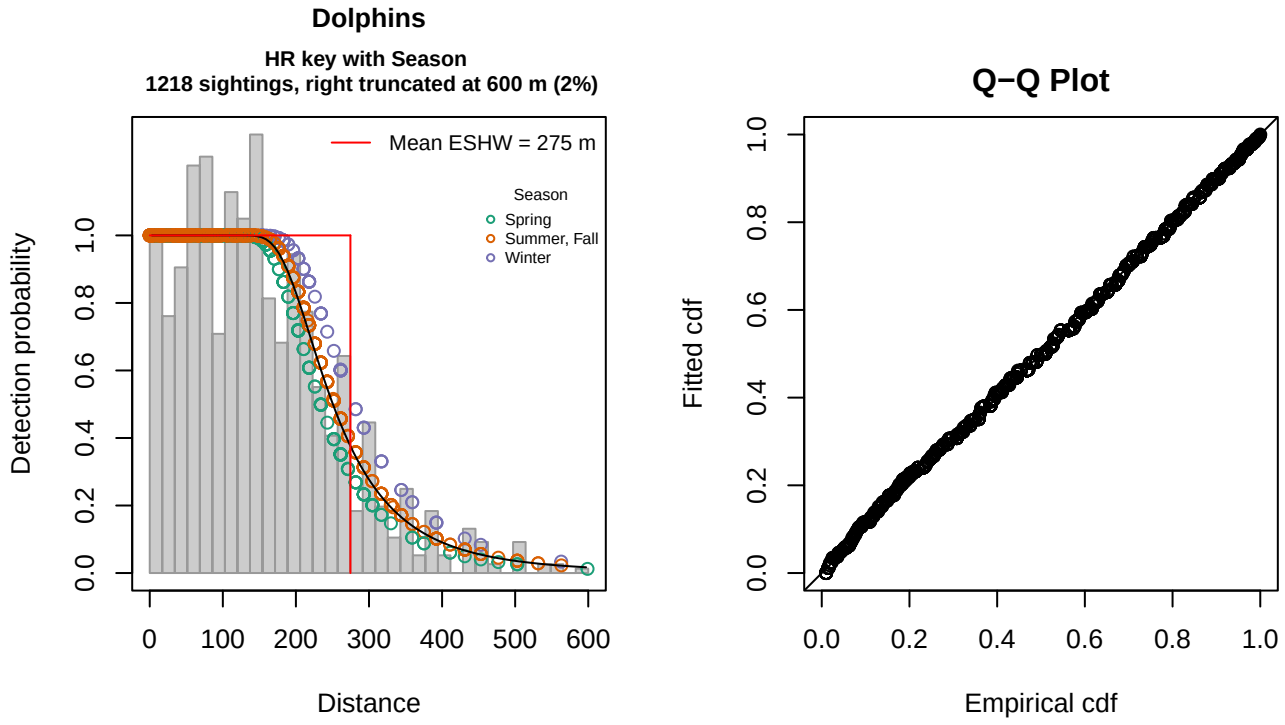

Figure 30: NEFSC AMAPPS detection function and Q-Q plot showing its goodness of fit.

Statistical output for this detection function:

```
Summary for ds object
Number of observations :  1218
Distance range         :  0  -  600
AIC                    :  14460.69

Detection function:
 Hazard-rate key function

Detection function parameters
Scale coefficient(s):
                     estimate         se
(Intercept)        5.36944749 0.04422696
SeasonSummer, Fall 0.08083579 0.04638562
SeasonWinter       0.17600218 0.07702020
```

```
Shape coefficient(s):
            estimate       se
(Intercept) 1.452854 0.065484

                        Estimate          SE         CV
Average p               0.456561  0.00970389 0.02125431
N in covered region 2667.770370 79.97999993 0.02998009

Distance sampling Cramer-von Mises test (unweighted)
Test statistic = 0.126854  p = 0.468488
```

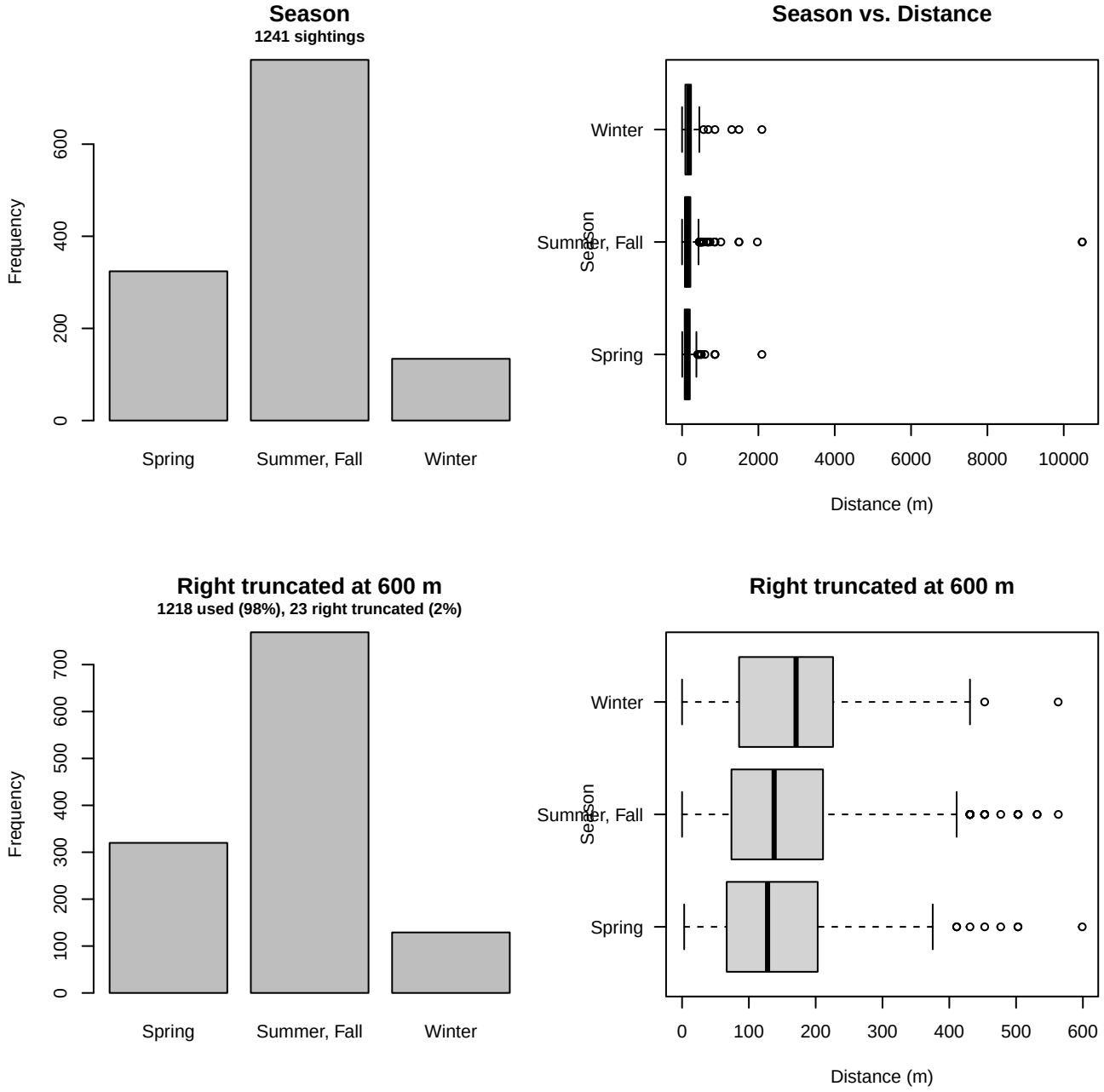

Figure 31: Distribution of the Season covariate before (top row) and after (bottom row) observations were truncated to fit the NEFSC AMAPPS detection function.

3.2.1.2 VAMSC and Riverhead MD DNR

After right-truncating observations greater than 400 m, we fitted the detection function to the 301 observations that remained (Table 13). The selected detection function (Figure 32) used a hazard rate key function with no covariates.

Table 13: Observations used to fit the VAMSC and Riverhead MD DNR detection function.

ScientificName	n
Delphinus delphis	22
Stenella frontalis	1
Tursiops truncatus	278
Total	**301**

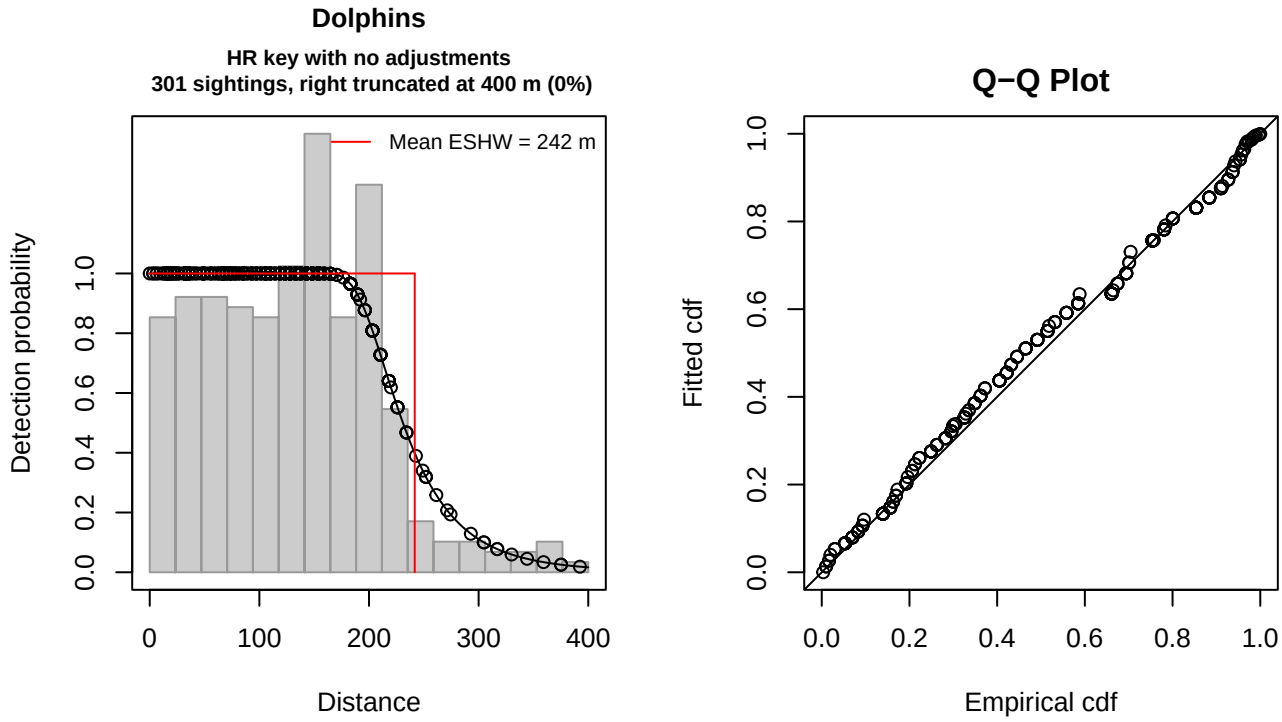

Figure 32: VAMSC and Riverhead MD DNR detection function and Q-Q plot showing its goodness of fit.

Statistical output for this detection function:

```
Summary for ds object
Number of observations :  301
Distance range         :  0  -  400
AIC                    :  3426.124

Detection function:
 Hazard-rate key function

Detection function parameters
Scale coefficient(s):
            estimate         se
(Intercept) 5.388208 0.04209556

Shape coefficient(s):
            estimate        se
(Intercept)  1.91525 0.1331166
```

```
                        Estimate         SE         CV
Average p               0.6042969  0.0203517 0.03367831
N in covered region 498.0995265 24.6489147 0.04948592

Distance sampling Cramer-von Mises test (unweighted)
Test statistic = 0.302011  p = 0.133421
```

3.2.1.3 MATS 2002-2005

After right-truncating observations greater than 629 m, we fitted the detection function to the 684 observations that remained (Table 14). The selected detection function (Figure 33) used a hazard rate key function with Beaufort (Figure 34) as a covariate.

Table 14: Observations used to fit the MATS 2002-2005 detection function.

ScientificName	n
Delphinus delphis	2
Stenella attenuata	2
Stenella frontalis	104
Tursiops truncatus	576
Total	**684**

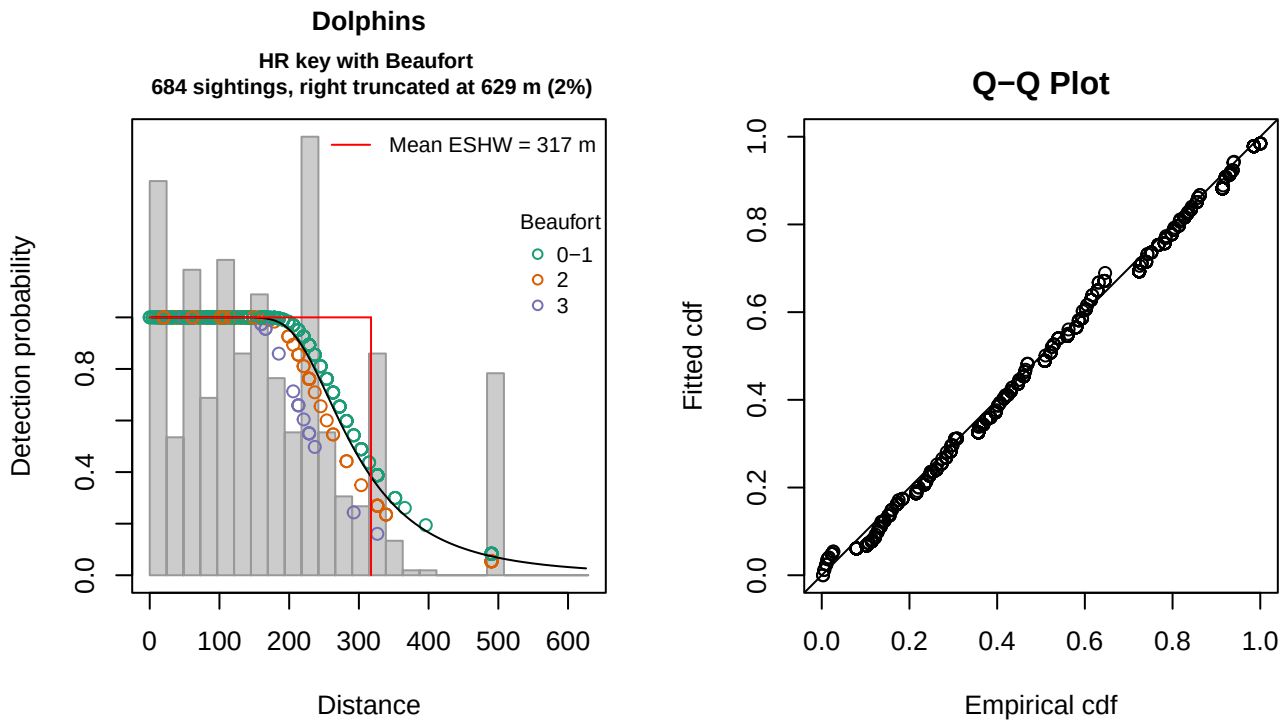

Figure 33: MATS 2002-2005 detection function and Q-Q plot showing its goodness of fit.

Statistical output for this detection function:

```
Summary for ds object
Number of observations :  684
Distance range         :  0  -  629
AIC                    :  8306.088

Detection function:
```

```
 Hazard-rate key function

Detection function parameters
Scale coefficient(s):
              estimate         se
(Intercept)  5.6213531 0.04325709
Beaufort2   -0.1046854 0.06814971
Beaufort3   -0.2421057 0.13060115

Shape coefficient(s):
            estimate         se
(Intercept) 1.449025 0.08965229

                        Estimate         SE         CV
Average p              0.5026836  0.0147185 0.02927984
N in covered region 1360.6968013 54.2106880 0.03984039

Distance sampling Cramer-von Mises test (unweighted)
Test statistic = 0.194502  p = 0.278380
```

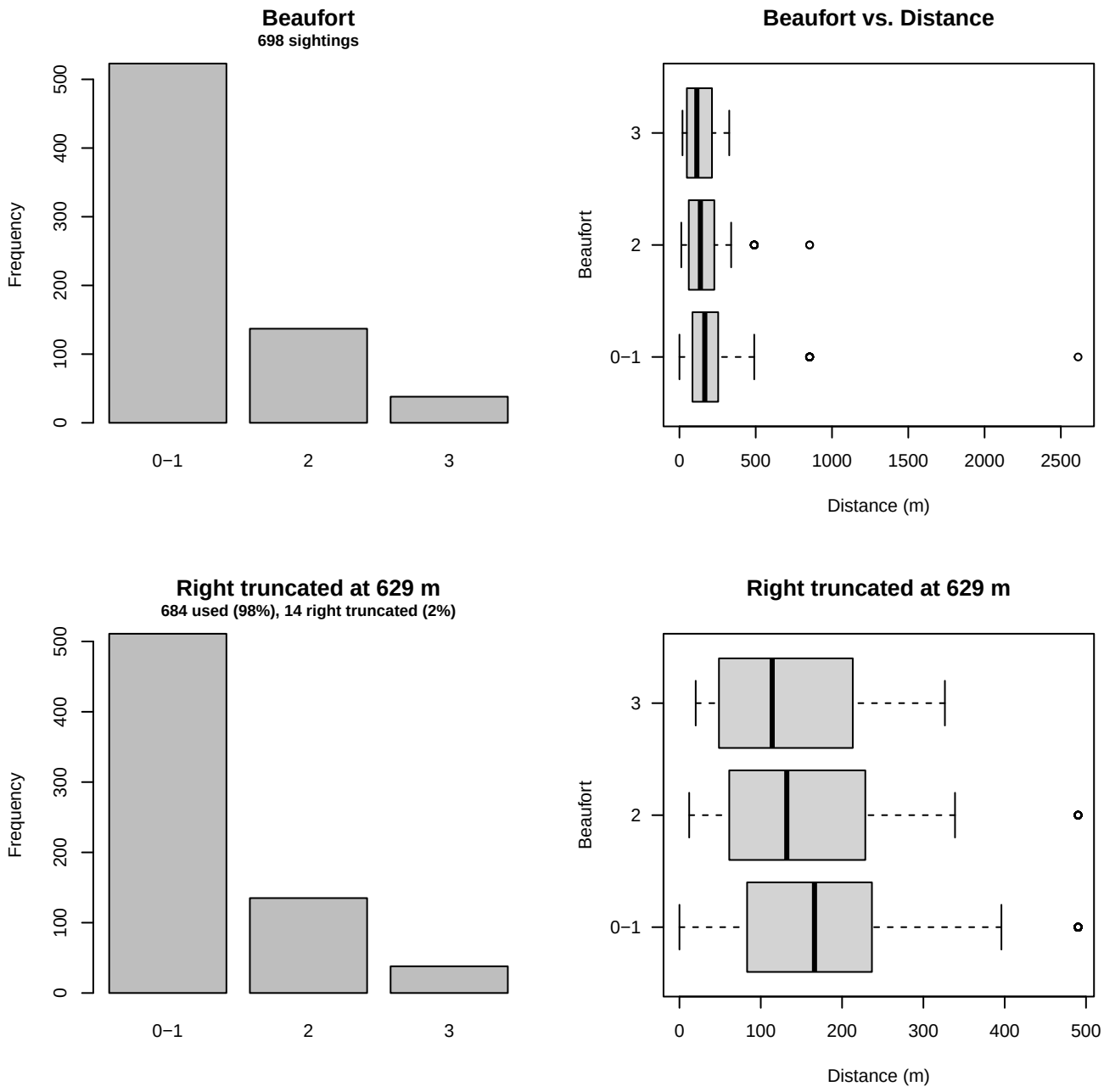

Figure 34: Distribution of the Beaufort covariate before (top row) and after (bottom row) observations were truncated to fit the MATS 2002-2005 detection function.

3.2.1.4 NARWSS 2003-2016

After right-truncating observations greater than 1367 m and left-truncating observations less than 61 m (Figure 36), we fitted the detection function to the 3073 observations that remained (Table 15). The selected detection function (Figure 35) used a hazard rate key function with Beaufort (Figure 37) and Season (Figure 38) as covariates.

Table 15: Observations used to fit the NARWSS 2003-2016 detection function.

ScientificName	n
Delphinus delphis	607
Lagenorhynchus acutus	2404
Lagenorhynchus albirostris	6
Tursiops truncatus	56
Total	**3073**

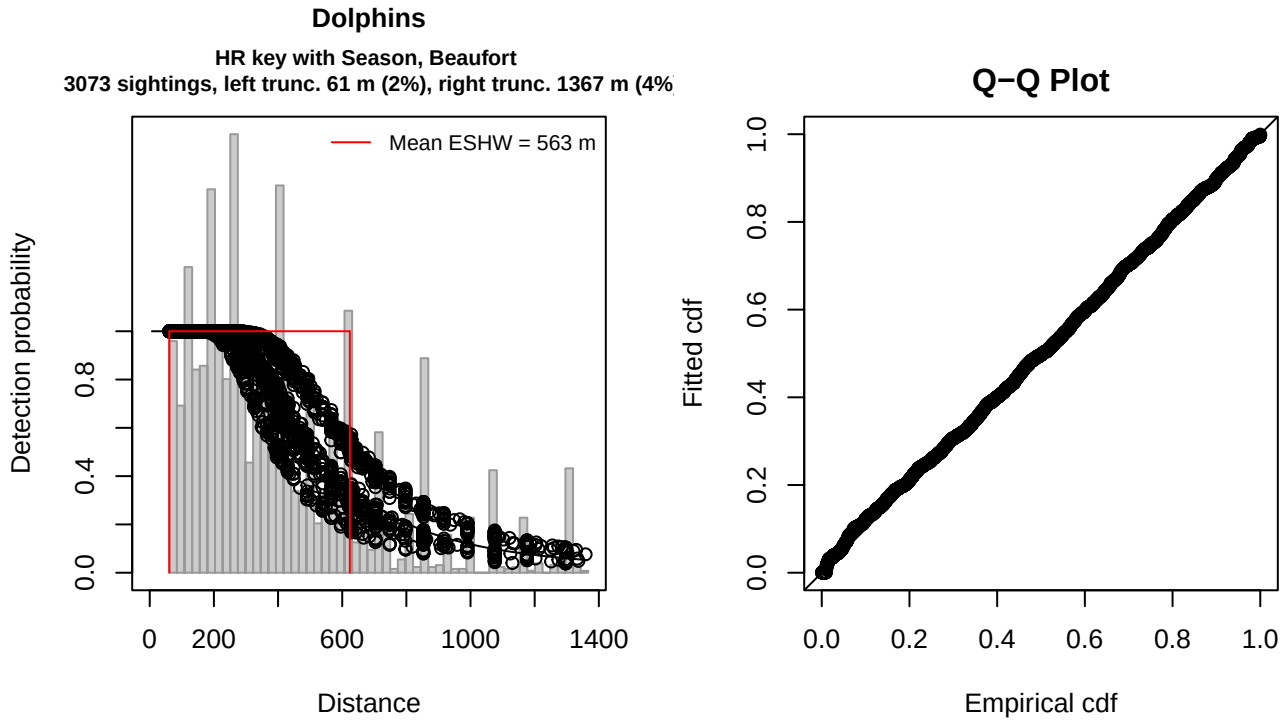

Figure 35: NARWSS 2003-2016 detection function and Q-Q plot showing its goodness of fit.

Statistical output for this detection function:

```
Summary for ds object
Number of observations :  3073
Distance range         :  61  -  1367
AIC                    :  41850.8

Detection function:
 Hazard-rate key function

Detection function parameters
Scale coefficient(s):
               estimate         se
(Intercept)   6.10469263 0.07579397
SeasonSpring  0.06689438 0.05622050
SeasonSummer  0.29278056 0.05383279
SeasonWinter -0.15259970 0.06804643
Beaufort     -0.03572691 0.02383833

Shape coefficient(s):
            estimate        se
(Intercept) 1.009361 0.0398862
```

```
                         Estimate           SE         CV
Average p              0.4196247 8.827249e-03 0.02103606
N in covered region 7323.2113220 1.845410e+02 0.02519946

Distance sampling Cramer-von Mises test (unweighted)
Test statistic = 0.246036  p = 0.193531
```

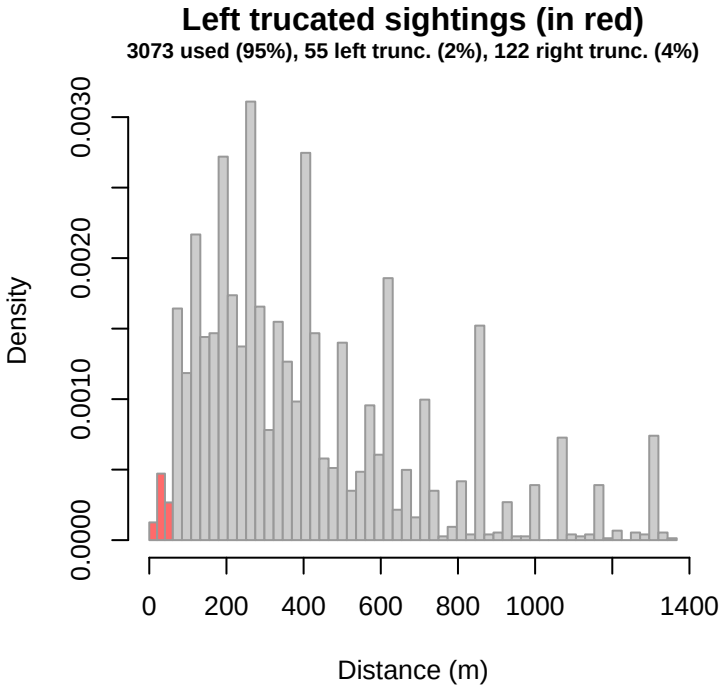

Figure 36: Density histogram of observations used to fit the NARWSS 2003-2016 detection function, with the left-most bar showing observations at distances less than 61 m, which were left-truncated and excluded from the analysis [Buckland et al. (2001)]. (This bar may be very short if there were very few left-truncated sightings, or very narrow if the left truncation distance was very small; in either case it may not appear red.)

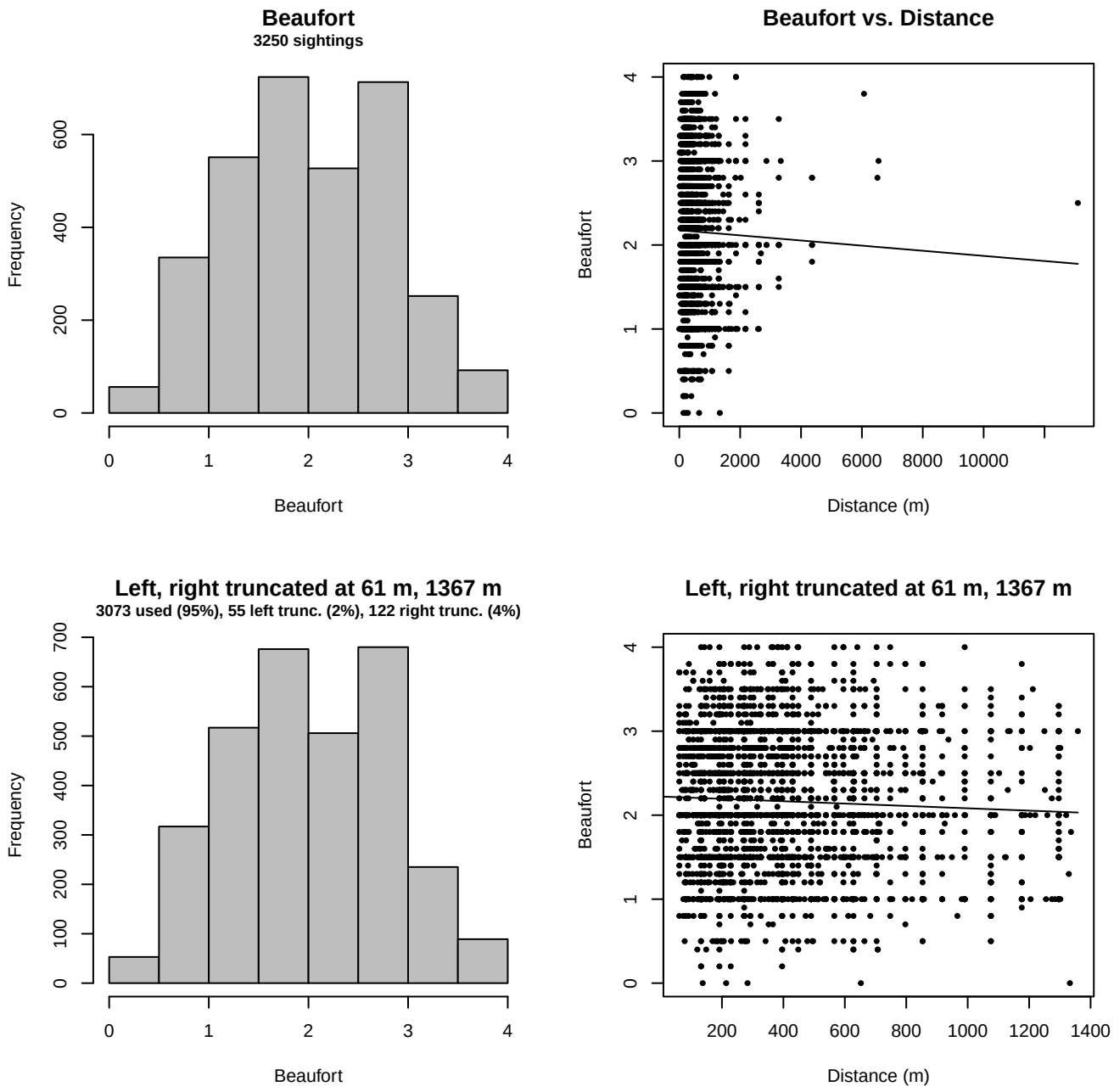

Figure 37: Distribution of the Beaufort covariate before (top row) and after (bottom row) observations were truncated to fit the NARWSS 2003-2016 detection function.

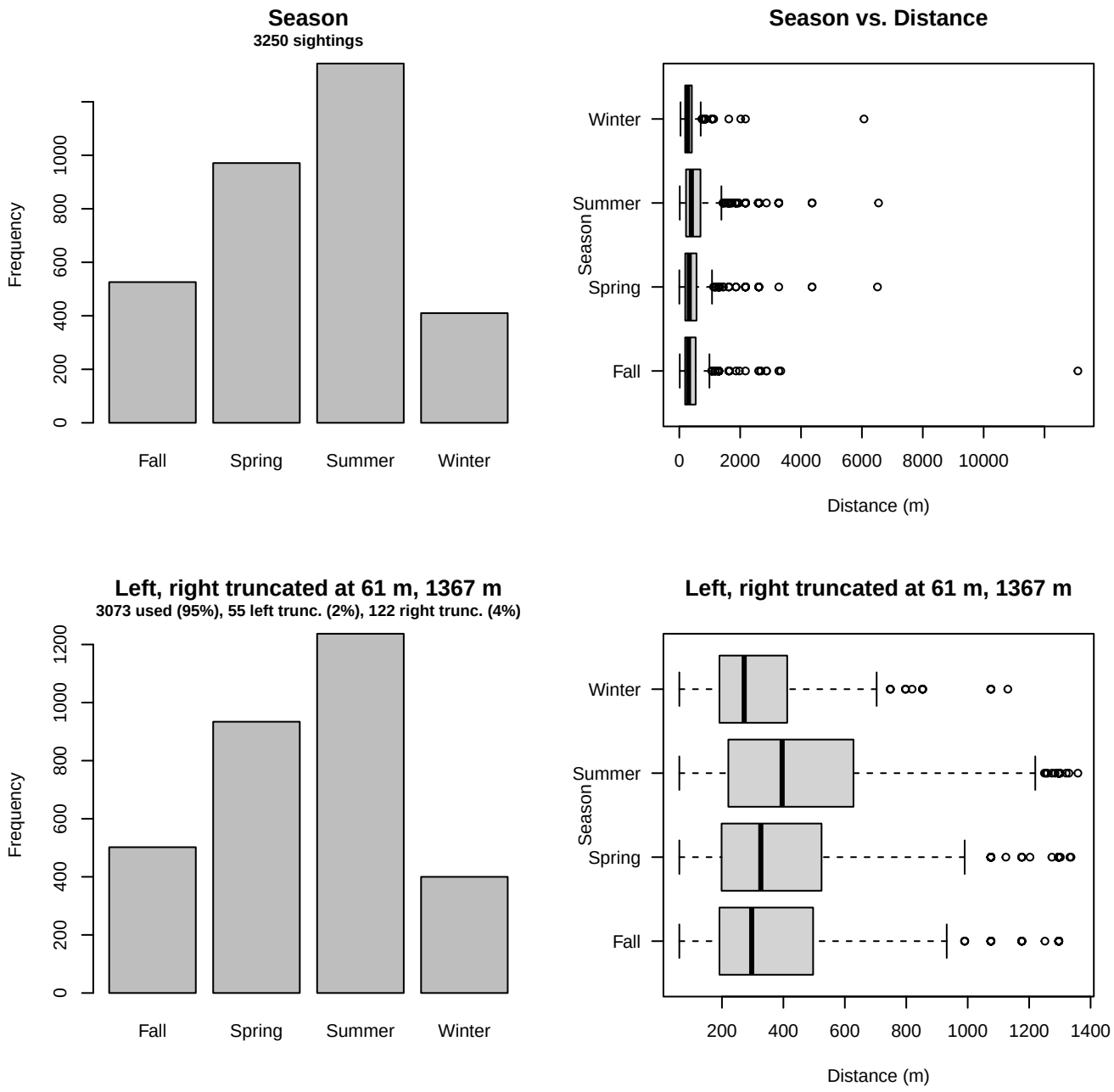

Figure 38: Distribution of the Season covariate before (top row) and after (bottom row) observations were truncated to fit the NARWSS 2003-2016 detection function.

3.2.1.5 UNCW Navy Surveys

After right-truncating observations greater than 1600 m, we fitted the detection function to the 1523 observations that remained (Table 16). The selected detection function (Figure 39) used a half normal key function with Glare (Figure 40) and Visibility (Figure 41) as covariates.

Table 16: Observations used to fit the UNCW Navy Surveys detection function.

ScientificName	n
Delphinus delphis	77
Lagenodelphis hosei	1
Stenella attenuata	2
Stenella clymene	11
Stenella coeruleoalba	19
Stenella frontalis	480
Stenella longirostris	1
Steno bredanensis	14
Tursiops truncatus	918
Total	**1523**

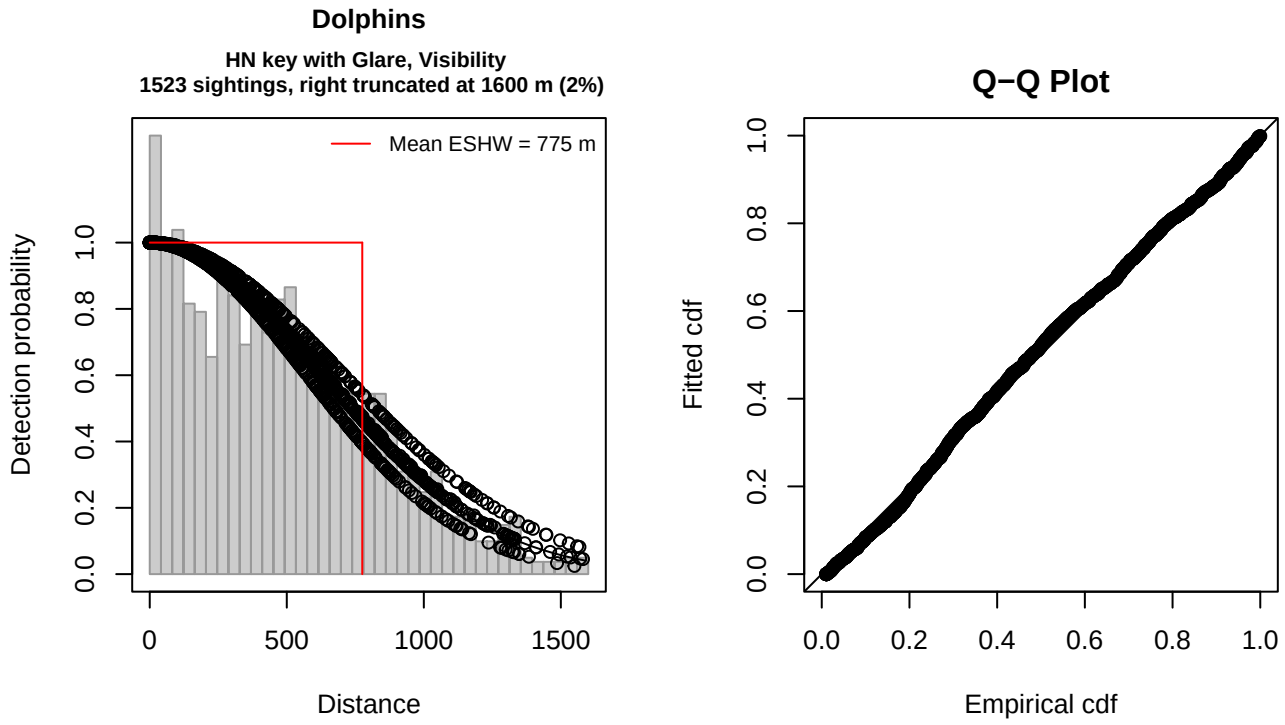

Figure 39: UNCW Navy Surveys detection function and Q-Q plot showing its goodness of fit.

Statistical output for this detection function:

```
Summary for ds object
Number of observations :  1523
Distance range         :  0  -  1600
AIC                    :  21665.78

Detection function:
 Half-normal key function

Detection function parameters
Scale coefficient(s):
                          estimate         se
(Intercept)             6.55223233 0.04798577
GlareNone, 0-25%, Unk. -0.10934970 0.05247015
VisibilityHalf         -0.09759271 0.04601702
```

```
                        Estimate          SE         CV
Average p               0.4827398  0.01003395 0.02078542
N in covered region 3154.9084328 87.71221948 0.02780183

Distance sampling Cramer-von Mises test (unweighted)
Test statistic = 0.331909  p = 0.110182
```

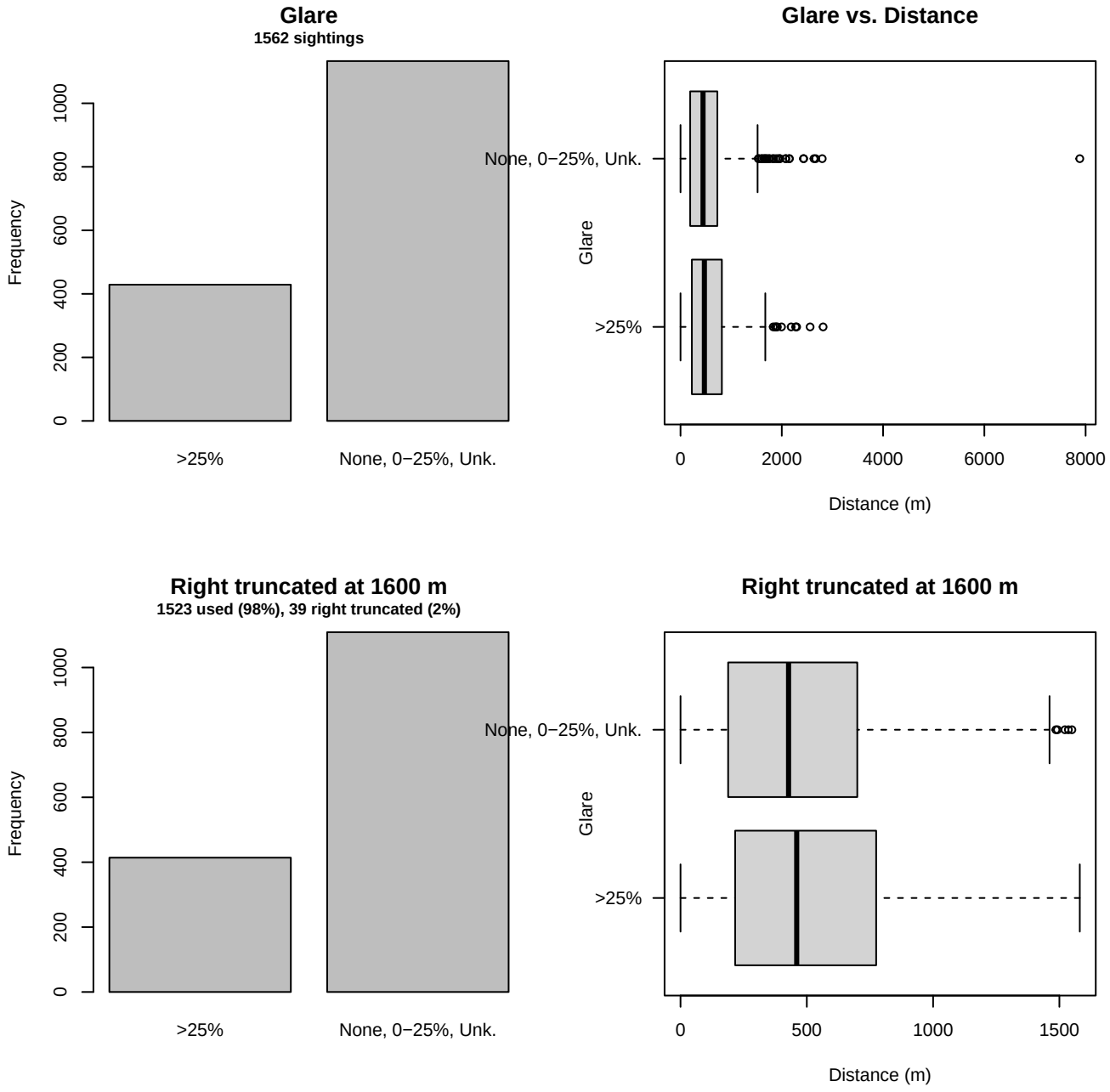

Figure 40: Distribution of the Glare covariate before (top row) and after (bottom row) observations were truncated to fit the UNCW Navy Surveys detection function.

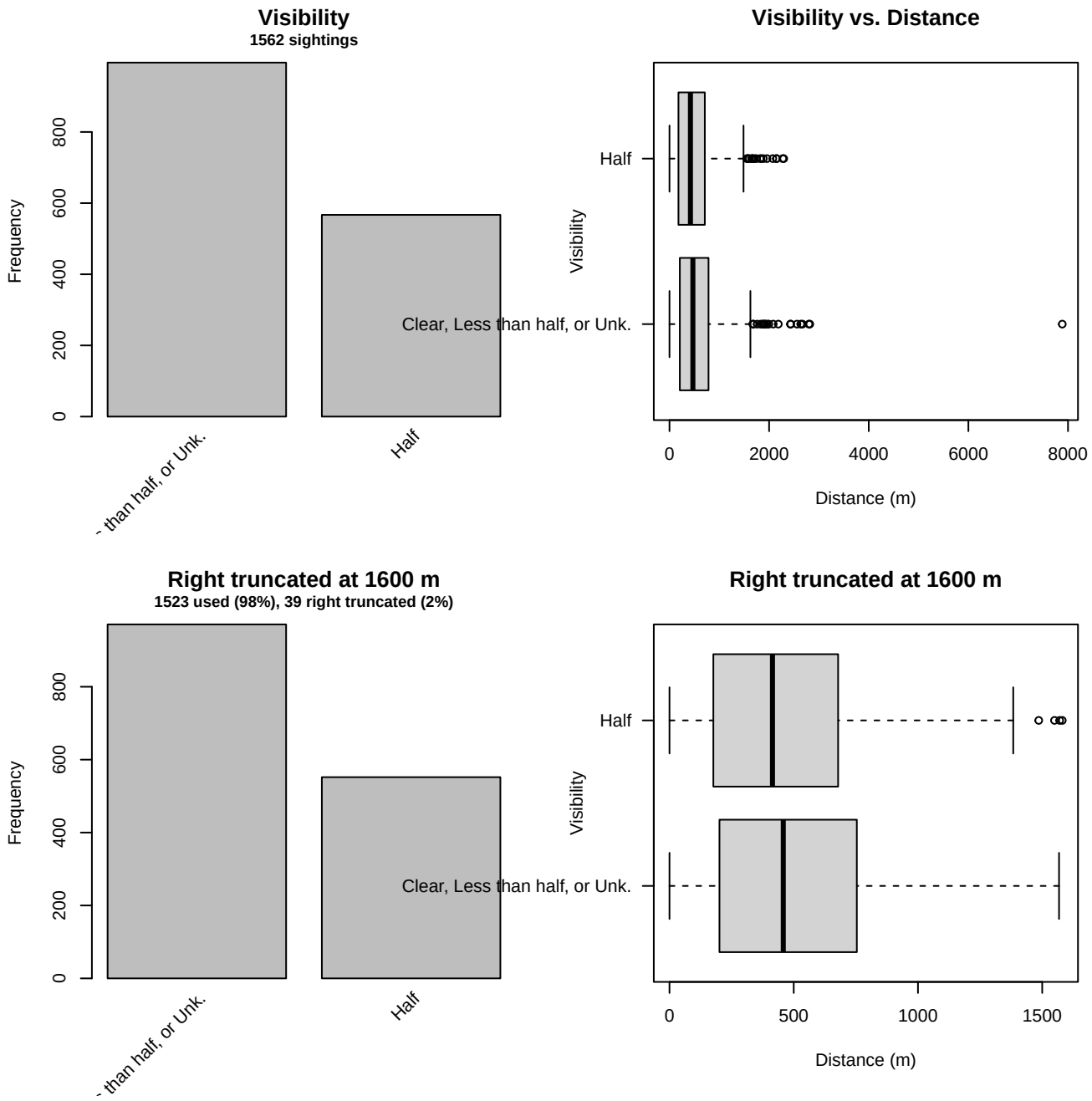

Figure 41: Distribution of the Visibility covariate before (top row) and after (bottom row) observations were truncated to fit the UNCW Navy Surveys detection function.

3.2.1.6 UNCW Right Whale Surveys

After right-truncating observations greater than 528 m and left-truncating observations less than 54 m (Figure 43), we fitted the detection function to the 1821 observations that remained (Table 17). The selected detection function (Figure 42) used a hazard rate key function with no covariates.

Table 17: Observations used to fit the UNCW Right Whale Surveys detection function.

ScientificName	n
Delphinus delphis	26
Stenella frontalis	4
Tursiops truncatus	1791
Total	**1821**

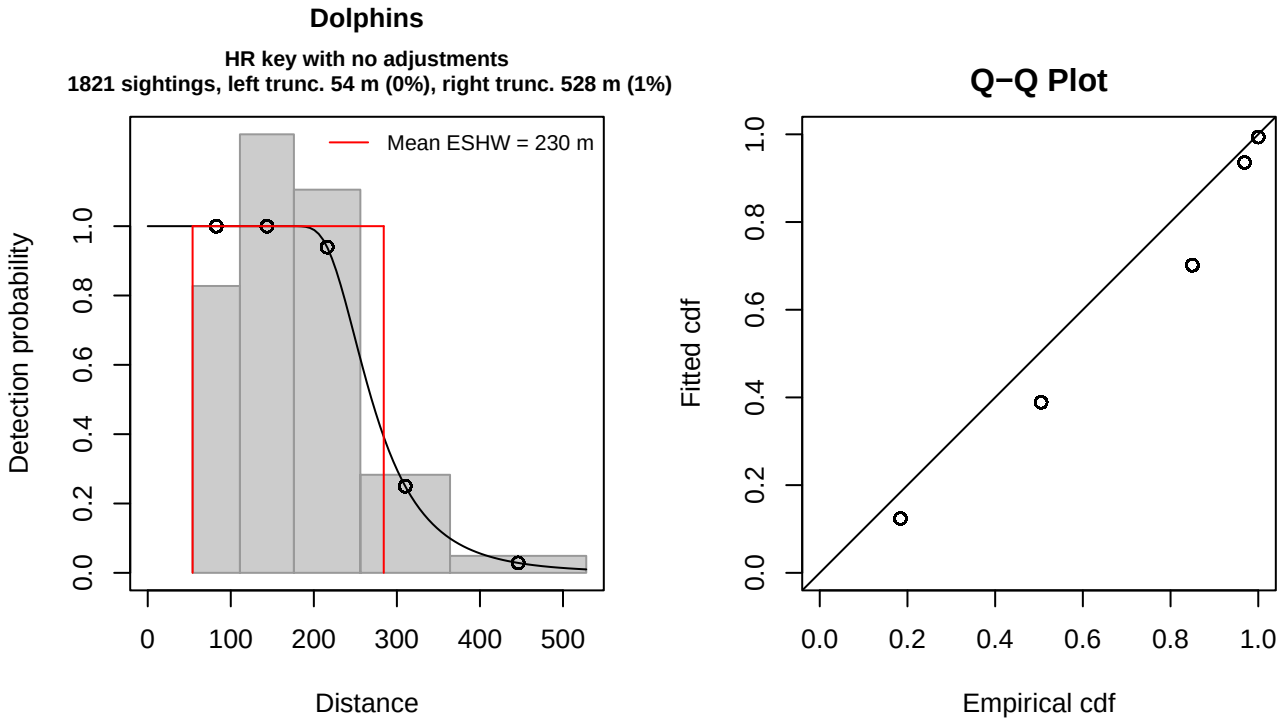

Figure 42: UNCW Right Whale Surveys detection function and Q-Q plot showing its goodness of fit.

Statistical output for this detection function:

```
Summary for ds object
Number of observations :  1821
Distance range         :  54  -  528
AIC                    :  5176.116

Detection function:
 Hazard-rate key function

Detection function parameters
Scale coefficient(s):
            estimate         se
(Intercept) 5.538954 0.02098751

Shape coefficient(s):
            estimate         se
(Intercept) 1.841299 0.06464608

                         Estimate           SE         CV
Average p                0.4855453  0.009233858 0.01901750
N in covered region 3750.4226341 95.188173832 0.02538065
```

```
Distance sampling Cramer-von Mises test (unweighted)
Test statistic = 14.468539  p = 0.010416
```

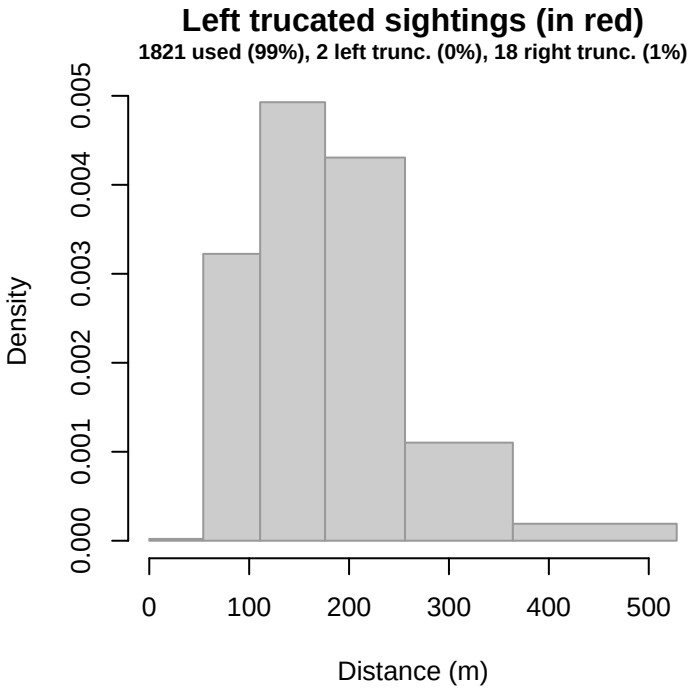

Figure 43: Density histogram of observations used to fit the UNCW Right Whale Surveys detection function, with the left-most bar showing observations at distances less than 54 m, which were left-truncated and excluded from the analysis [Buckland et al. (2001)]. (This bar may be very short if there were very few left-truncated sightings, or very narrow if the left truncation distance was very small; in either case it may not appear red.)

3.2.1.7 UNCW Early Surveys

After right-truncating observations greater than 333 m and left-truncating observations less than 14 m (Figure 45), we fitted the detection function to the 349 observations that remained (Table 18). The selected detection function (Figure 44) used a half normal key function with Beaufort (Figure 46) as a covariate.

Table 18: Observations used to fit the UNCW Early Surveys detection function.

ScientificName	n
Delphinus delphis	5
Stenella frontalis	1
Tursiops truncatus	343
Total	**349**

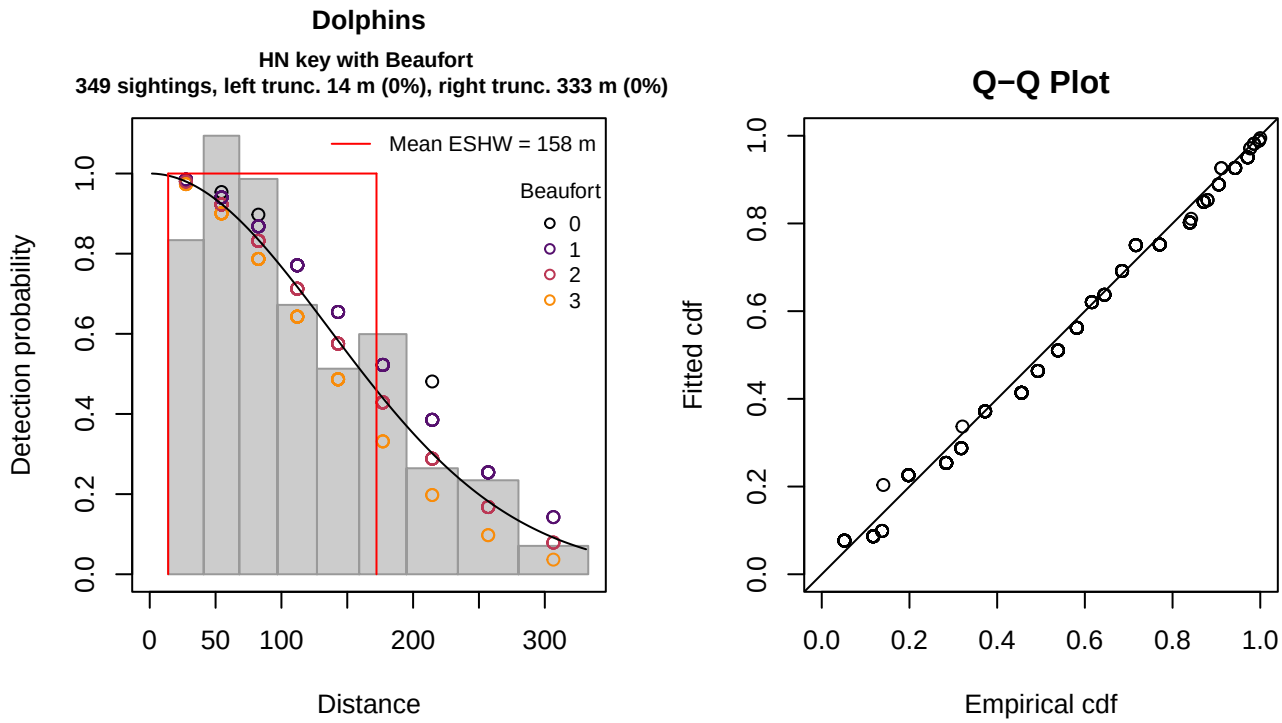

Figure 44: UNCW Early Surveys detection function and Q-Q plot showing its goodness of fit.

Statistical output for this detection function:

```
Summary for ds object
Number of observations :  349
Distance range         :  14  -  333
AIC                    :  1464.597

Detection function:
 Half-normal key function

Detection function parameters
Scale coefficient(s):
             estimate         se
(Intercept)  5.1778911 0.14575211
Beaufort    -0.1325498 0.07066838

                       Estimate          SE         CV
Average p              0.4915207  0.02352103 0.04785360
N in covered region 710.0413079 43.53534195 0.06131382

Distance sampling Cramer-von Mises test (unweighted)
Test statistic = 0.278162  p = 0.155953
```

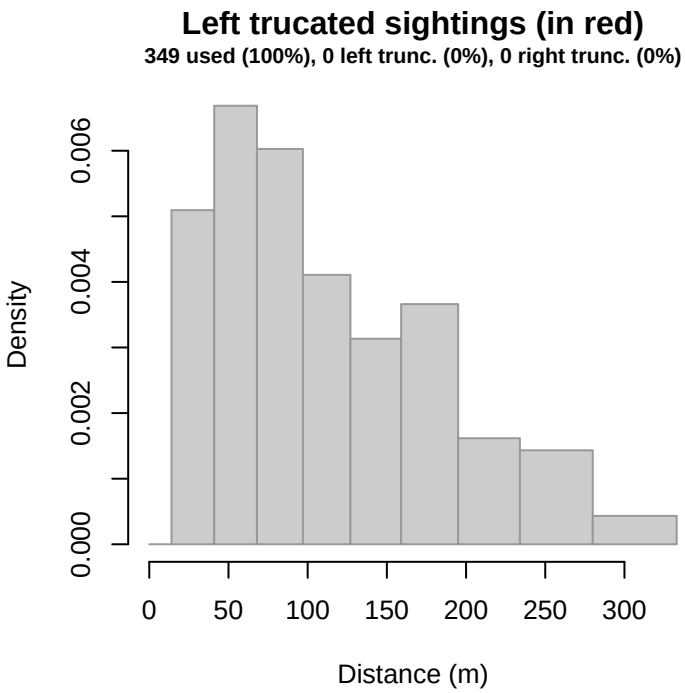

Figure 45: Density histogram of observations used to fit the UNCW Early Surveys detection function, with the left-most bar showing observations at distances less than 14 m, which were left-truncated and excluded from the analysis [Buckland et al. (2001)]. (This bar may be very short if there were very few left-truncated sightings, or very narrow if the left truncation distance was very small; in either case it may not appear red.)

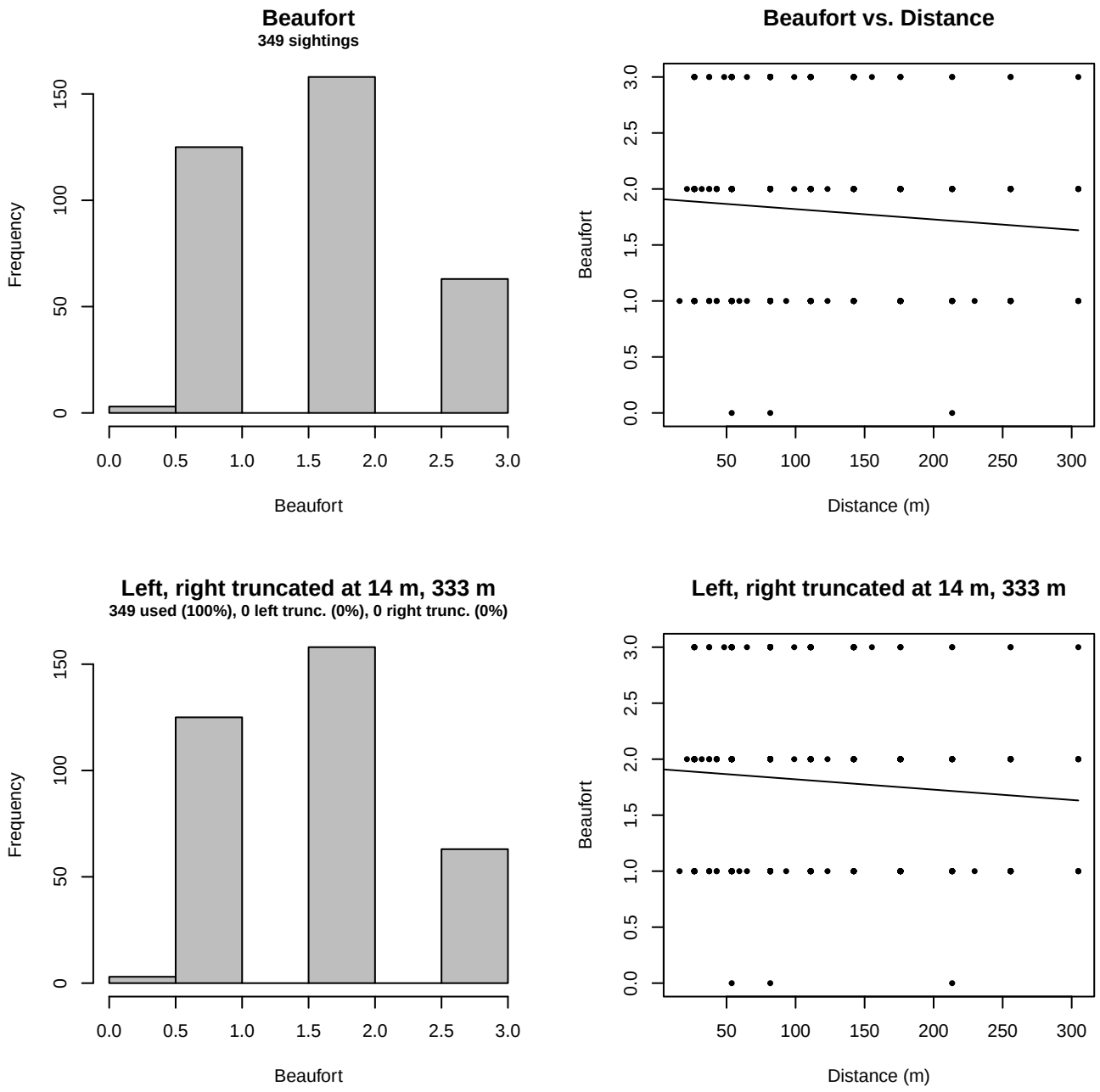

Figure 46: Distribution of the Beaufort covariate before (top row) and after (bottom row) observations were truncated to fit the UNCW Early Surveys detection function.

3.2.1.8 VAMSC

After right-truncating observations greater than 1000 m, we fitted the detection function to the 303 observations that remained (Table 19). The selected detection function (Figure 47) used a hazard rate key function with no covariates.

Table 19: Observations used to fit the VAMSC detection function.

ScientificName	n
Delphinus delphis	30
Stenella frontalis	4
Tursiops truncatus	269
Total	**303**

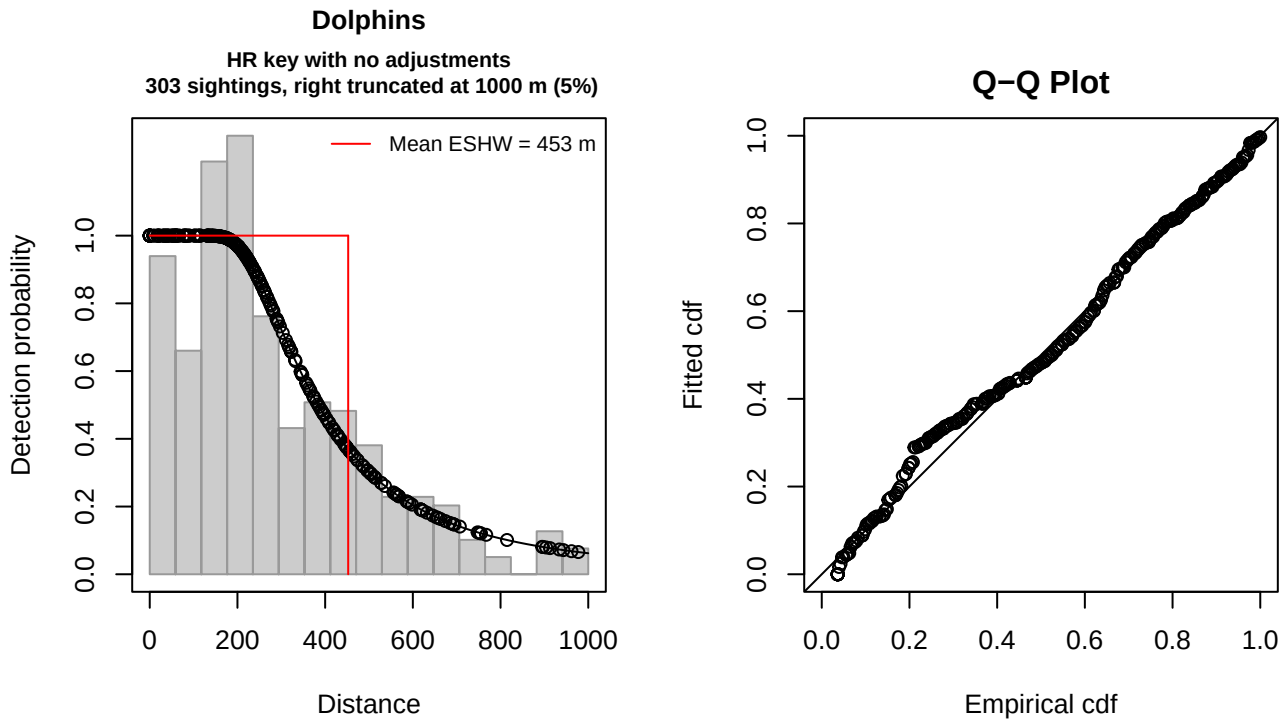

Figure 47: VAMSC detection function and Q-Q plot showing its goodness of fit.

Statistical output for this detection function:

```
Summary for ds object
Number of observations :  303
Distance range         :  0  -  1000
AIC                    :  3992.632

Detection function:
 Hazard-rate key function

Detection function parameters
Scale coefficient(s):
            estimate        se
(Intercept) 5.803823 0.1019737

Shape coefficient(s):
             estimate        se
(Intercept) 0.9119562 0.1438459

                       Estimate          SE         CV
Average p             0.4525805  0.02853931 0.06305908
N in covered region 669.4942067 50.91287837 0.07604678

Distance sampling Cramer-von Mises test (unweighted)
Test statistic = 0.212402  p = 0.244680
```

3.2.1.9 HDR

After right-truncating observations greater than 1500 m and left-truncating observations less than 111 m (Figure 49), we fitted the detection function to the 203 observations that remained (Table 20). The selected detection function (Figure 48) used a hazard rate key function with Season (Figure 50) and Swell (Figure 51) as covariates.

Table 20: Observations used to fit the HDR detection function.

ScientificName	n
Delphinus delphis	47
Stenella coeruleoalba	14
Stenella frontalis	19
Tursiops truncatus	123
Total	**203**

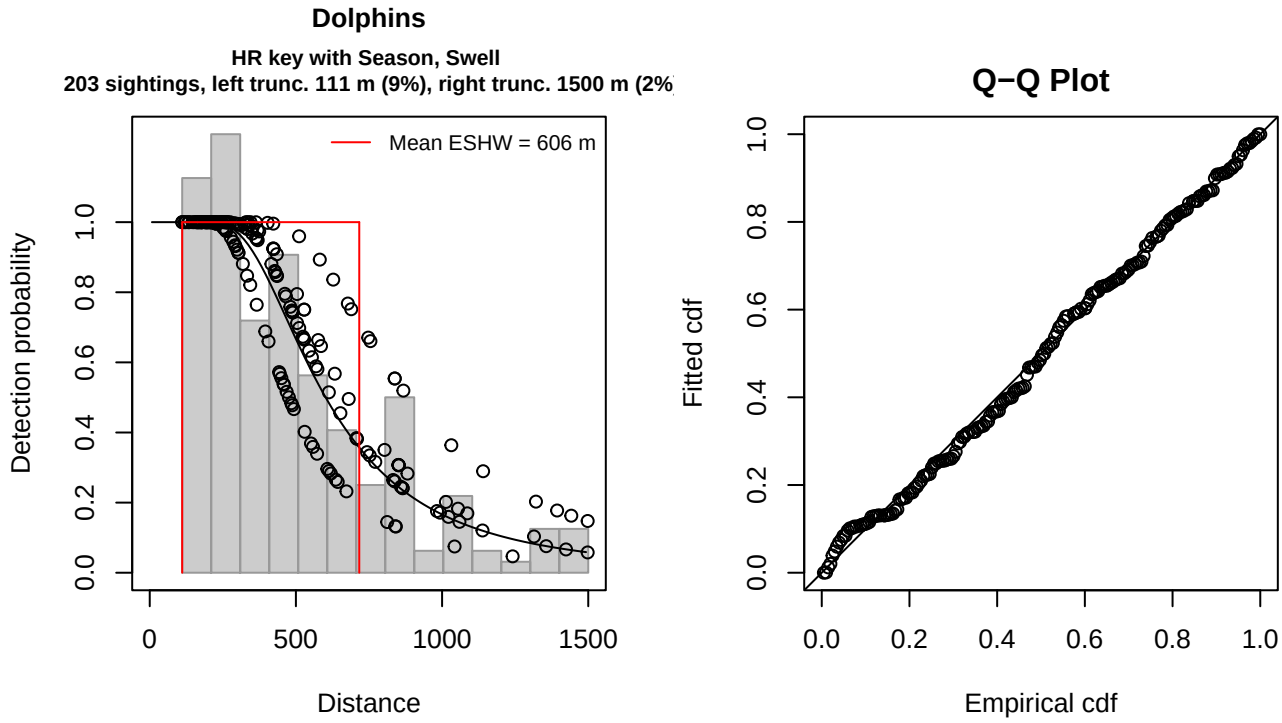

Figure 48: HDR detection function and Q-Q plot showing its goodness of fit.

Statistical output for this detection function:

```
Summary for ds object
Number of observations :  203
Distance range         :  111  -  1500
AIC                    :  2802.845

Detection function:
 Hazard-rate key function

Detection function parameters
Scale coefficient(s):
                       estimate        se
(Intercept)           6.3015171 0.1328018
SeasonWinter, Spring -0.2671651 0.1458664
Swell3-4              0.3527933 0.1530784

Shape coefficient(s):
            estimate        se
(Intercept) 1.026101 0.1620057

                     Estimate          SE         CV
```

```
Average p             0.419883  0.03654238 0.08702991
N in covered region 483.467993 49.56848062 0.10252691

Distance sampling Cramer-von Mises test (unweighted)
Test statistic = 0.059652  p = 0.816171
```

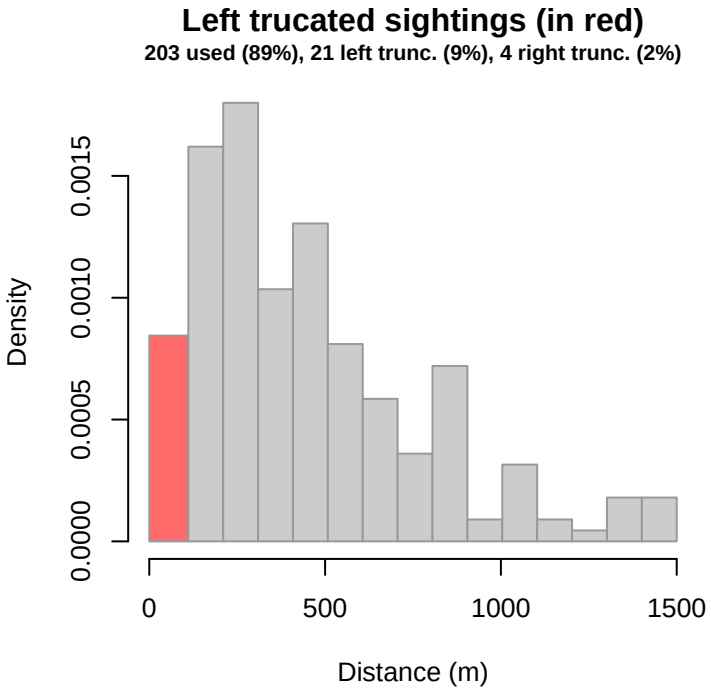

Figure 49: Density histogram of observations used to fit the HDR detection function, with the left-most bar showing observations at distances less than 111 m, which were left-truncated and excluded from the analysis [Buckland et al. (2001)]. (This bar may be very short if there were very few left-truncated sightings, or very narrow if the left truncation distance was very small; in either case it may not appear red.)

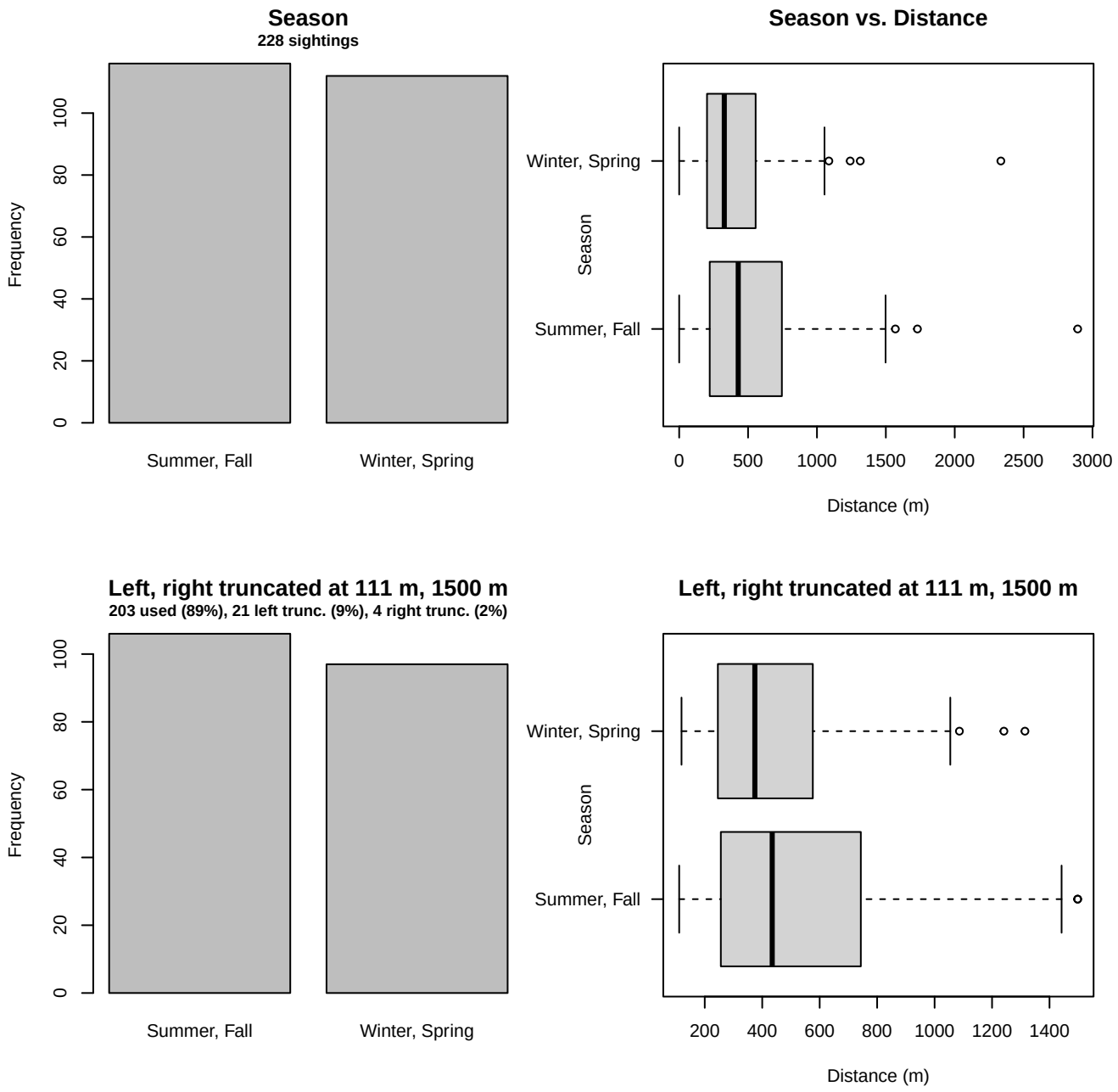

Figure 50: Distribution of the Season covariate before (top row) and after (bottom row) observations were truncated to fit the HDR detection function.

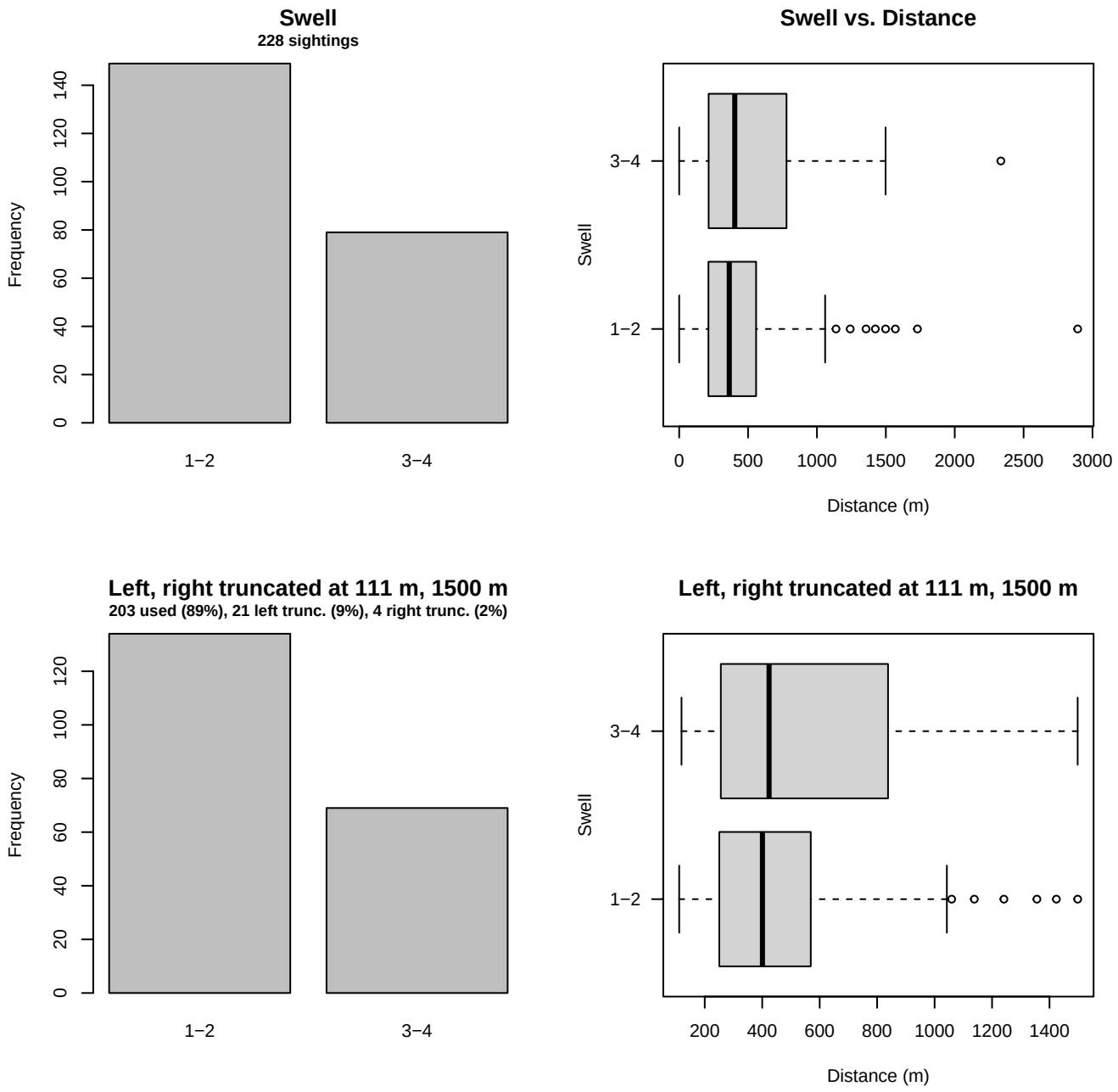

Figure 51: Distribution of the Swell covariate before (top row) and after (bottom row) observations were truncated to fit the HDR detection function.

3.2.2 Shipboard Surveys

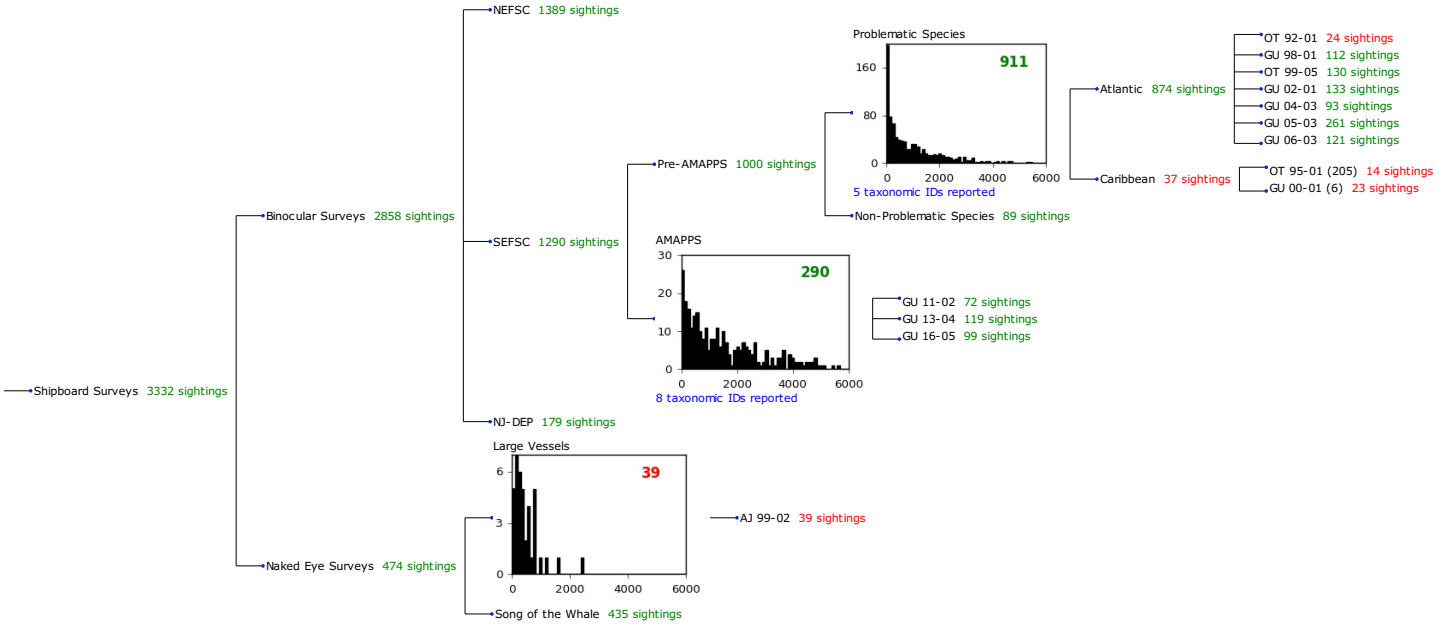

Figure 52: Detection hierarchy for shipboard surveys, showing how they were pooled during detectability modeling, for detection functions that pooled multiple taxa but could not use a taxonomic covariate to account for differences between them. Each histogram represents a detection function and summarizes the perpendicular distances of observations that were pooled to fit it, prior to truncation. Observation counts, also prior to truncation, are shown in green when they met the recommendation of Buckland et al. (2001) that detection functions utilize at least 60 sightings, and red otherwise. For rare taxa, it was not always possible to meet this recommendation, yielding higher statistical uncertainty. During the spatial modeling stage of the analysis, effective strip widths were computed for each survey using the closest detection function above it in the hierarchy (i.e. moving from right to left in the figure). Surveys that do not have a detection function above them in this figure were either addressed by a detection function presented in a different section of this report, or were omitted from the analysis.

3.2.2.1 SEFSC Pre-AMAPPS Problematic Species

After right-truncating observations greater than 4000 m and left-truncating observations less than 200 m (Figure 54), we fitted the detection function to the 616 observations that remained (Table 21). The selected detection function (Figure 53) used a hazard rate key function with Beaufort (Figure 55) and VesselName (Figure 56) as covariates.

Table 21: Observations used to fit the SEFSC Pre-AMAPPS Problematic Species detection function.

ScientificName	n
Delphinus delphis	34
Stenella attenuata	14
Stenella frontalis	262
Steno bredanensis	4
Tursiops truncatus	302
Total	**616**

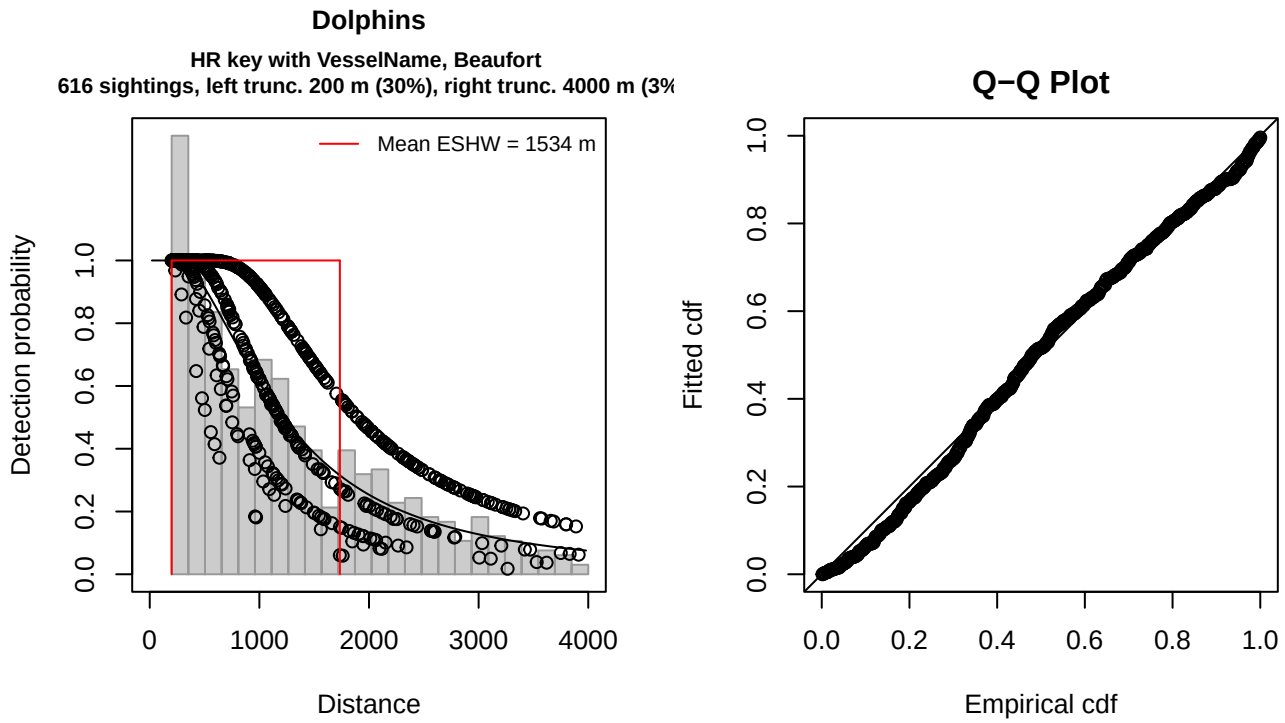

Figure 53: SEFSC Pre-AMAPPS Problematic Species detection function and Q-Q plot showing its goodness of fit.

Statistical output for this detection function:

```
Summary for ds object
Number of observations :  616
Distance range         :  200  -  4000
AIC                    :  9753.004

Detection function:
 Hazard-rate key function

Detection function parameters
Scale coefficient(s):
                     estimate         se
(Intercept)          7.3628462 0.09422017
VesselNameOregon II -0.4793018 0.17480366
Beaufort3           -0.4668391 0.14302976
Beaufort4-5         -0.8137669 0.16103824

Shape coefficient(s):
            estimate         se
(Intercept) 0.689867 0.09372714

                         Estimate           SE         CV
Average p               0.3555714   0.02671315 0.07512737
N in covered region 1732.4228173 142.52885613 0.08227140

Distance sampling Cramer-von Mises test (unweighted)
Test statistic = 0.313292  p = 0.124062
```

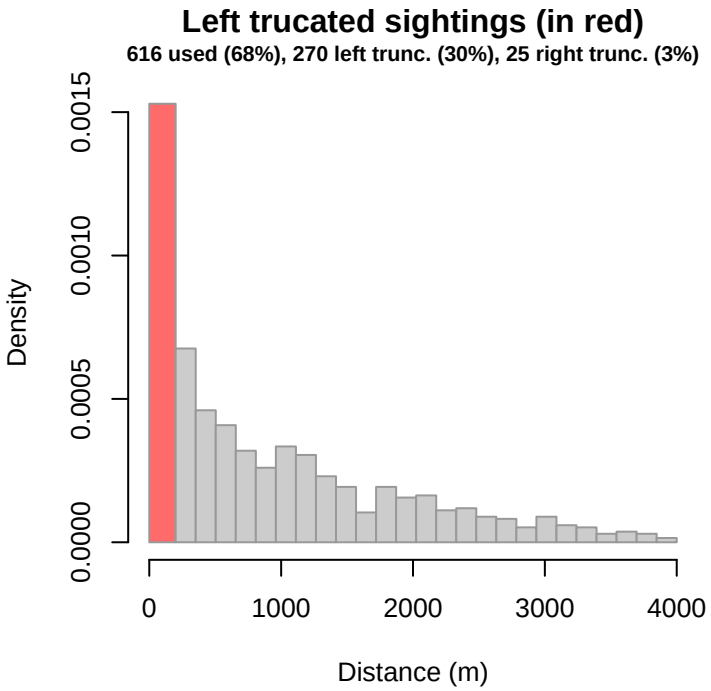

Figure 54: Density histogram of observations used to fit the SEFSC Pre-AMAPPS Problematic Species detection function, with the left-most bar showing observations at distances less than 200 m, which were left-truncated and not used to fit the detection function. (This bar may be very short if there were very few left-truncated sightings, or very narrow if the left truncation distance was very small; in either case it may not appear red.) These were excluded because they formed a problematic "spike" in detections close to the trackline, suggesting that animals approached the vessel (e.g. to bow-ride) prior to being detected. To address this, we fitted the detection function to the observations beyond the spike and assumed that within it, detection probability was 1, effectively treating it like a strip transect. We then added the left-truncated observations back into the analysis as if they occurred in this strip. This treatment may have resulted in an underestimation of detection probability.

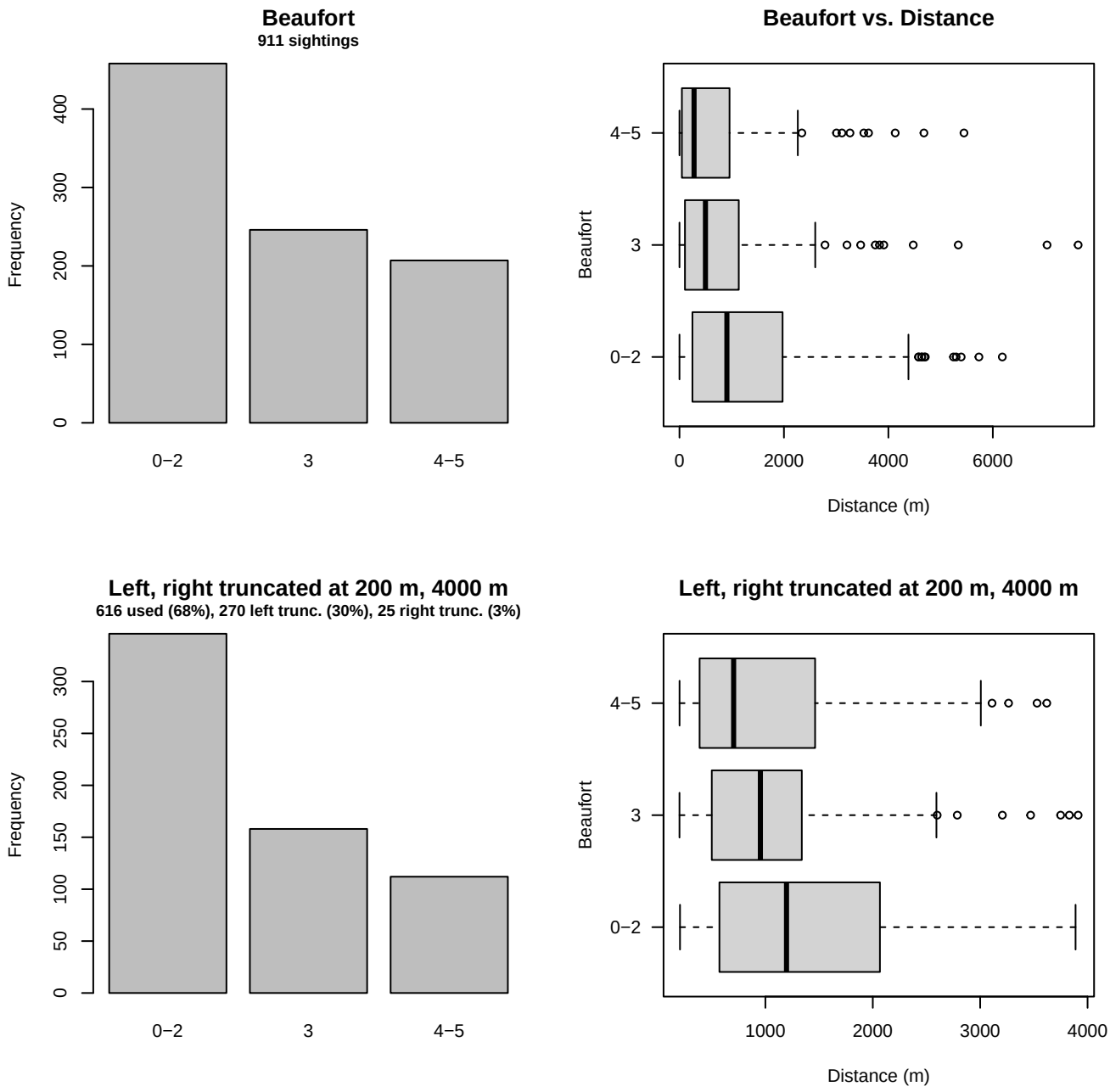

Figure 55: Distribution of the Beaufort covariate before (top row) and after (bottom row) observations were truncated to fit the SEFSC Pre-AMAPPS Problematic Species detection function.

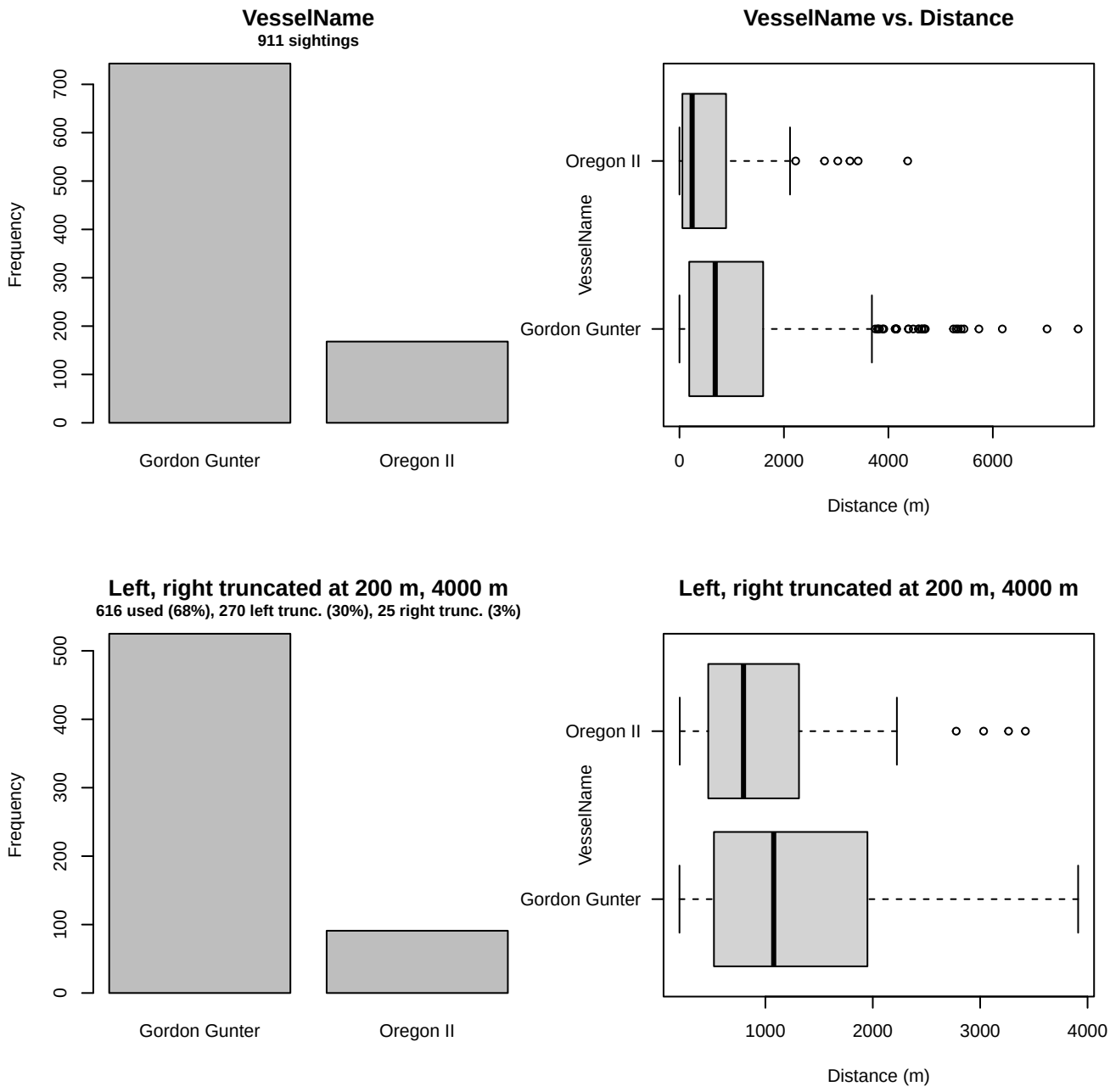

Figure 56: Distribution of the VesselName covariate before (top row) and after (bottom row) observations were truncated to fit the SEFSC Pre-AMAPPS Problematic Species detection function.

3.2.2.2 SEFSC AMAPPS

After right-truncating observations greater than 5000 m, we fitted the detection function to the 284 observations that remained (Table 22). The selected detection function (Figure 57) used a hazard rate key function with Beaufort (Figure 58) as a covariate.

Table 22: Observations used to fit the SEFSC AMAPPS detection function.

ScientificName	n
Delphinus delphis	2
Stenella attenuata	10
Stenella clymene	3
Stenella coeruleoalba	11
Stenella frontalis	84
Stenella longirostris	1
Steno bredanensis	2
Tursiops truncatus	171
Total	**284**

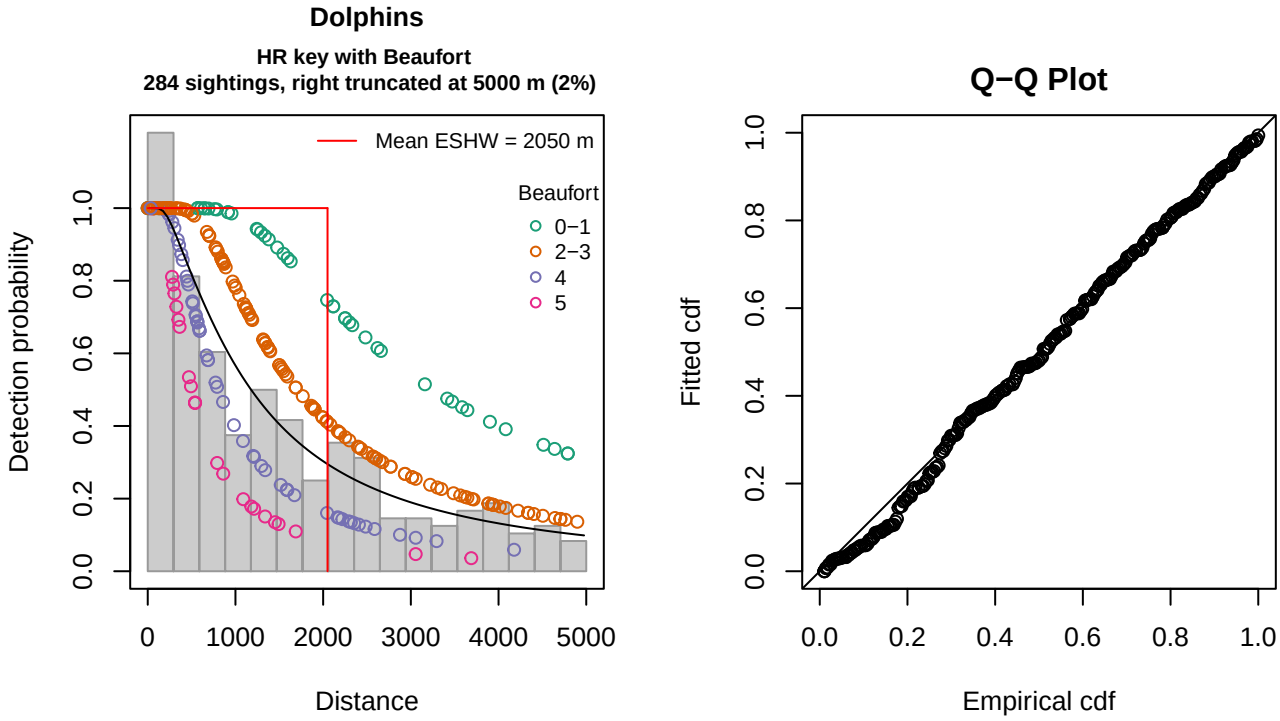

Figure 57: SEFSC AMAPPS detection function and Q-Q plot showing its goodness of fit.

Statistical output for this detection function:

```
Summary for ds object
Number of observations :  284
Distance range         :  0  -  5000
AIC                    :  4678.464

Detection function:
 Hazard-rate key function

Detection function parameters
Scale coefficient(s):
              estimate        se
(Intercept)  7.8386611 0.3487749
Beaufort2-3 -0.6450433 0.3816484
Beaufort4   -1.3990617 0.4441169
Beaufort5   -1.8689041 0.5186901
```

```
Shape coefficient(s):
             estimate        se
(Intercept) 0.3878689 0.1380351

                        Estimate           SE        CV
Average p              0.3478259   0.03965009 0.1139941
N in covered region 816.5004271 101.68622285 0.1245391

Distance sampling Cramer-von Mises test (unweighted)
Test statistic = 0.107898  p = 0.547527
```

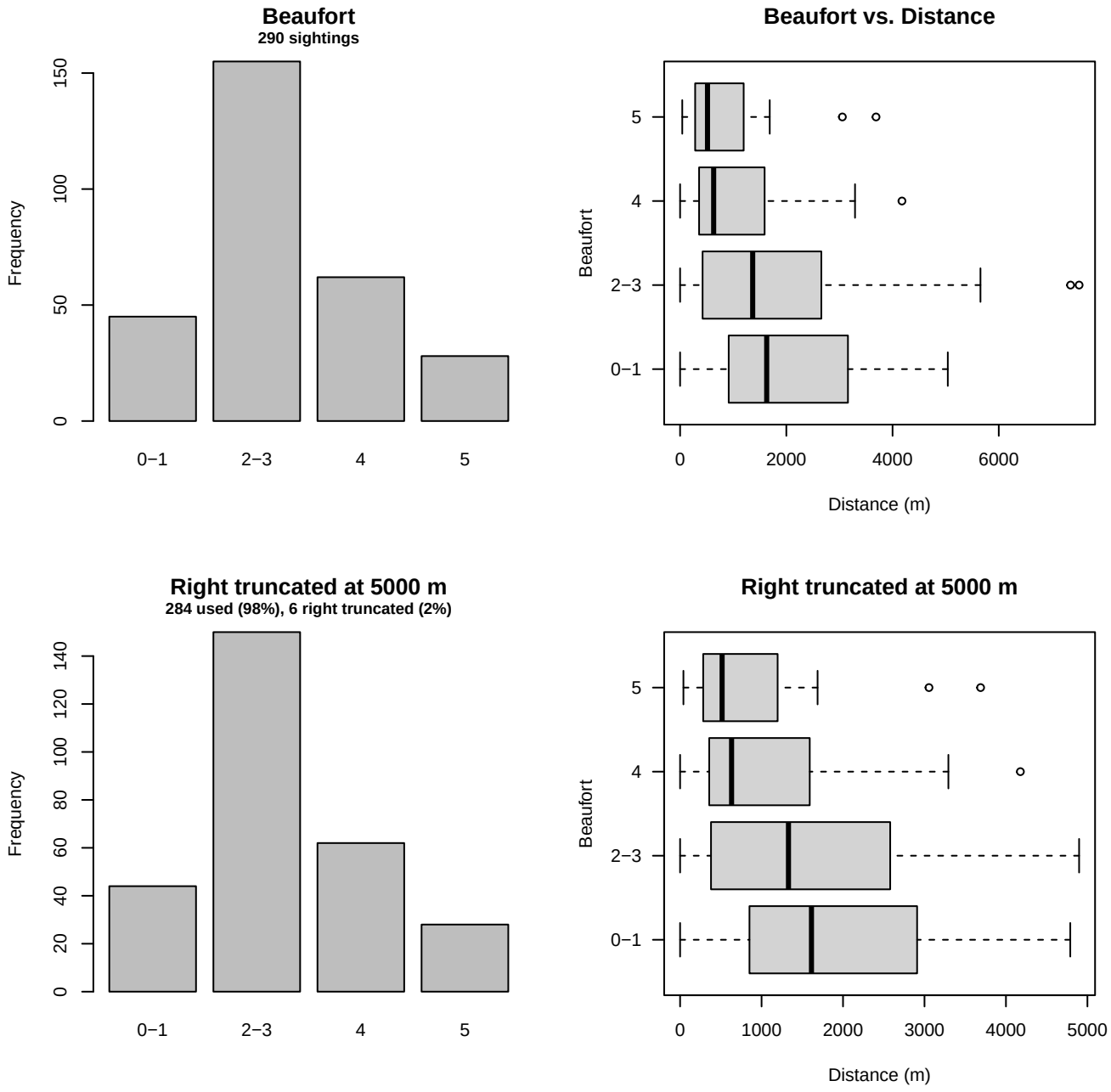

Figure 58: Distribution of the Beaufort covariate before (top row) and after (bottom row) observations were truncated to fit the SEFSC AMAPPS detection function.

3.2.2.3 Large Vessels

After right-truncating observations greater than 1100 m, we fitted the detection function to the 36 observations that remained (Table 23). The selected detection function (Figure 59) used a half normal key function with no covariates.

Table 23: Observations used to fit the Large Vessels detection function.

ScientificName	n
Lagenorhynchus acutus	36
Total	**36**

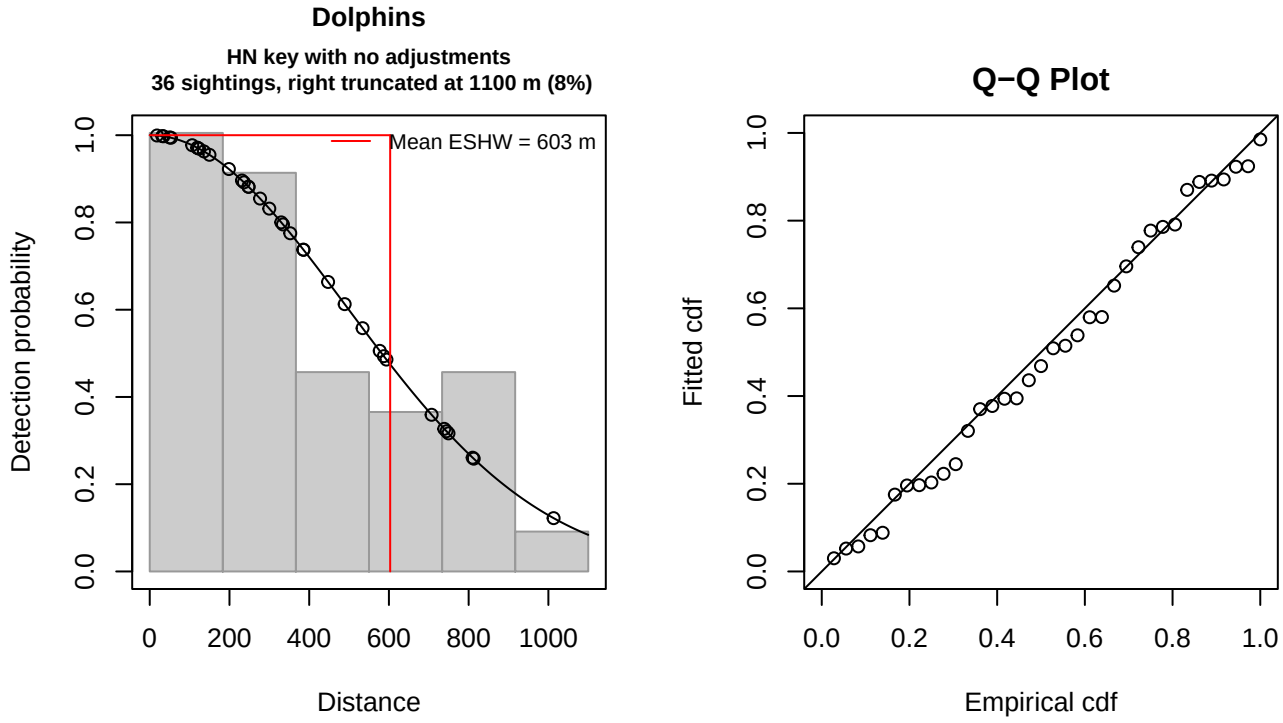

Figure 59: Large Vessels detection function and Q-Q plot showing its goodness of fit.

Statistical output for this detection function:

```
Summary for ds object
Number of observations :  36
Distance range         :  0  -  1100
AIC                    :  493.4472

Detection function:
 Half-normal key function

Detection function parameters
Scale coefficient(s):
            estimate        se
(Intercept) 6.202683 0.1646341

                     Estimate          SE        CV
Average p            0.5483057  0.07646146 0.1394504
N in covered region 65.6568085 11.74385160 0.1788672

Distance sampling Cramer-von Mises test (unweighted)
Test statistic = 0.026241  p = 0.986825
```

4 Bias Corrections

Density surface modeling methodology uses *distance sampling* (Buckland et al. 2001) to model the probability that an observer on a line transect survey will detect an animal given the perpendicular distance to it from the transect line. Distance sampling assumes that detection probability is 1 when perpendicular distance is 0. When this assumption is not met, detection probability is biased high, leading to an underestimation of density and abundance. This is known as the $g_0 < 1$ problem, where g_0 refers to the detection probability at distance 0. Modelers often try to address this problem by estimating g_0 empirically and dividing it into estimated density or abundance, thereby correcting those estimates to account for the animals that were presumed missed.

Two important sources of bias for visual surveys are known as *availability bias*, in which an animal was present on the transect line but impossible to detect, e.g. because it was under water, and *perception bias*, in which an animal was present and available but not noticed, e.g. because of its small size or cryptic coloration or behavior (Marsh and Sinclair 1989). Modelers often estimate the influence of these two sources of bias on detection probability independently, yielding two estimates of g_0, hereafter referred to as g_{0A} and g_{0P}, and multiply them together to obtain a final, combined estimate: $g_0 = g_{0A}.g_{0P}$.

Our overall approach was to perform this correction on a per-observation basis, to have the flexibility to account for many factors such as platform type, surveyor institution, group size, group composition (e.g. singleton, mother-calf pair, or surface active group), and geographic location (e.g. feeding grounds vs. calving grounds). The level of complexity of the corrections varied by species according to the amount of information available, with North Atlantic right whale having the most elaborate corrections, derived from a substantial set of publications documenting its behavior, and various lesser known odontocetes having corrections based only on platform type (aerial or shipboard), derived from comparatively sparse information. Here we document the corrections used for common bottlenose dolphin.

4.1 Aerial Surveys

Palka et al. (2021) developed perception bias corrections using two team, mark recapture distance sampling (MRDS) methodology (Burt et al. 2014) for aerial surveys conducted in 2010-2017 by NOAA NEFSC and SEFSC during the AMAPPS program. These were the only extant perception bias estimates developed from aerial surveys used in our analysis, aside from estimates developed earlier by Palka and colleagues (Palka 2006; Palka et al. 2017). Those earlier efforts utilized older methods and less data than their 2021 analysis, so we applied the Palka et al. (2021) estimates to all aerial survey programs (Table 24).

We applied Palka's estimate for NEFSC to all programs other than SEFSC on the basis that those programs employed a similar visual scanning protocol that allowed observers to scan from the trackline up to the horizon, while SEFSC's protocol generally limited scanning only up to 50° from the trackline. This difference between NEFSC and SEFSC is apparent in the maximum distances of the most distant (untruncated) sightings, which was over 2000 m for NEFSC (Figure 31, upper right, ignoring spurious sighting at 10,000 m) but only about 500 m for SEFSC (Figure 11).

For all aerial surveys, to account for the influence of large group sizes on perception bias, we followed Carretta et al. (2000) and set the perception bias correction factor for sightings of more than 25 animals to $g_{0P} = 0.994$. Roughly 88% of NEFSC's and 92% of SEFSC's sightings were of 25 animals or less.

We caution that it is possible that perception bias was different on the other aerial programs, as they often used different aircraft, flew at different altitudes, and were staffed by different personnel. Of particular concern are that many programs flew Cessna 337 Skymasters, which had flat windows, while NOAA flew de Havilland Twin Otters, which had bubble windows, which likely afforded a better view of the transect line and therefore might have required less of a correction than the Skymasters. Correcting the other programs using NOAA's estimate as we have done is likely to yield less bias than leaving them uncorrected, but we urge all programs to undertake their own efforts to estimate perception bias, as resources allow.

We estimated availability bias corrections using the Laake et al. (1997) estimator and dive intervals reported by Palka et al. (2017) (Table 25). To estimate time in view, needed by the Laake estimator, we used results reported by Robertson et al. (2015), rescaled linearly for each survey program according to its target altitude and speed. We caution that Robertson's analysis was done for a de Havilland Twin Otter, which may have a different field of view than that of the other aircraft used here, which mainly comprised Cessna 337 Skymasters with flat windows. However, we note that McLellan et al. (2018) conducted a sensitivity analysis on the influence of the length of the "window of opportunity" to view beaked whales from a Cessna Skymaster on their final density estimates and found that they varied by only a few thousandths of an animal per kilometer when the window of opportunity more than doubled. Still, we urge additional program-specific research into estimation of availability bias.

To address the influence of group size on availability bias, we applied the group availability estimator of McLellan et al. (2018) on a per-observation basis. Following Palka et al. (2021), who also used that method, we assumed that individuals

in the group dived asynchronously. The resulting g_{0A} corrections ranged from about 0.65 to 1.0 (Figure 60), with the majority of observations having a correction of 0.95 or higher, owing to large group sizes. We caution that the assumption of asynchronous diving can lead to an underestimation of density and abundance if diving is actually synchronous; see McLellan et al. (2018) for an exploration of this effect. However, if future research finds that this species conducts synchronous dives and characterizes the degree of synchronicity, the model can be updated to account for this knowledge.

Table 24: Perception bias corrections for common bottlenose dolphin applied to aerial surveys.

Surveys	Group Size	g_{0P}	g_{0P} Source
SEFSC	≤ 25	0.860	Palka et al. (2021): SEFSC
All others	≤ 25	0.670	Palka et al. (2021): NEFSC
All	> 25	0.994	Carretta et al. (2000)

Table 25: Surface and dive intervals for common bottlenose dolphin used to estimate availability bias corrections.

Surface Interval (s)	Dive Interval (s)	Source
3	26.6	Palka et al. (2017)

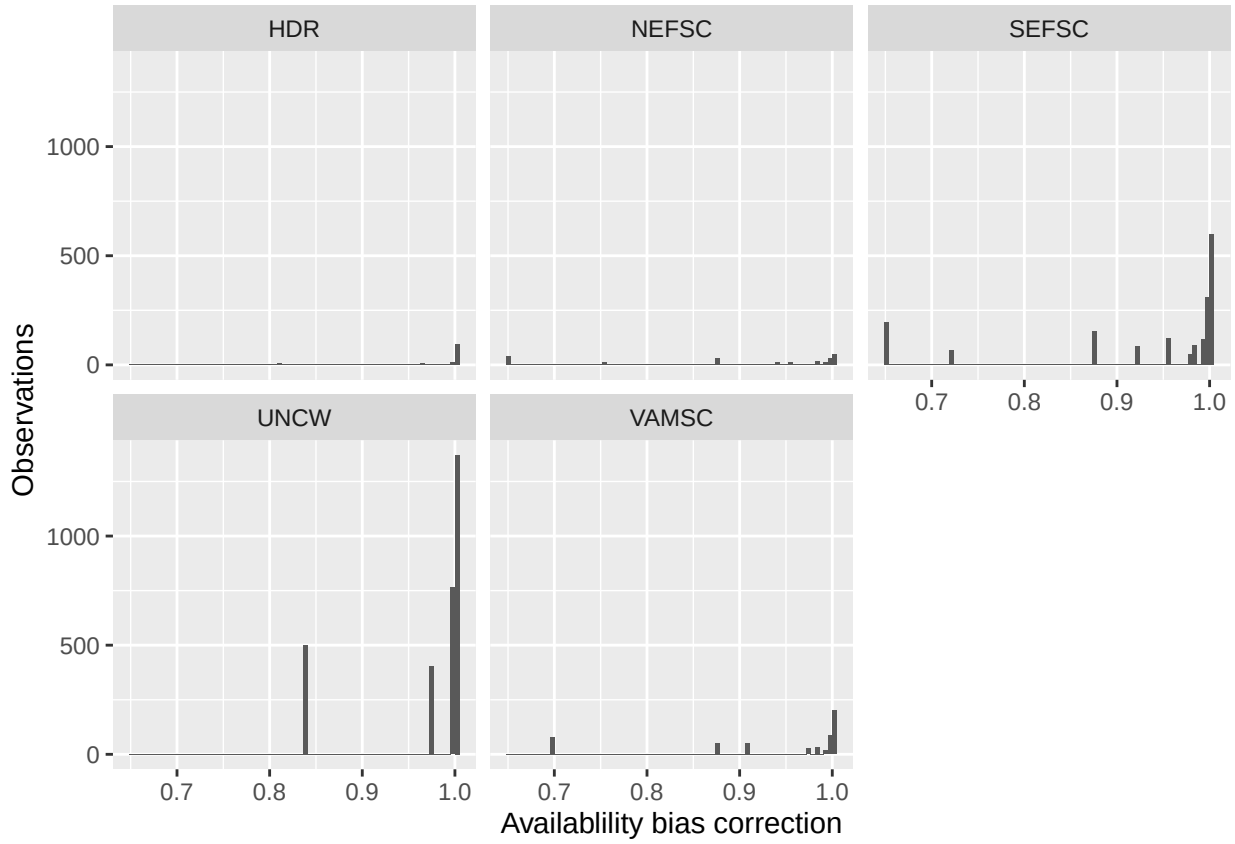

Figure 60: Availability bias corrections for common bottlenose dolphin for aerial surveys, by institution.

4.2 Shipboard Surveys

Most of the shipboard surveys in our analysis used high-power (25x150), pedestal-mounted binoculars. Similar to aerial surveys, Palka et al. (2021) developed perception bias corrections using two team, MRDS methodology (Burt et al. 2014) for high-power binocular surveys conducted in 2010-2017 by NOAA NEFSC and SEFSC during the AMAPPS program. These were the only extant perception bias estimates developed from high-power binocular surveys used in our analysis, aside from estimates developed earlier by Palka and colleagues (Palka 2006; Palka et al. 2017). Those earlier efforts utilized older

methods and less data than their 2021 analysis, so we applied the Palka et al. (2021) estimates to all shipboard surveys that searched with high-power binoculars (Table 26).

A few surveys used naked eyes rather than high-power binoculars, but none of these programs prepared perception bias estimates for common bottlenose dolphin, nor could we locate any in the literature for shipboard naked eye observations of this species. As a proxy, we used the estimate from Palka (2006) developed for Atlantic white-sided dolphin for the AJ 99-02 naked eye survey.

For all surveys, to account for the influence of large group sizes on perception bias, we followed Barlow and Forney (2007) and set the perception bias correction factor for sightings of more than 20 animals to $g_{0P} = 0.97$. Given that the dive interval of this species (Table 25) was short relative to the amount of time a given patch of water remained in view to shipboard observers, we assumed that no availability bias correction was needed ($g_{0A} = 1$), following Palka et al. (2021).

Table 26: Perception and availability bias corrections for common bottlenose dolphin applied to shipboard surveys.

Surveys	Searching Method	Group Size	g_{0P}	g_{0P} Source	g_{0A}	g_{0A} Source
NEFSC, NJDEP	Binoculars	≤ 20	0.59	Palka et al. (2021): NEFSC	1	Assumed
SEFSC	Binoculars	≤ 20	0.69	Palka et al. (2021): SEFSC	1	Assumed
MCR	Naked eye	≤ 20	0.27	Palka et al. (2006)	1	Assumed
All	All	> 20	0.97	Barlow and Forney (2007)	1	Assumed

5 Density Model

The common bottlenose dolphin is the most abundant cetacean in U.S. Atlantic waters, with the possible exception of the short-beaked common dolphin. Owing to its high abundance and distribution close to shore, the surveys available for our analysis reported more sightings of bottlenose dolphin than any other cetacean species (Table 1).

Bottlenose dolphins exhibit the most complex population structure yet documented for any cetacean in the U.S. Atlantic or Gulf of Mexico. The Marine Mammal Protection Act (MMPA) requires that cetaceans be managed on a per-"stock" basis, and defines a stock as "a group of marine mammals of the same species or smaller taxa in a common spatial arrangement, that interbreed when mature". NOAA Fisheries is responsible for defining stocks and estimating their abundance, and periodically issues Stock Assessment Reports (SARs) that summarize the latest research and promulgate stock definitions and abundance estimates. At the time of this writing, NOAA had last updated the relevant Atlantic stocks in SARs dated 2017 through 2020 (Table 29). The SARs described the western North Atlantic stocks of bottlenose dolphin as follows:

Two morphologically and genetically distinct morphotypes of bottlenose dolphins, known as the coastal and offshore forms, inhabit the western North Atlantic. A recent integrative taxonomic investigation proposed the two forms be recognized as different species (Costa et al. 2022). The offshore form is larger and more robust, and consists of a single stock, which inhabits off-shelf, slope, and shelf-break waters, as well as outer portions of the continental shelf. The spatiotemporal extent and dynamics of its on-shelf distribution (e.g. how close it comes to shore) are a topic of active research and appear to vary spatially and seasonally. The coastal morphotype consists of multiple "coastal" and "estuarine" stocks. At the time of this writing, NOAA had defined five coastal stocks for the east coast, each genetically distinct. They generally inhabit the inner portions of the continental shelf, and some migrate north along the shelf in summer and return south in winter. NOAA also defined at least 10 estuarine stocks for the east coast. These inhabit particular bays, sounds, rivers, and other estuarine systems and may be genetically distinct from each other as well as the other coastal stocks. They generally do not migrate.

There is spatiotemporal overlap between many of these stocks: between the offshore and coastal stocks, among the coastal stocks, between the estuarine and coastal stocks, and among the estuarine stocks. At present, we lack the information necessary to model each stock individually. The core problem is that there is no reliable and comprehensive way to determine which stock a given sighting belongs to. Some surveys in our study reported "coastal bottlenose dolphin" or "offshore bottlenose dolphin", but none reported a more precise identification than that, and the large majority of surveys simply reported "bottlenose dolphin".

NOAA SARs and the literature (e.g. Torres et al. 2003; Toth et al. 2012) discussed potential methods for classifying sightings based on geographic location, distance to shore, depth, and other variables, but these proposals did not cover all of the stocks or definitively address the overlaps between them, and there was no widespread agreement among the research community on the efficacy of proposed approaches. At the time of this writing, the only foolproof method of classifying a sighting into a stock was through genetics. Therefore we have made no attempt to model bottlenose dolphins on a per-stock basis from the sightings, and have instead modeled all stocks in a single model. Prior to fitting our spatial model, we discarded all estuarine

survey transects, thus it is probably reasonable to assume that our model estimates the aggregate density of the offshore and coastal stocks, and excludes the estuarine stocks (although some estuarine stocks are known to range into coastal areas beyond their home estuaries; presumably some of these were sighted and we failed to discard them).

The surveys incorporated into our model, spanning 1998-2019 (see Section 1), reported over 6800 sightings. Consistent with the presence of two morphotypes with differing habitat preferences, the densest clusters of sightings stretched along two isobaths, the first along the shore between Palm Beach, Florida and the eastern tip of Long Island, New York, and the second along the continental shelf break from Florida through eastern edge of Georges Bank. Although a seasonal shift in sightings was apparent in monthly aggregate maps of surveys and sightings (see figures in Section 6.1), similar to that described for the coastal migratory stocks, we could find no description in the literature that indicated a clear seasonal switch in the species' relationship to environmental covariates (as with certain baleen whales migrating between cold feeding grounds and warm calving grounds). Given that, we fitted a single year-round model that incorporated all available survey data.

The model selection procedure was straightforward. When ranked by REML score (Wood 2011), the highest ranked models with contemporaneous covariates outranked those with climatological covariates and explained 0.3% more deviance. We selected the highest ranked contemporaneous model, which included eight terms (Table 27). Functional relationships (Figure 64) for several covariates were bimodal, likely reflecting the differing stock-environment relationships of the multiple stocks included in the model. The relationship with Depth was positive for depths less than about 25 m, consistent with some descriptions of the preferred habitat of coastal stocks (Hayes et al. 2020), and greater than about 150 m, indicative of the shelf-break and slope habitat preferred by the offshore stock. The DistTo125m relationship was positive out to about 10 km beyond the isobath, with three peaks, indicating complex structure over the continental shelf and decreasing density beyond it. The relationship with bottom salinity peaked at the highest values, corresponding to salty offshore waters, and again just below 35 PSU, consistent with more southerly shelf waters, and steadily decreased as salinity decreased, indicating an avoidance of northerly shelf waters such as the Gulf of Maine and the Scotian Shelf, where the species was sighted only rarely.

North of Long Island, only one sighting occurred very close to shore, while along Long Island and south of it to the southern tip of Florida, sightings regularly occurred very close to shore. To address this ecological pattern, we introduced a bivariate interaction of fetch, a measure of how enclosed an area is, with distance to Hudson Canyon, with positive distances being north and negative distances south. This term showed an elevated relationship south of Hudson Canyon, with peak values occurring between 0-500 km south of it, roughly corresponding to the stretch of coastline between New York-New Jersey Harbor and Cape Lookout, North Carolina. The term showed a strong drop north of Hudson Canyon for low fetch values, consistent with the lack of sightings in nearshore areas in the northern regions of the study area.

The remaining oceanographic covariates indicated positive relationships with sea surface temperature (SST) greater than about 9 °C, consistent with finding that the species "northern distribution in winter appears to be limited by water temperatures <9.5 °C" (Hayes et al. 2018), and across a wide range of values of epipelagic micronekton biomass but not the highest biomasses sampled. Both of these relationships were consistent with a distribution that was widespread, but low in the Gulf of Maine and Scotian Shelf where waters are cold and epipelagic micronekton biomass is the highest in the study area. High densities were also indicated close to SST fronts and greater than 100 km from mesoscale eddies, which likely reflects the offshore morphotypes's apparent preference for the shelf break and upper continental slope rather than deeper, more distant waters.

5.1 Final Model

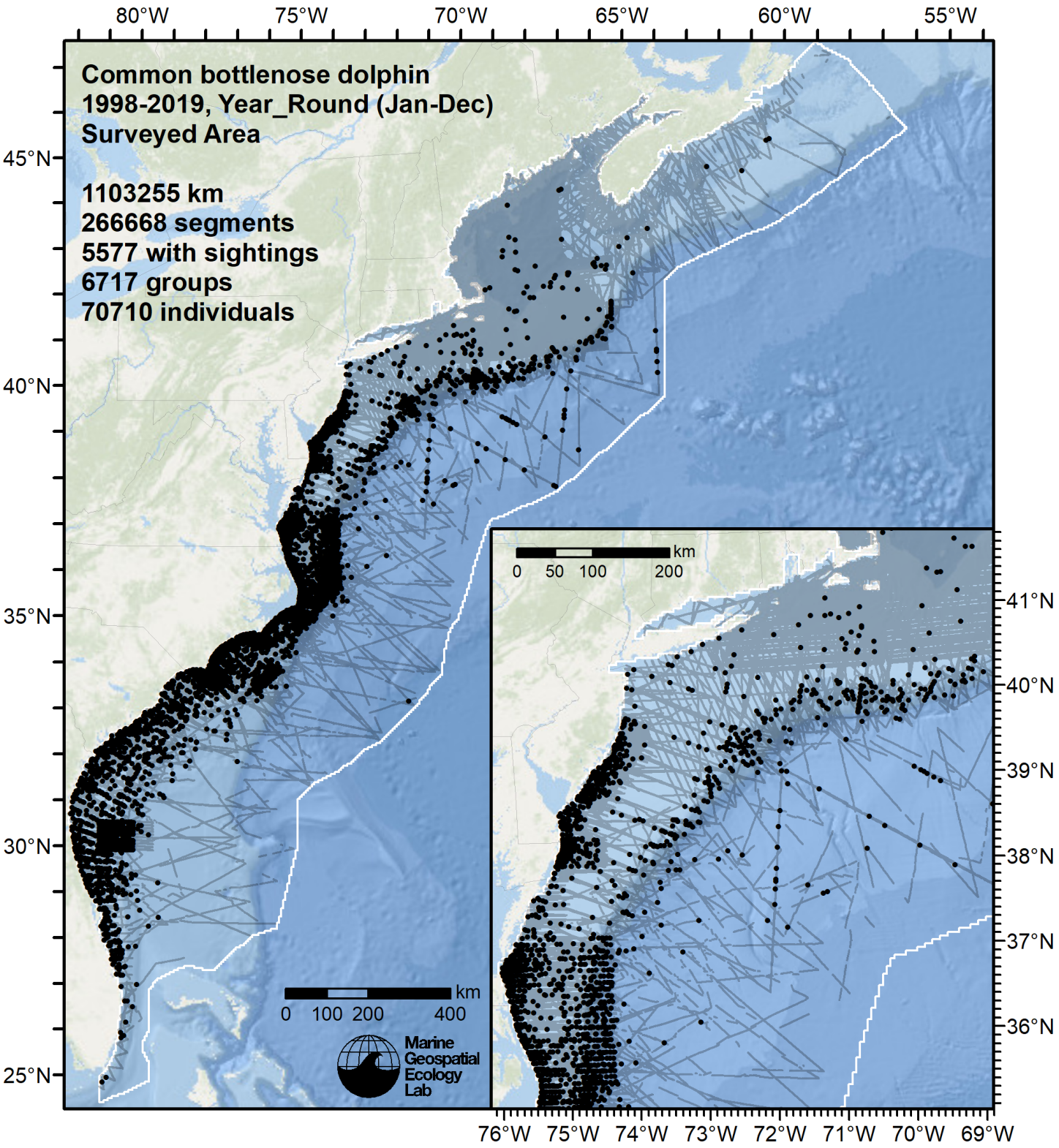

Figure 61: Survey segments used to fit the model. Black points indicate segments with observations.

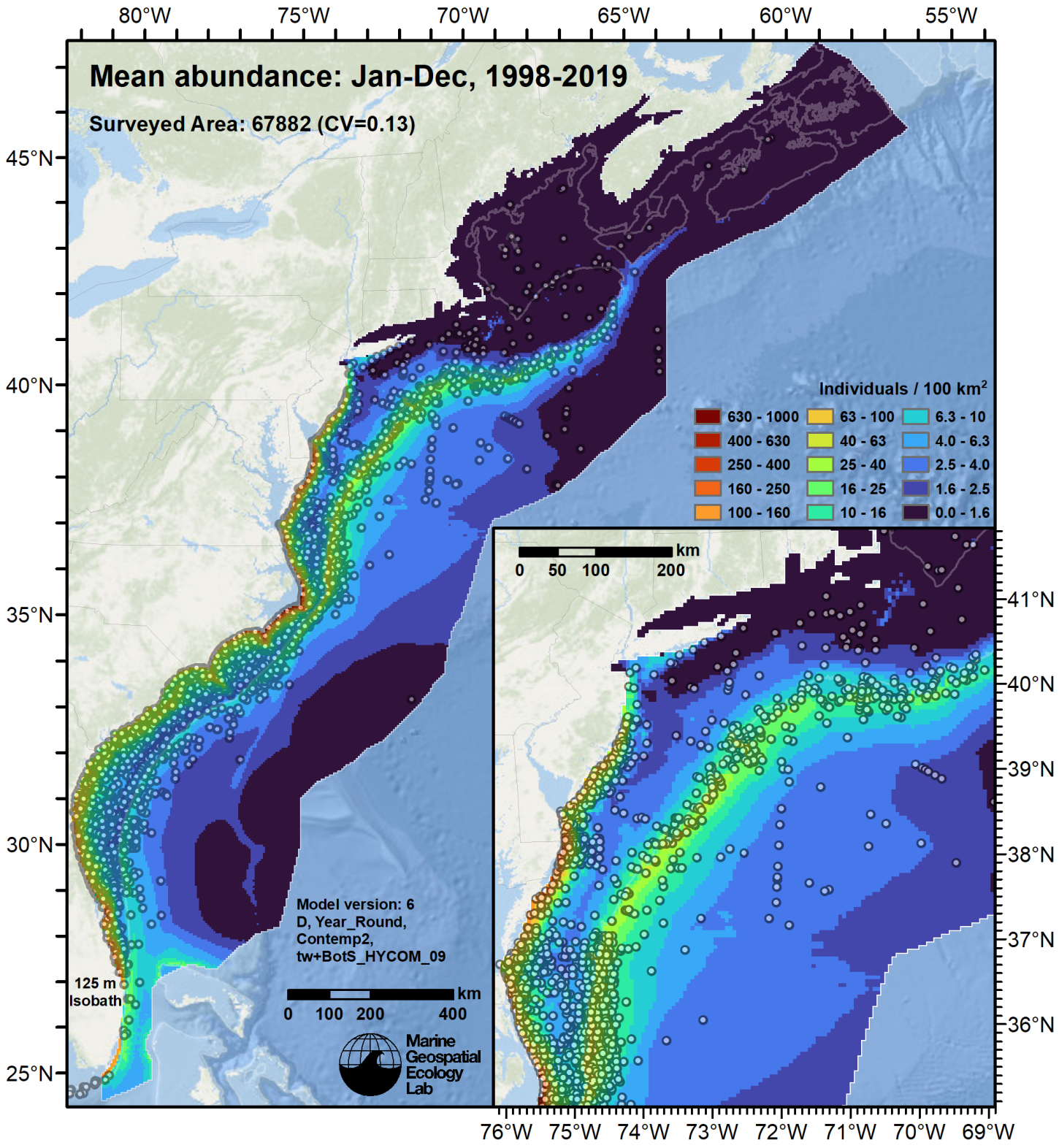

Figure 62: Common bottlenose dolphin mean density for the indicated period, as predicted by the model. Open circles indicate segments with observations. Mean total abundance and its coefficient of variation (CV) are given in the subtitle. Variance was estimated with the analytic approach given by Miller et al. (2022), Appendix S1, and accounts both for uncertainty in model parameter estimates and for seasonal and interannual variability in dynamic covariates.

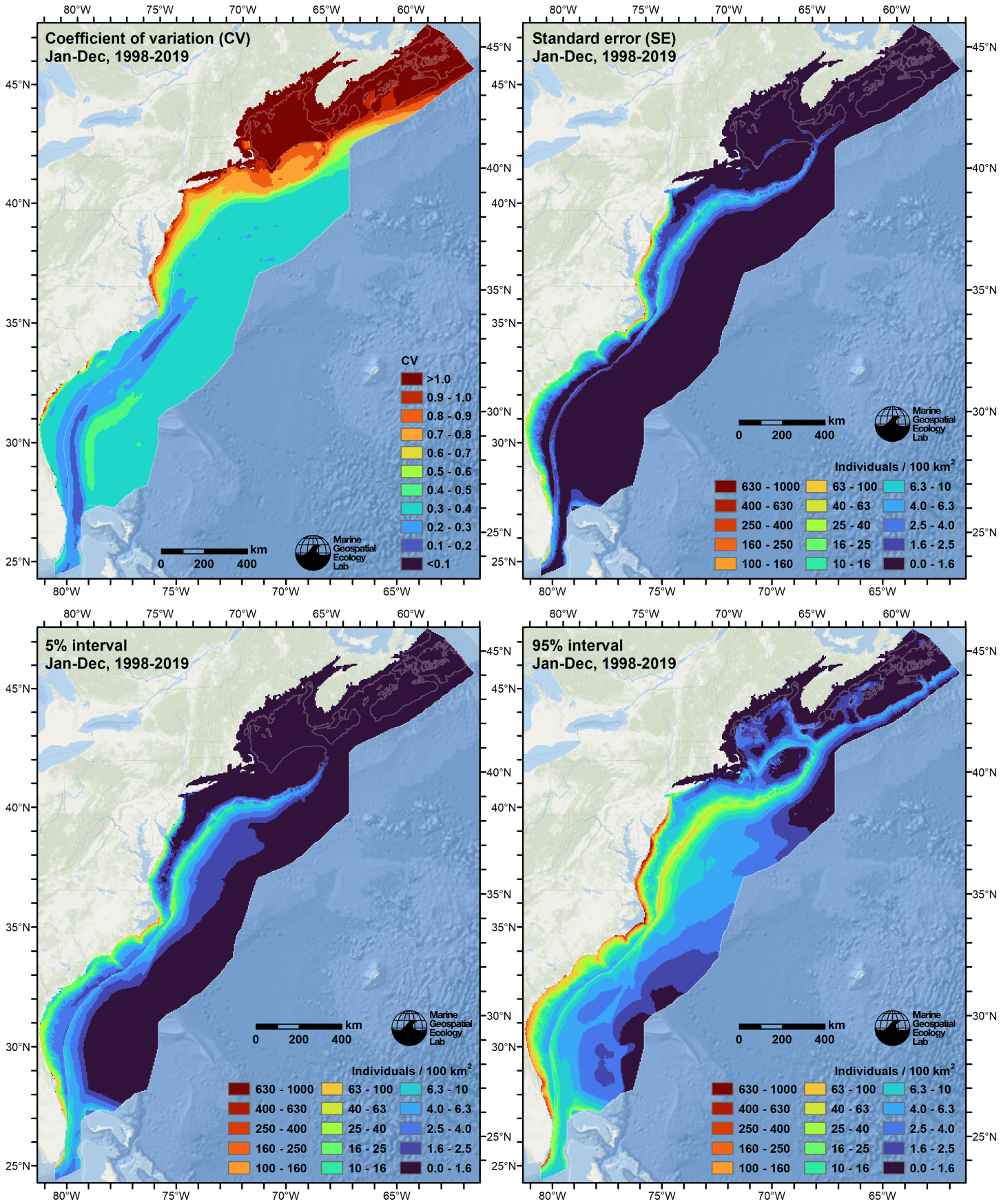

Figure 63: Uncertainty statistics for the common bottlenose dolphin mean density surface (Figure 62) predicted by the model. Variance was estimated with the analytic approach given by Miller et al. (2022), Appendix S1, and accounts both for uncertainty in model parameter estimates and for seasonal and interannual variability in dynamic covariates.

Statistical output for this model:

```
Family: Tweedie(p=1.407)
Link function: log

Formula:
IndividualsCorrected ~ offset(log(SegmentArea)) + te(Fetch_50km,
    pmax(-1300, pmin(I(DistToHudCan/1000), 800)), bs = "ts") +
    s(log10(pmax(3, pmin(Depth, 4000))), bs = "ts") + s(pmax(-100,
    pmin(I(DistTo125m/1000), 100)), bs = "ts") + s(pmax(3, pmin(SST_CMC,
    30)), bs = "ts") + s(pmax(31, pmin(BotS_HYCOM, 36.5)), bs = "ts") +
    s(pmin(I(DistToFront105/1000), 75), bs = "ts") + s(pmax(-50,
    pmin(I(DistToEddy/1000), 200)), bs = "ts") + s(pmax(0.5,
    pmin(MnkEpi, 26)), bs = "ts")

Parametric coefficients:
             Estimate Std. Error t value Pr(>|t|)
(Intercept) -18.09326    0.06083  -297.4   <2e-16 ***
---
Signif. codes:  0 '***' 0.001 '**' 0.01 '*' 0.05 '.' 0.1 ' ' 1

Approximate significance of smooth terms:
                                                        edf Ref.df      F p-value
te(Fetch_50km,pmax(-1300, pmin(I(DistToHudCan/1000), 800))) 16.235     24 41.219 < 2e-16 ***
s(log10(pmax(3, pmin(Depth, 4000))))                     8.484      9 47.746 < 2e-16 ***
s(pmax(-100, pmin(I(DistTo125m/1000), 100)))             7.596      9 10.642 < 2e-16 ***
s(pmax(3, pmin(SST_CMC, 30)))                            7.789      9 34.814 < 2e-16 ***
s(pmax(31, pmin(BotS_HYCOM, 36.5)))                      6.802      9 25.882 < 2e-16 ***
s(pmin(I(DistToFront105/1000), 75))                      4.993      9 12.765 < 2e-16 ***
s(pmax(-50, pmin(I(DistToEddy/1000), 200)))              2.319      9  1.349 0.00163 **
s(pmax(0.5, pmin(MnkEpi, 26)))                           7.472      9 25.390 < 2e-16 ***
---
Signif. codes:  0 '***' 0.001 '**' 0.01 '*' 0.05 '.' 0.1 ' ' 1

R-sq.(adj) =  0.0306   Deviance explained = 33.1%
-REML =  44765  Scale est. = 31.729    n = 266668
```

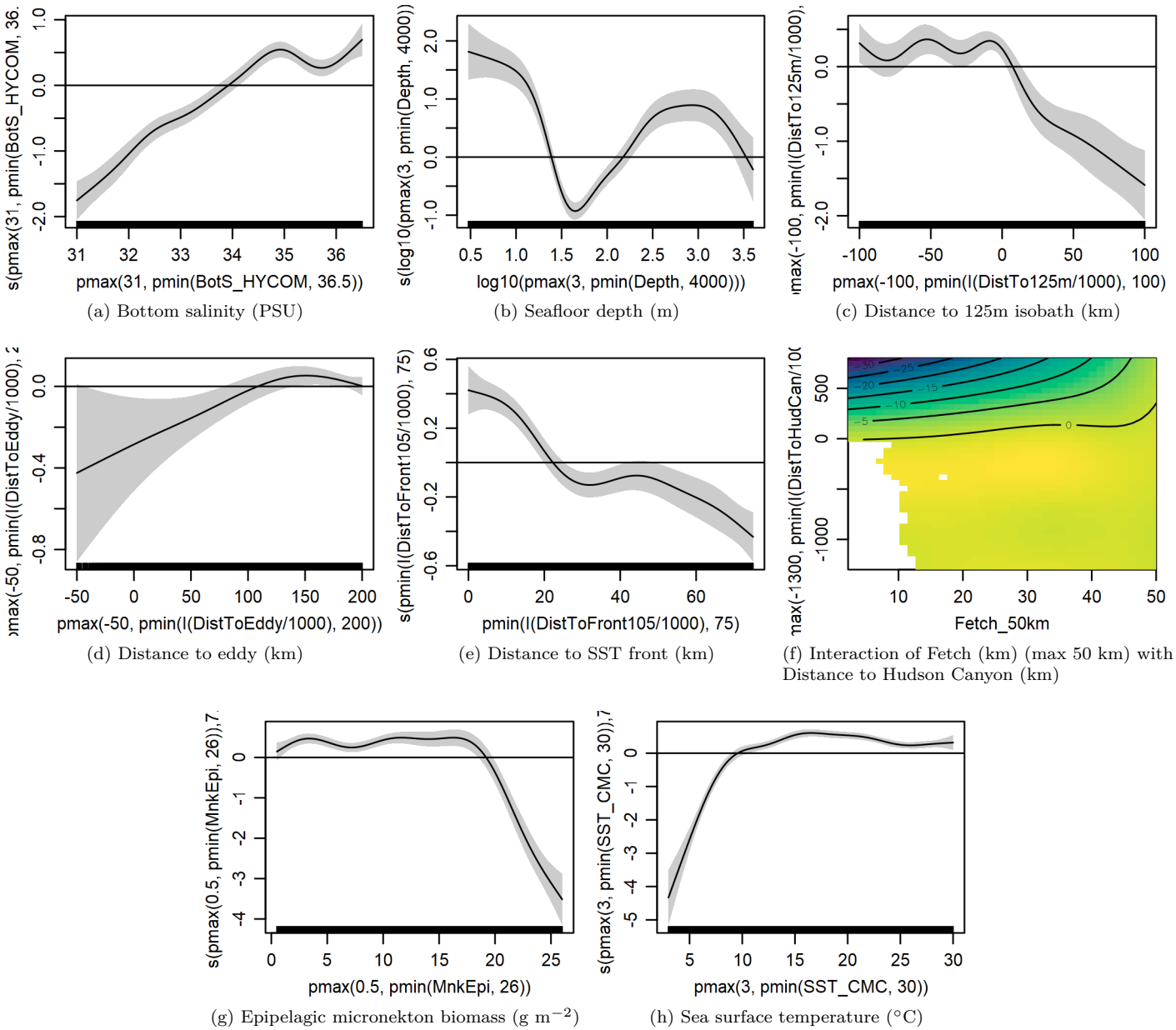

(a) Bottom salinity (PSU)

(b) Seafloor depth (m)

(c) Distance to 125m isobath (km)

(d) Distance to eddy (km)

(e) Distance to SST front (km)

(f) Interaction of Fetch (km) (max 50 km) with Distance to Hudson Canyon (km)

(g) Epipelagic micronekton biomass (g m^{-2})

(h) Sea surface temperature (°C)

Figure 64: Functional plots for the final model. Transforms and other treatments are indicated in axis labels. *log10* indicates the covariate was $\log_{10}$ transformed. *pmax* and *pmin* indicate the covariate's minimum and maximum values, respectively, were Winsorized to the values shown. Winsorization was used to prevent runaway extrapolations during prediction when covariates exceeded sampled ranges, or for ecological reasons, depending on the covariate. */1000* indicates meters were transformed to kilometers for interpretation convenience.

Table 27: Covariates used in the final model.

Covariate	Description
BotS_HYCOM	Monthly mean bottom salinity (PSU) from the HYCOM GOFS 3.1 1/12° ocean model (Chassignet et al. (2009))
Depth	Depth (m) of the seafloor, from SRTM30_PLUS (Becker et al. (2009))
DistTo125m	Distance (km) to the 125m isobath, derived from SRTM30_PLUS (Becker et al. (2009))

Table 27: Covariates used in the final model. *(continued)*

Covariate	Description
DistToEddy	Monthly mean distance (km) to the edge of the closest mesoscale eddy of any polarity and age, derived with MGET (Roberts et al. (2010)) from the Aviso Mesoscale Eddy Trajectories Atlas (META2.0), produced by SSALTO/DUACS and distributed by AVISO+ (https://aviso.altimetry.fr) with support from CNES, in collaboration with Oregon State University with support from NASA, using the method of Schlax and Chelton (2016), based on Chelton et al. (2011)
DistToFront105	Monthly mean distance (km) to the closest sea surface temperature front detected in daily GHRSST Level 4 CMC0.2deg and CMC0.1deg images (Brasnett (2008); Canada Meteorological Center (2012); Meissner et al. (2016); Canada Meteorological Center (2016)) with MGET's implementation of the Canny edge detector (Roberts et al. (2010); Canny (1986))
DistToHudCan	Distance (km) to Hudson Canyon, derived from SRTM30_PLUS (Becker et al. (2009))
Fetch_50km	Fetch (km): mean distance to shore averaged over 16 radial directions, limited to a maximum of 50 km
MnkEpi	Monthly mean micronekton biomass available in the epipelagic zone, expressed as wet weight (g m^{-2}), from SEAPODYM (Lehodey et al. (2008); Lehodey et al. (2015)), provided by E.U. Copernicus Marine Service. doi: 10.48670/moi-00020. Computed as the sum of the SEAPODYM mnkc_epi, mnkc_mumeso, and mnkc_hmlmeso variables.
SST_CMC	Monthly mean sea surface temperature (°C) from GHRSST Level 4 CMC0.2deg and CMC0.1deg (Brasnett (2008); Canada Meteorological Center (2012); Meissner et al. (2016); Canada Meteorological Center (2016))

5.2 Diagnostic Plots

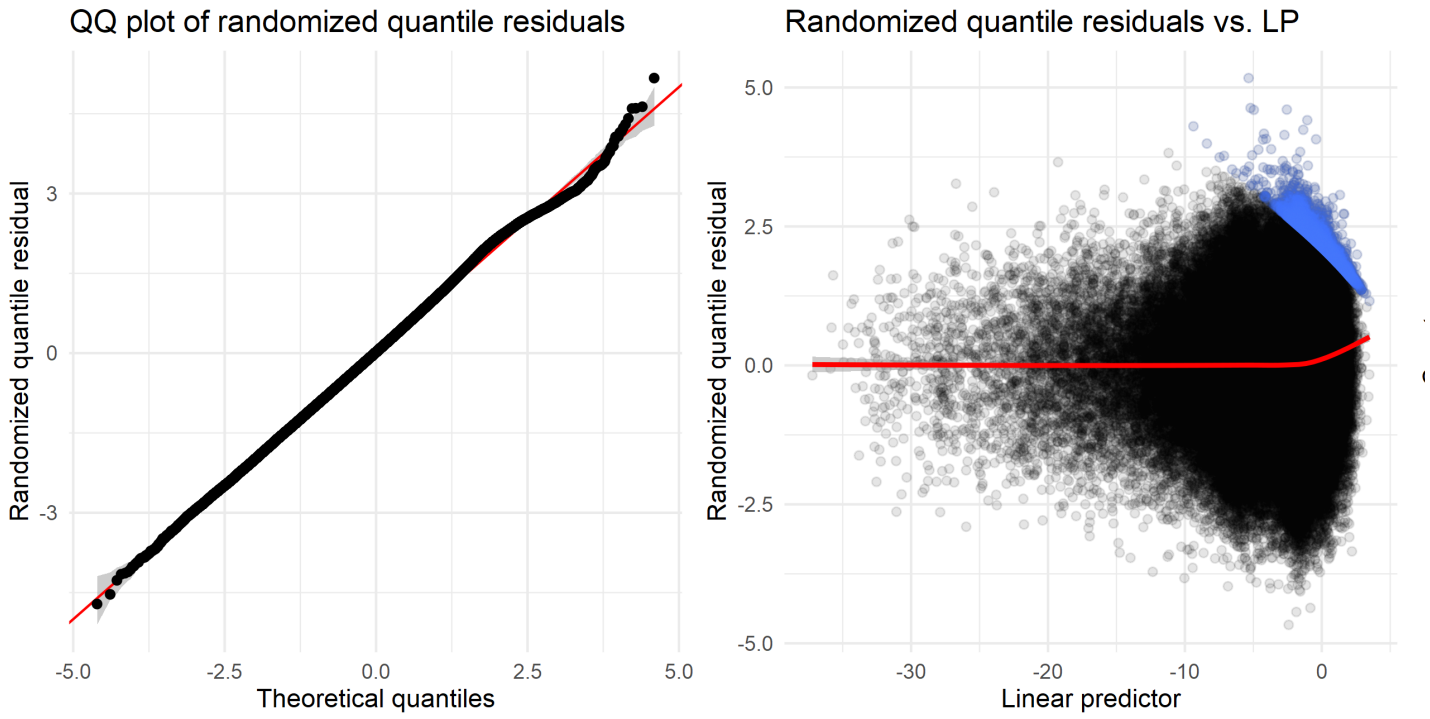

Figure 65: Residual plots for the final model.

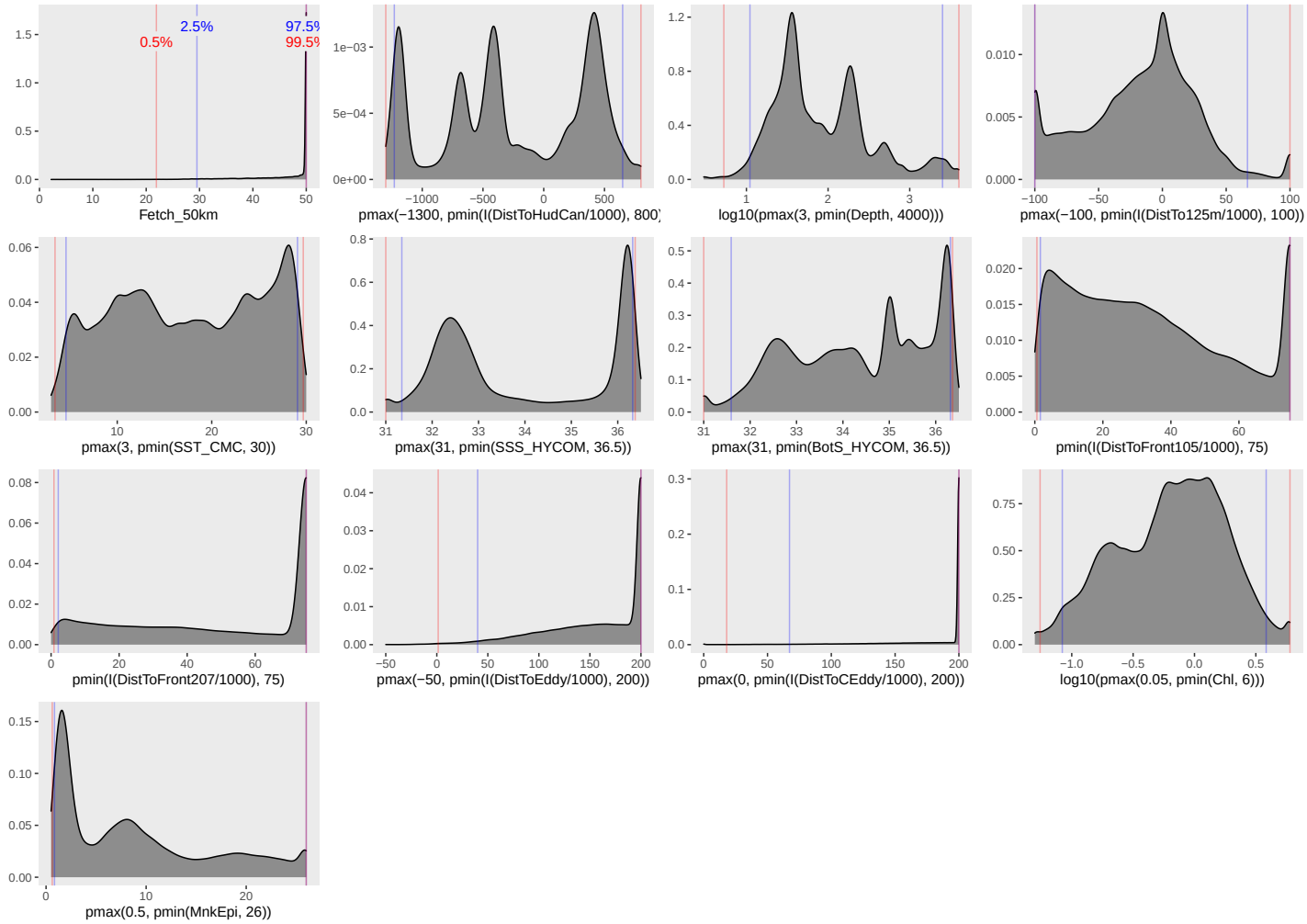

Figure 66: Density histograms showing the distributions of the covariates considered during the final model selection step. The final model may have included only a subset of the covariates shown here (see Figure 64), and additional covariates may have been considered in preceding selection steps. Red and blue lines enclose 99% and 95% of the distributions, respectively. Transforms and other treatments are indicated in axis labels. *log10* indicates the covariate was $\log_{10}$ transformed. *pmax* and *pmin* indicate the covariate's minimum and maximum values, respectively, were Winsorized to the values shown. Winsorization was used to prevent runaway extrapolations during prediction when covariates exceeded sampled ranges, or for ecological reasons, depending on the covariate. */1000* indicates meters were transformed to kilometers for interpretation convenience.

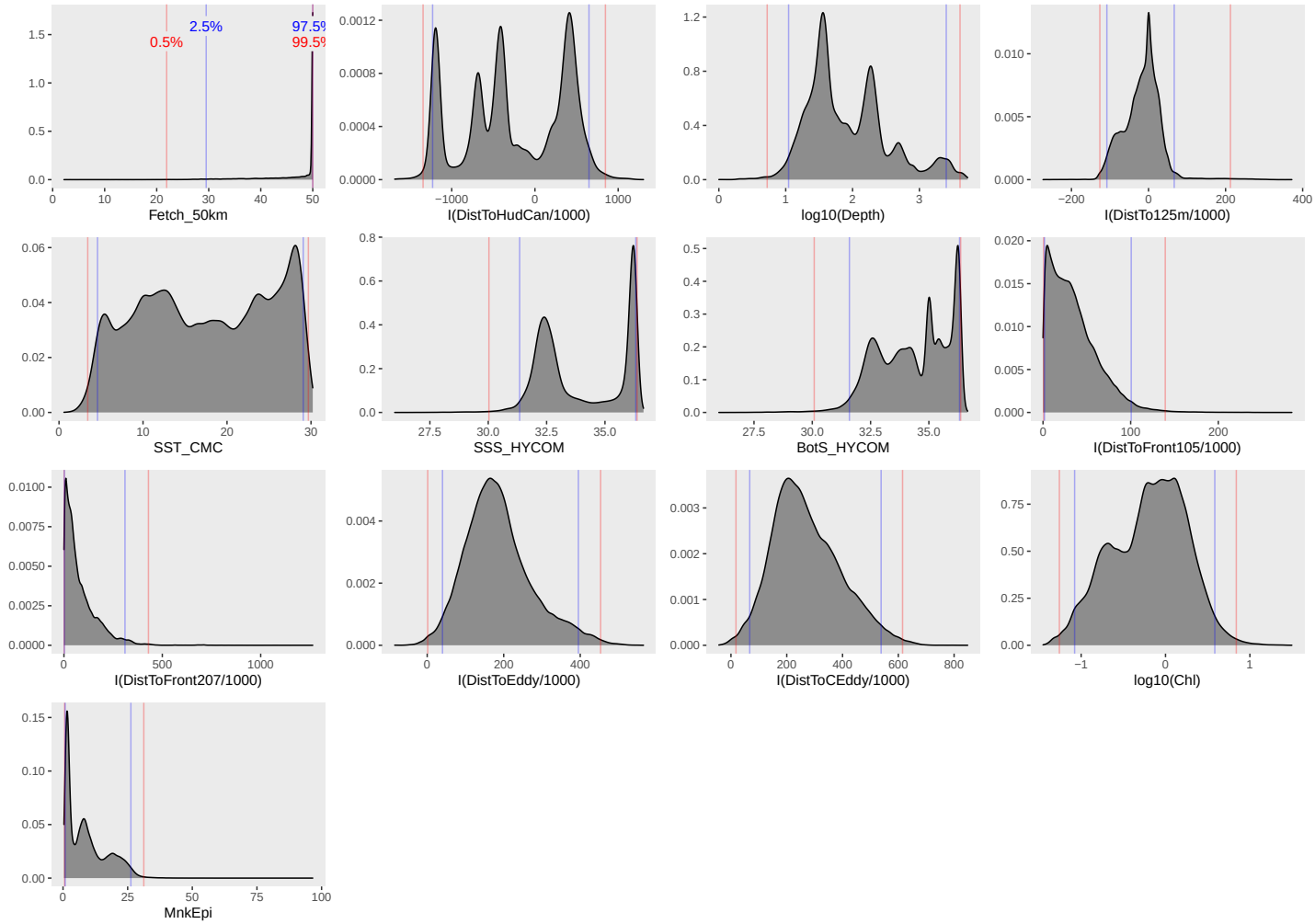

Figure 67: Density histograms shown in Figure 66 replotted without Winsorization, to show the full range of sampling represented by survey segments.

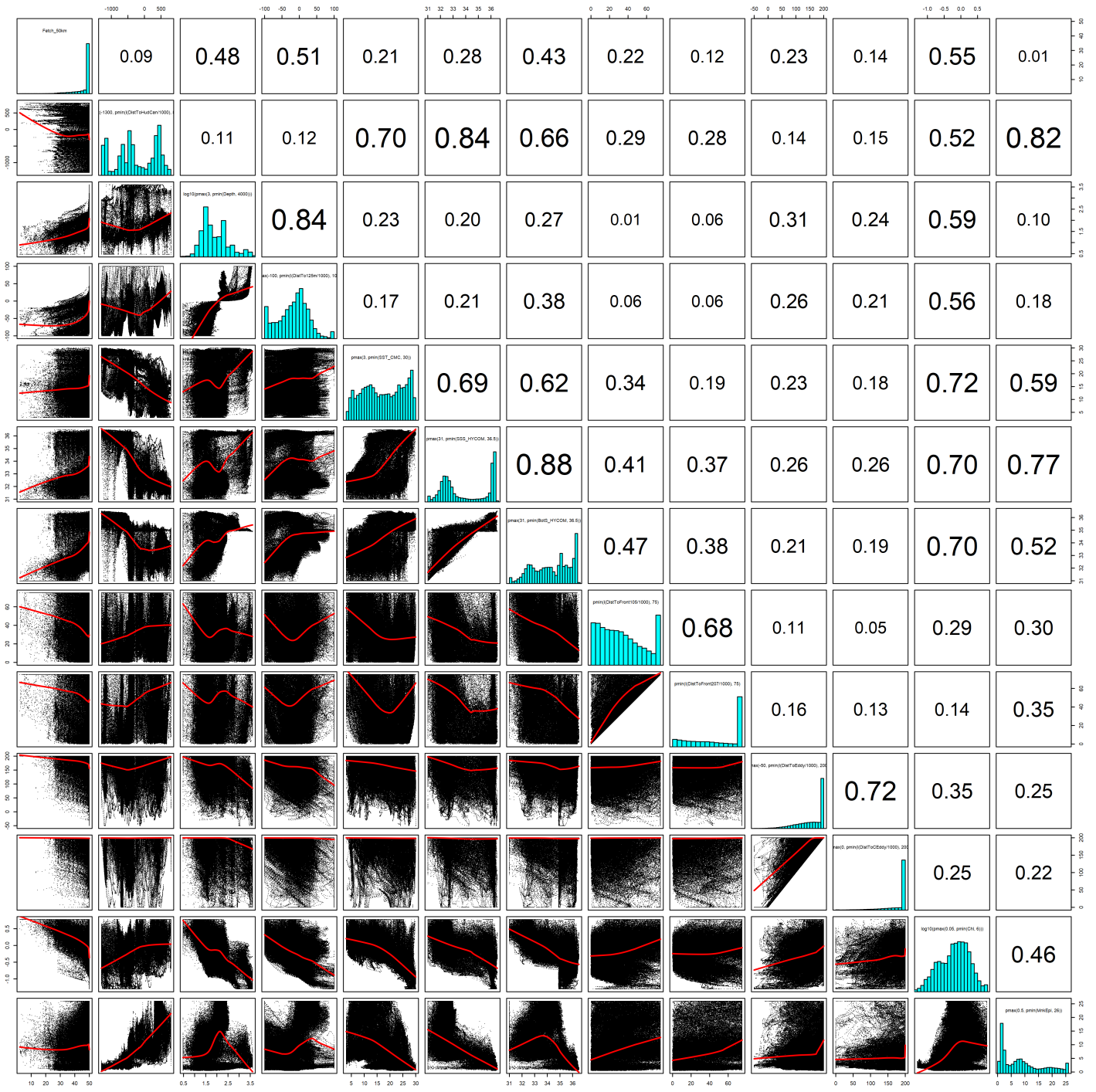

Figure 68: Scatterplot matrix of the covariates considered during the final model selection step. The final model may have included only a subset of the covariates shown here (see Figure 64), and additional covariates may have been considered in preceding selection steps. Covariates are transformed and Winsorized as shown in Figure 66. This plot is used to check simple correlations between covariates (via pairwise Pearson coefficients above the diagonal) and visually inspect for concurvity (via scatterplots and red lowess curves below the diagonal).

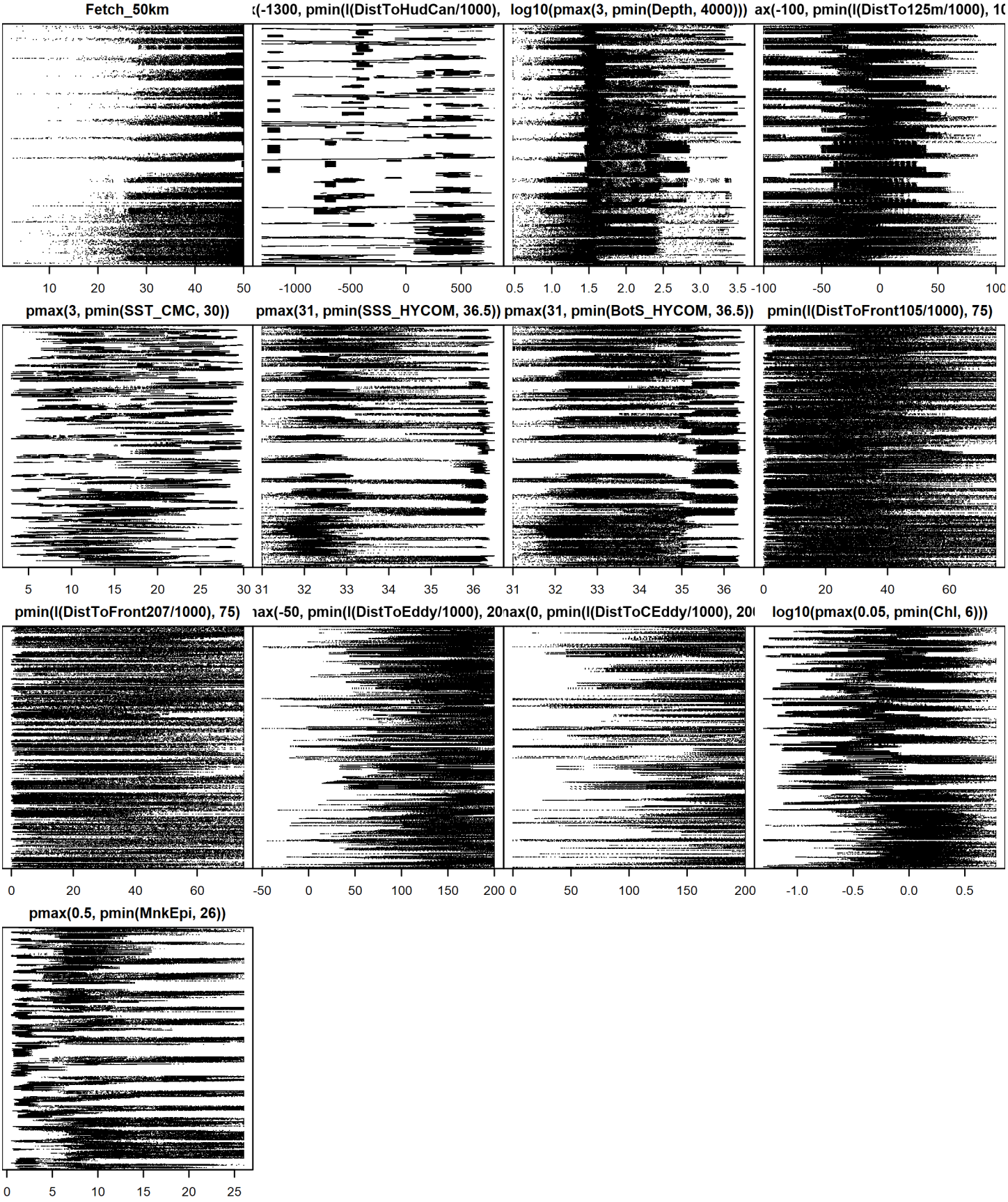

Figure 69: Dotplot of the covariates considered during the final model selection step. The final model may have included only a subset of the covariates shown here (see Figure 64), and additional covariates may have been considered in preceding selection steps. Covariates are transformed and Winsorized as shown in Figure 66. This plot is used to check for suspicious patterns and outliers in the data. Points are ordered vertically by segment ID, sequentially in time.

5.3 Extrapolation Diagnostics

5.3.1 Univariate Extrapolation

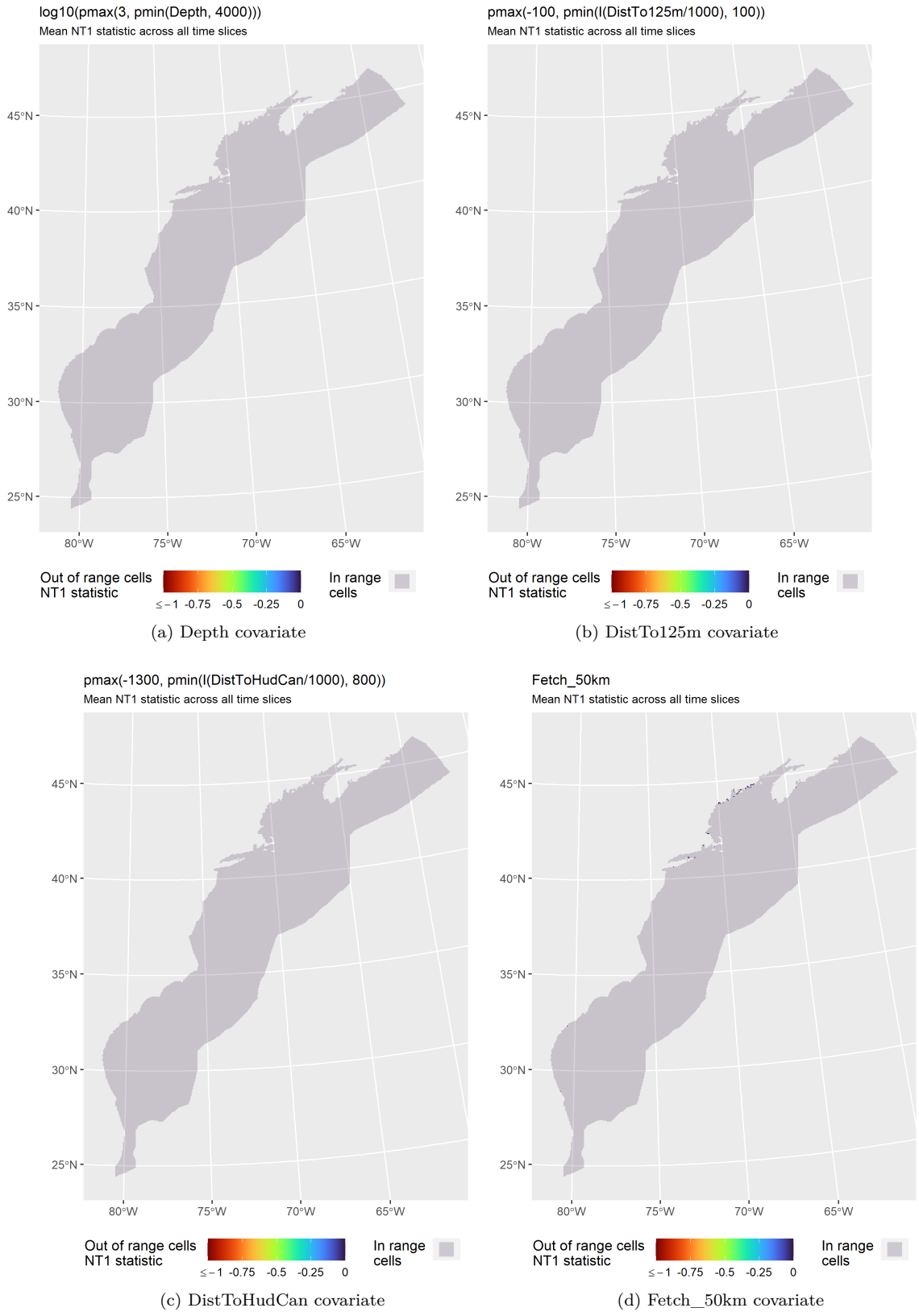

(a) Depth covariate

(b) DistTo125m covariate

(c) DistToHudCan covariate

(d) Fetch_50km covariate

Figure 70: NT1 statistic (Mesgaran et al. (2014)) for static covariates used in the model. Areas outside the sampled range of a covariate appear in color, indicating univariate extrapolation of that covariate occurred there. Areas within the sampled range appear in gray, indicating it did not occur.

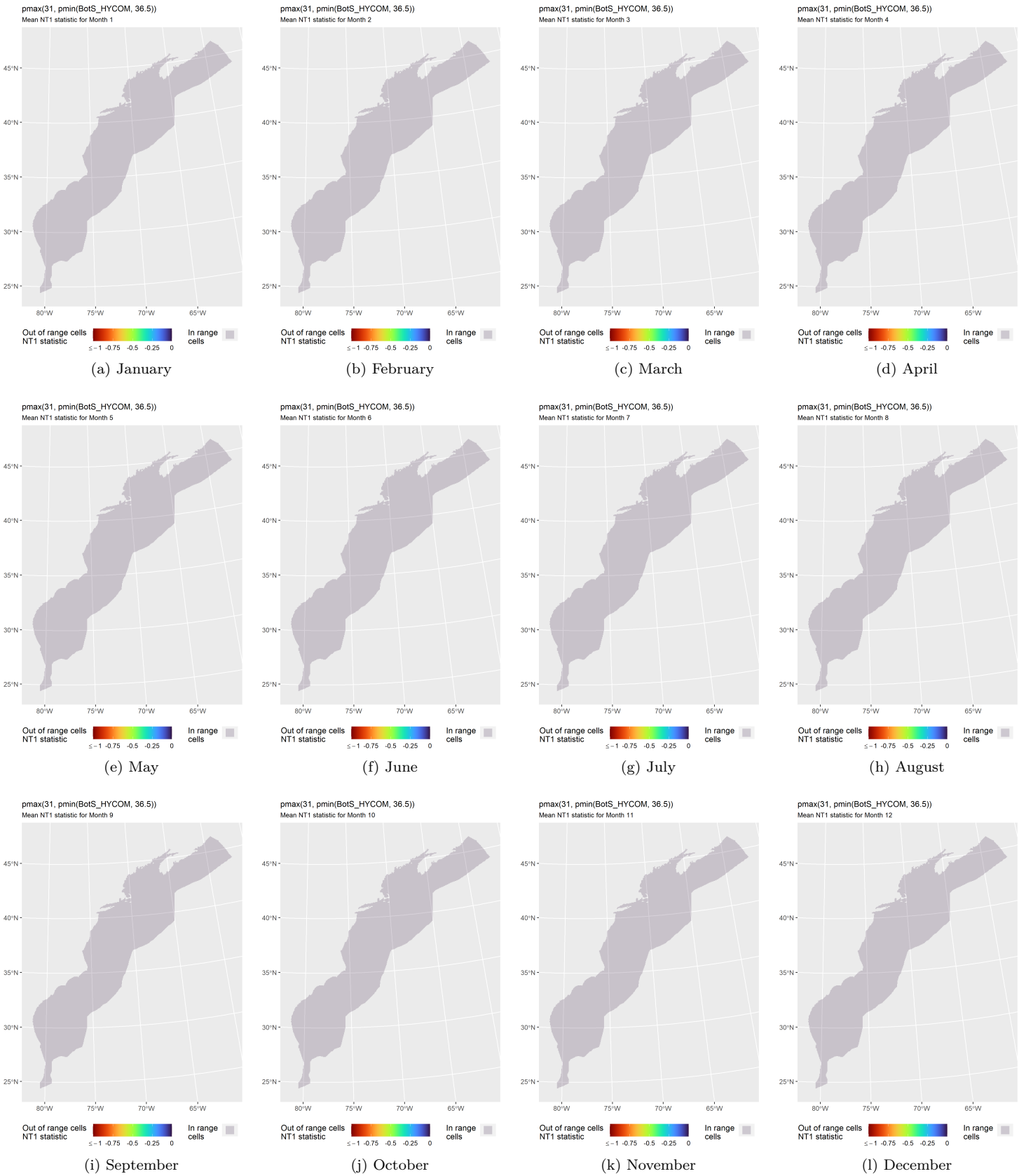

(a) January (b) February (c) March (d) April

(e) May (f) June (g) July (h) August

(i) September (j) October (k) November (l) December

Figure 71: NT1 statistic (Mesgaran et al. (2014)) for the BotS_HYCOM covariate in the model. Areas outside the sampled range of a covariate appear in color, indicating univariate extrapolation of that covariate occurred there during the month. Areas within the sampled range appear in gray, indicating it did not occur.

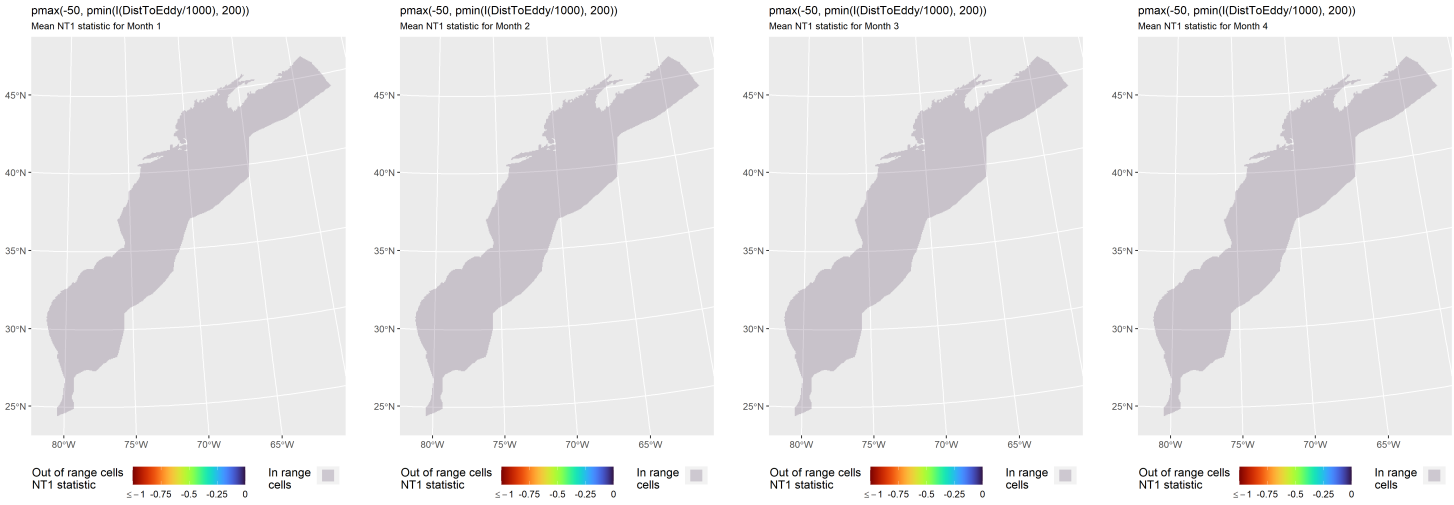

(a) January

(b) February

(c) March

(d) April

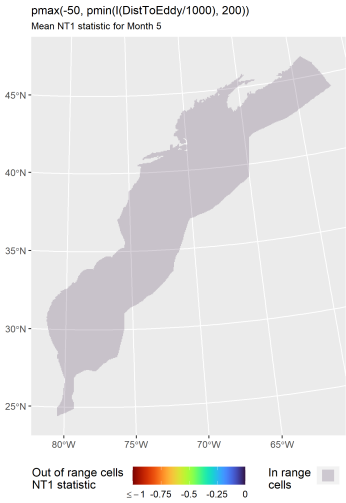

(e) May

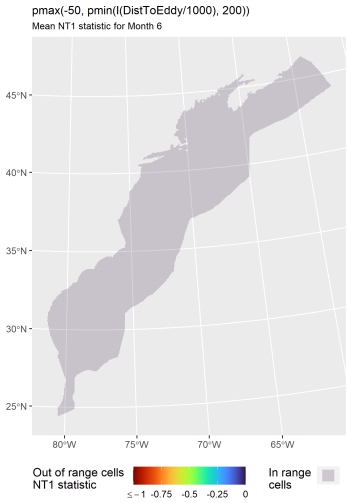

(f) June

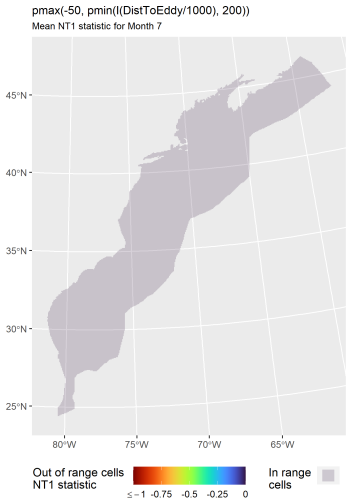

(g) July

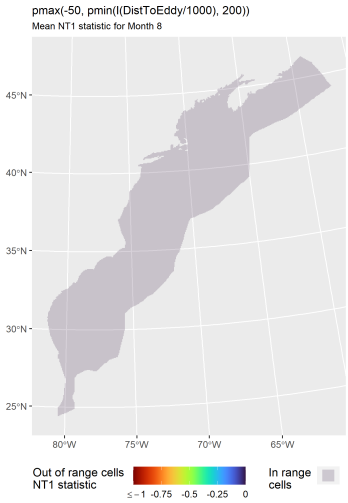

(h) August

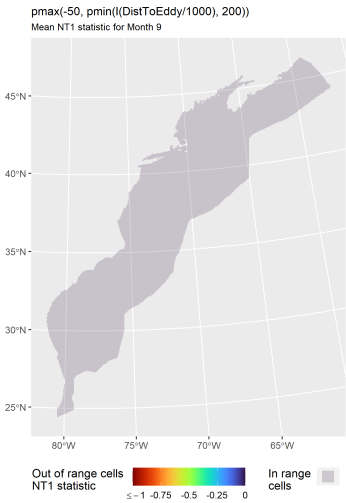

(i) September

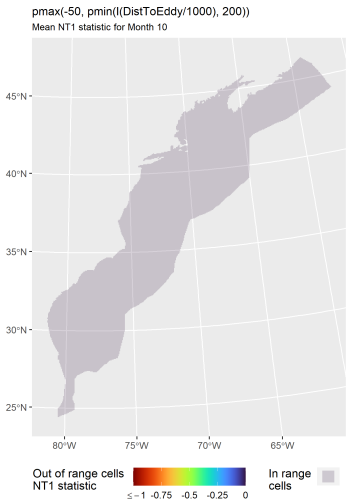

(j) October

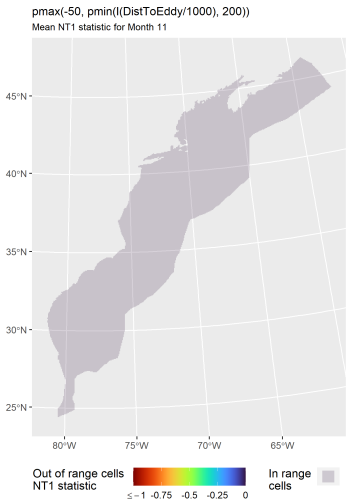

(k) November

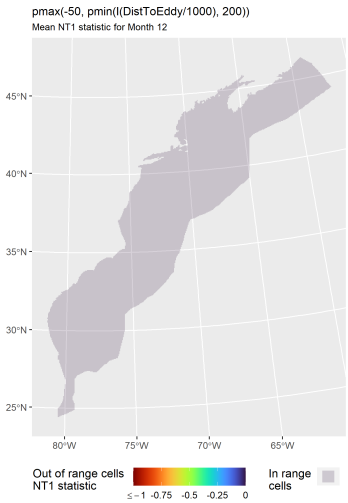

(l) December

Figure 72: NT1 statistic (Mesgaran et al. (2014)) for the DistToEddy covariate in the model. Areas outside the sampled range of a covariate appear in color, indicating univariate extrapolation of that covariate occurred there during the month. Areas within the sampled range appear in gray, indicating it did not occur.

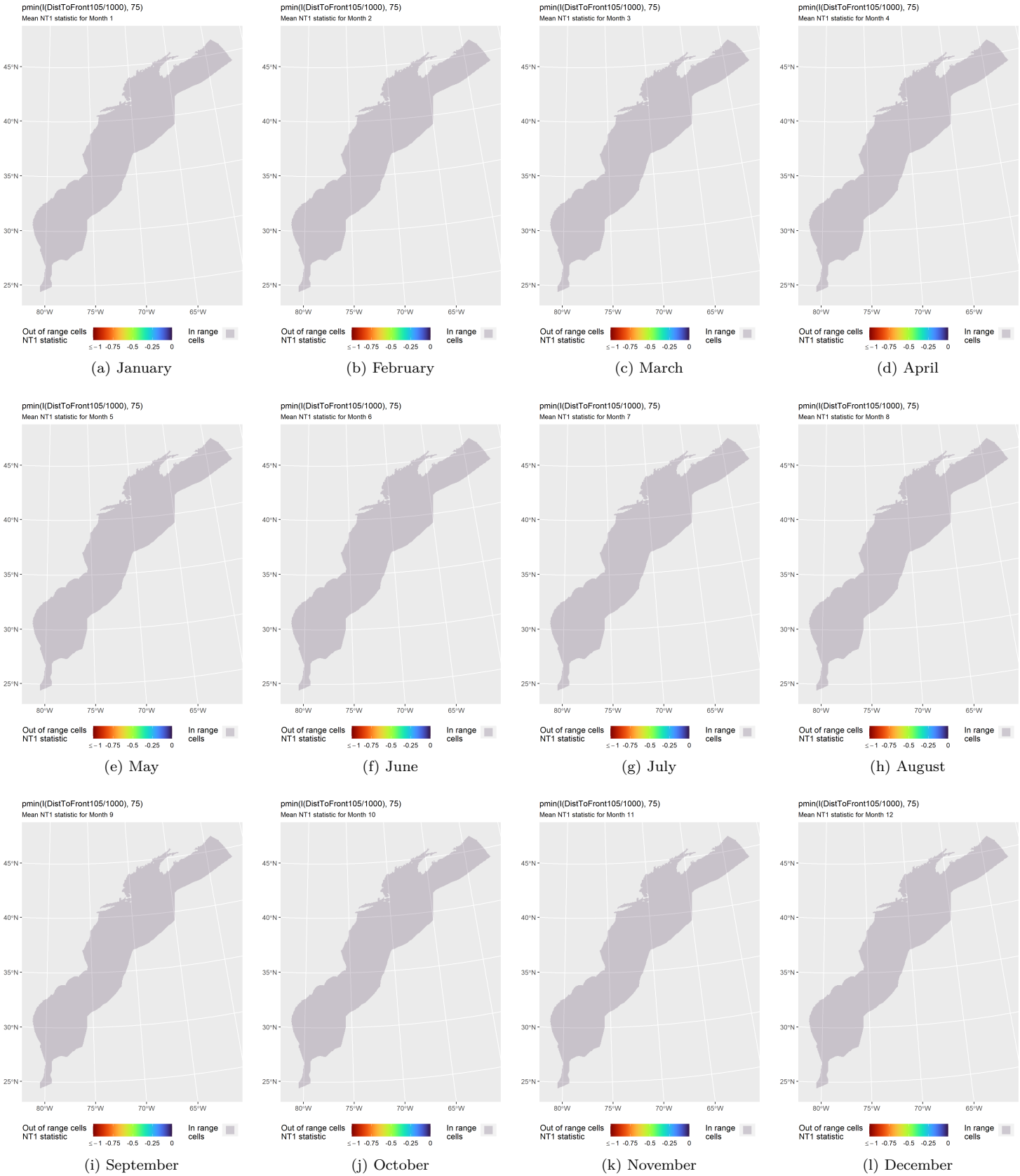

(a) January (b) February (c) March (d) April

(e) May (f) June (g) July (h) August

(i) September (j) October (k) November (l) December

Figure 73: NT1 statistic (Mesgaran et al. (2014)) for the DistToFront105 covariate in the model. Areas outside the sampled range of a covariate appear in color, indicating univariate extrapolation of that covariate occurred there during the month. Areas within the sampled range appear in gray, indicating it did not occur.

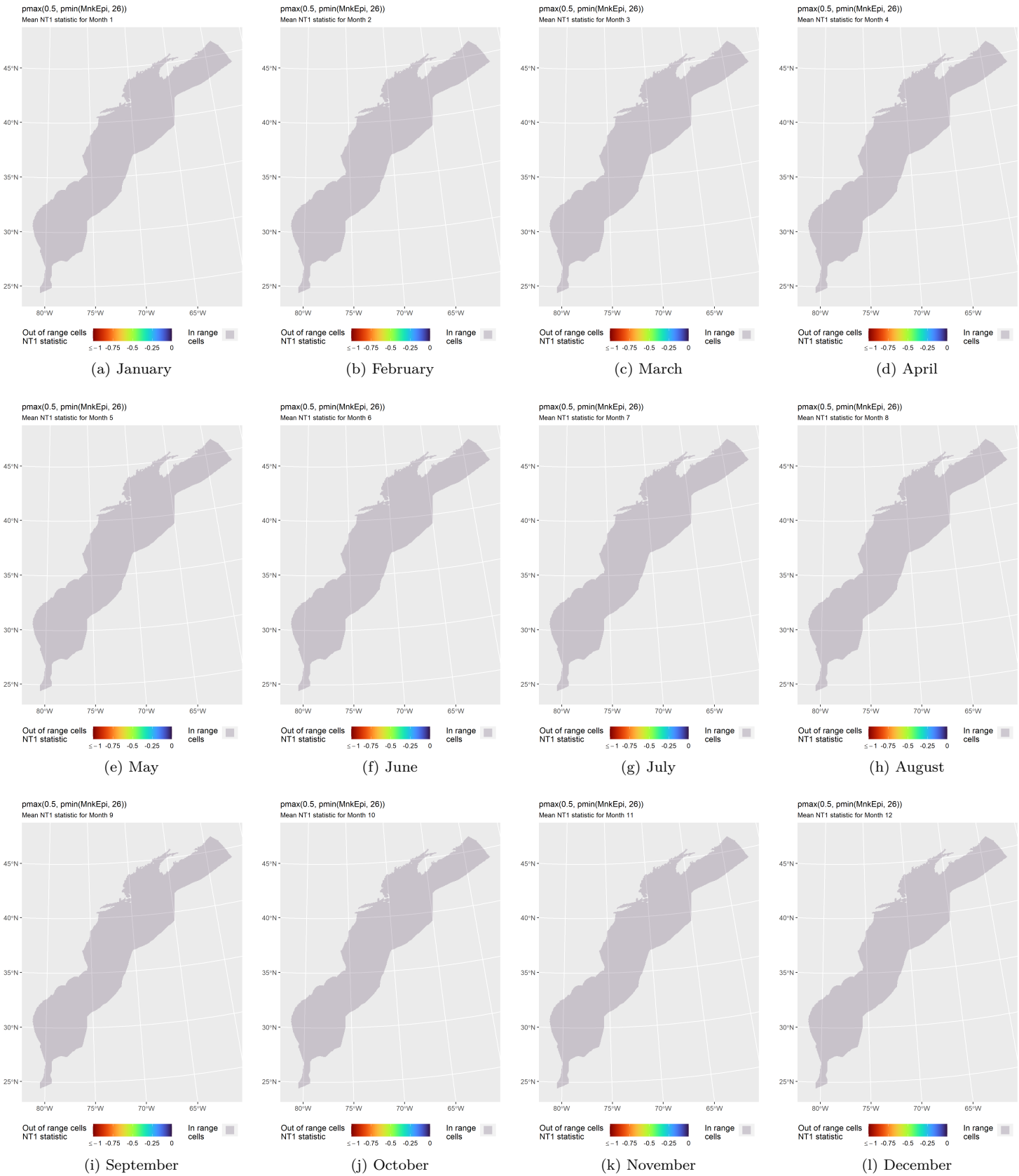

(a) January (b) February (c) March (d) April

(e) May (f) June (g) July (h) August

(i) September (j) October (k) November (l) December

Figure 74: NT1 statistic (Mesgaran et al. (2014)) for the MnkEpi covariate in the model. Areas outside the sampled range of a covariate appear in color, indicating univariate extrapolation of that covariate occurred there during the month. Areas within the sampled range appear in gray, indicating it did not occur.

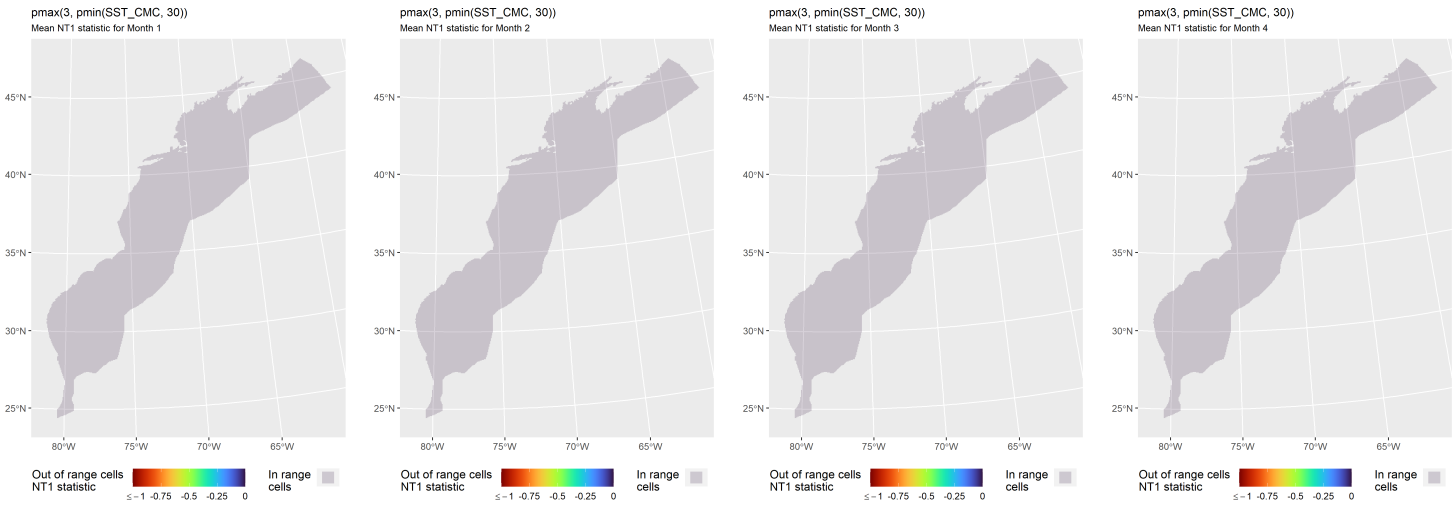

(a) January

(b) February

(c) March

(d) April

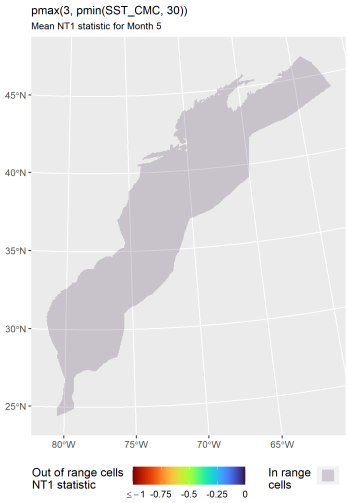

(e) May

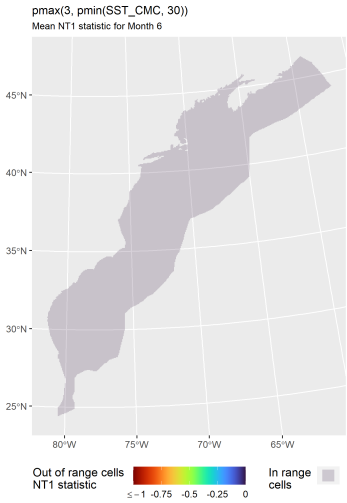

(f) June

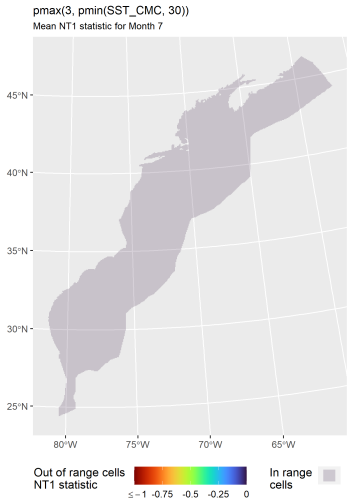

(g) July

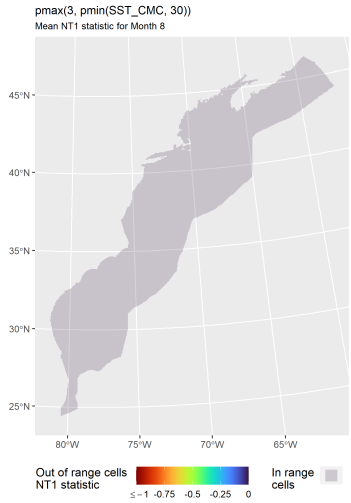

(h) August

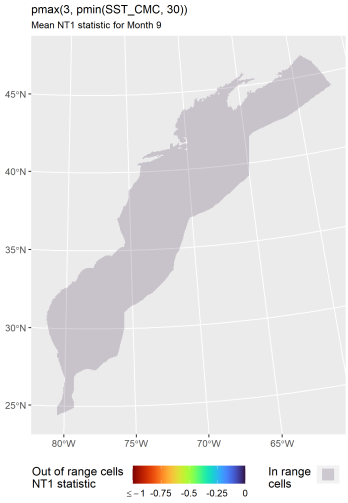

(i) September

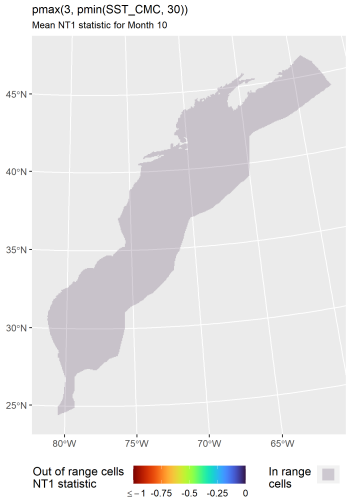

(j) October

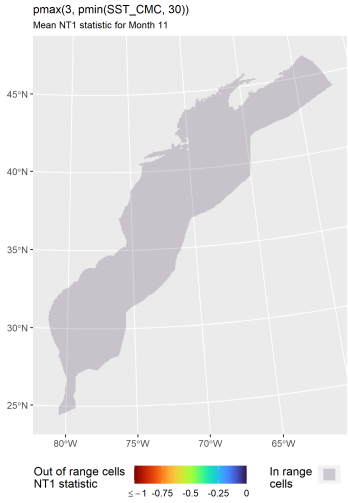

(k) November

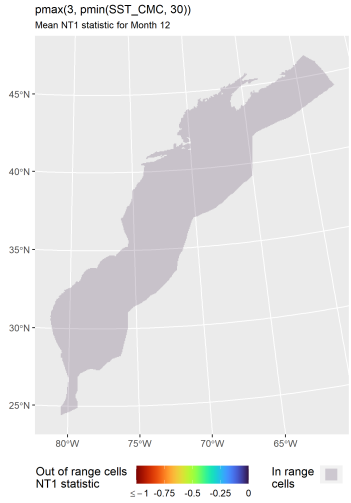

(l) December

Figure 75: NT1 statistic (Mesgaran et al. (2014)) for the SST_CMC covariate in the model. Areas outside the sampled range of a covariate appear in color, indicating univariate extrapolation of that covariate occurred there during the month. Areas within the sampled range appear in gray, indicating it did not occur.

5.3.2 Multivariate Extrapolation

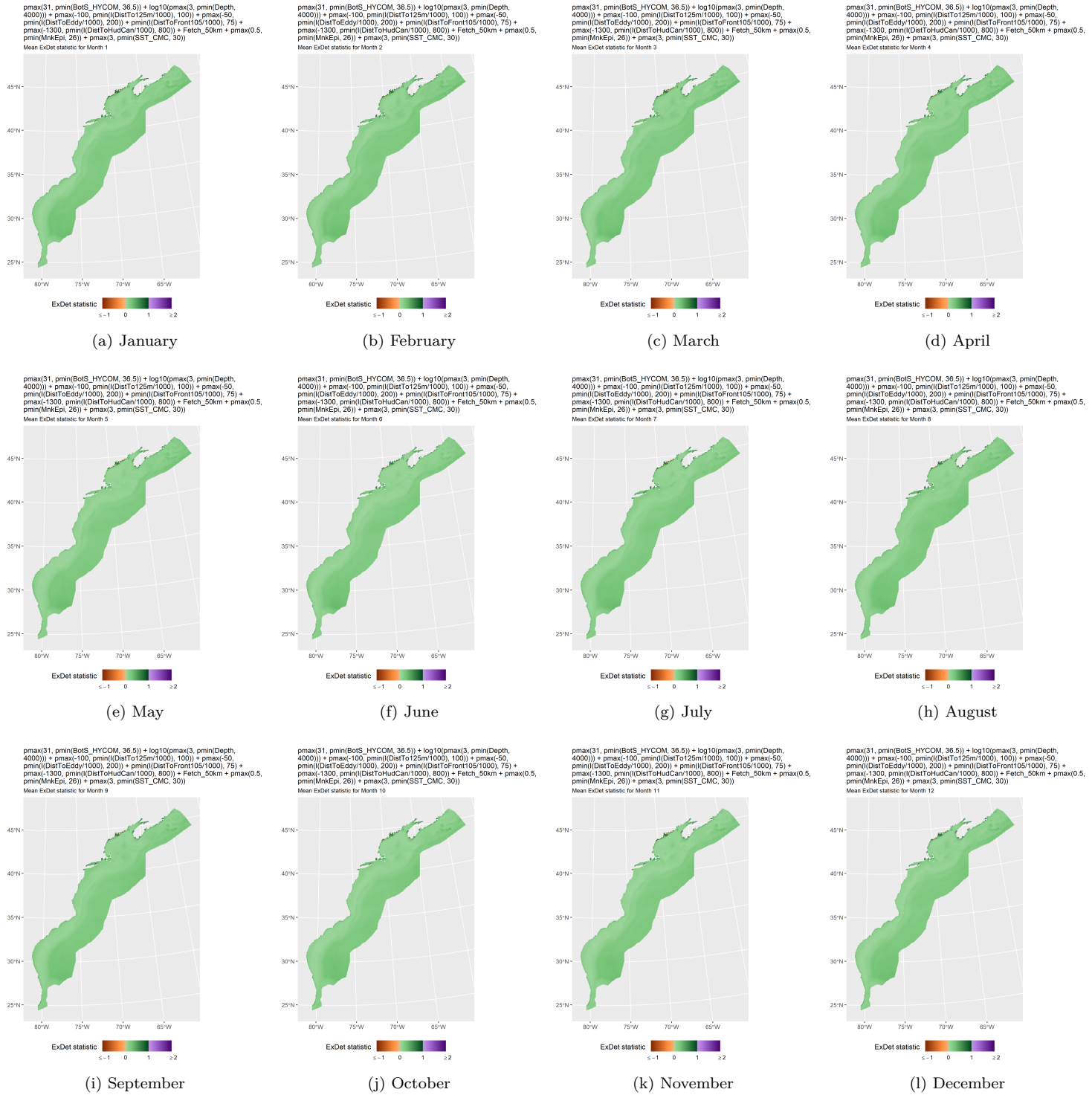

(a) January (b) February (c) March (d) April

(e) May (f) June (g) July (h) August

(i) September (j) October (k) November (l) December

Figure 76: ExDet statistic (Mesgaran et al. (2014)) for all of the covariates used in the model. Areas in orange (ExDet < 0) required univariate extrapolation of one or more covariates (see previous section). Areas in purple (ExDet > 1), did not require univariate extrapolation but did require multivariate extrapolation, by virtue of having novel combinations of covariates not represented in the survey data, according to the NT2 statistic (Mesgaran et al. (2014)). Areas in green ($0 \geq$ ExDet ≤ 1) did not require either type of extrapolation.

6 Predictions

Based on our evaluation of this model in the context of what is known of this species (see Section 7), we summarized its predictions into monthly climatological density and uncertainty surfaces, shown in the maps below.

6.1 Summarized Predictions

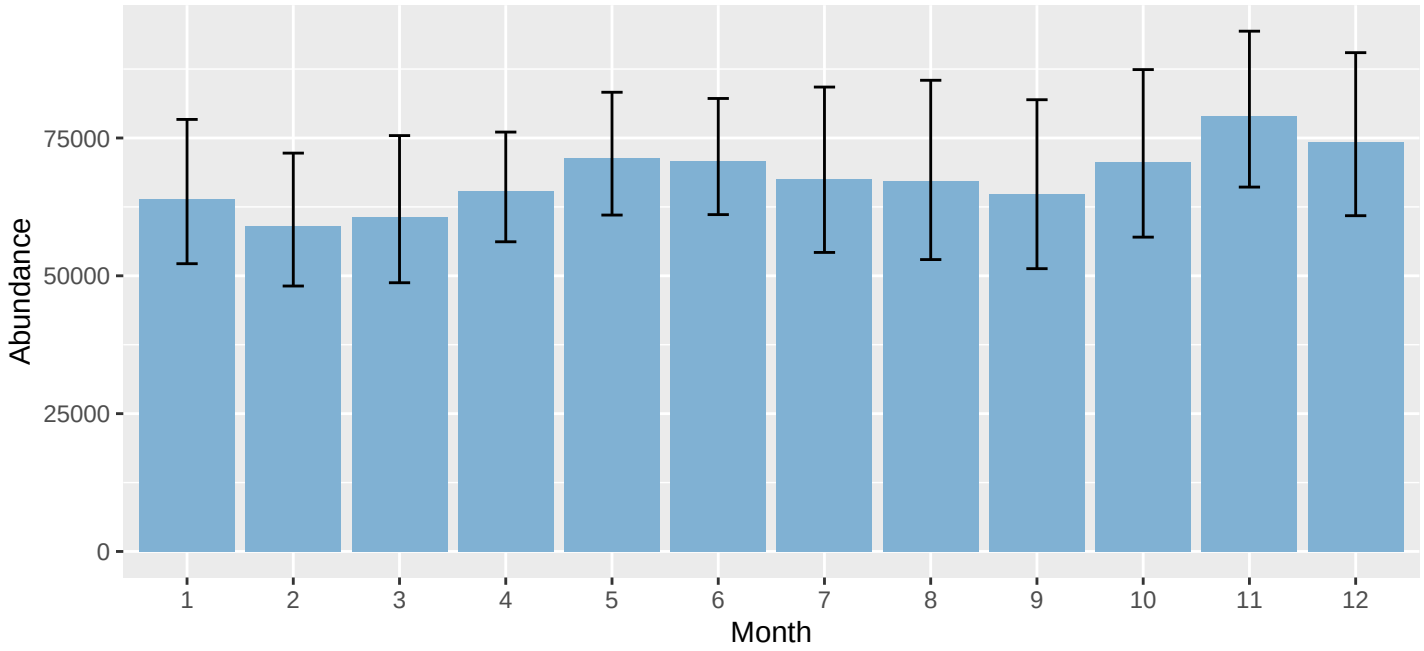

Figure 77: Mean monthly abundance for the prediction area for 1998-2019. Error bars are a 95% interval, made with a log-normal approximation using the prediction's CV. The CV was estimated with the analytic approach given by Miller et al. (2022), Appendix S1, and accounts both for uncertainty in model parameter estimates and for temporal variability in dynamic covariates.

Table 28: Mean monthly abundance and density for the prediction area for 1998-2019. CV and intervals estimated as described for the previous figure.

Month	Abundance	CV	95% Interval	Area (km^2)	Density (individuals / 100 km^2)
1	63,955	0.104	52,195 - 78,365	1,272,925	5.02
2	58,984	0.104	48,150 - 72,255	1,272,925	4.63
3	60,637	0.112	48,742 - 75,435	1,272,925	4.76
4	65,369	0.077	56,173 - 76,071	1,272,925	5.14
5	71,291	0.080	61,018 - 83,294	1,272,925	5.60
6	70,856	0.076	61,102 - 82,166	1,272,925	5.57
7	67,592	0.113	54,237 - 84,235	1,272,925	5.31
8	67,269	0.123	52,948 - 85,464	1,272,925	5.28
9	64,831	0.120	51,297 - 81,936	1,272,925	5.09
10	70,595	0.109	57,017 - 87,406	1,272,925	5.55
11	78,974	0.091	66,091 - 94,367	1,272,925	6.20
12	74,231	0.101	60,904 - 90,475	1,272,925	5.83

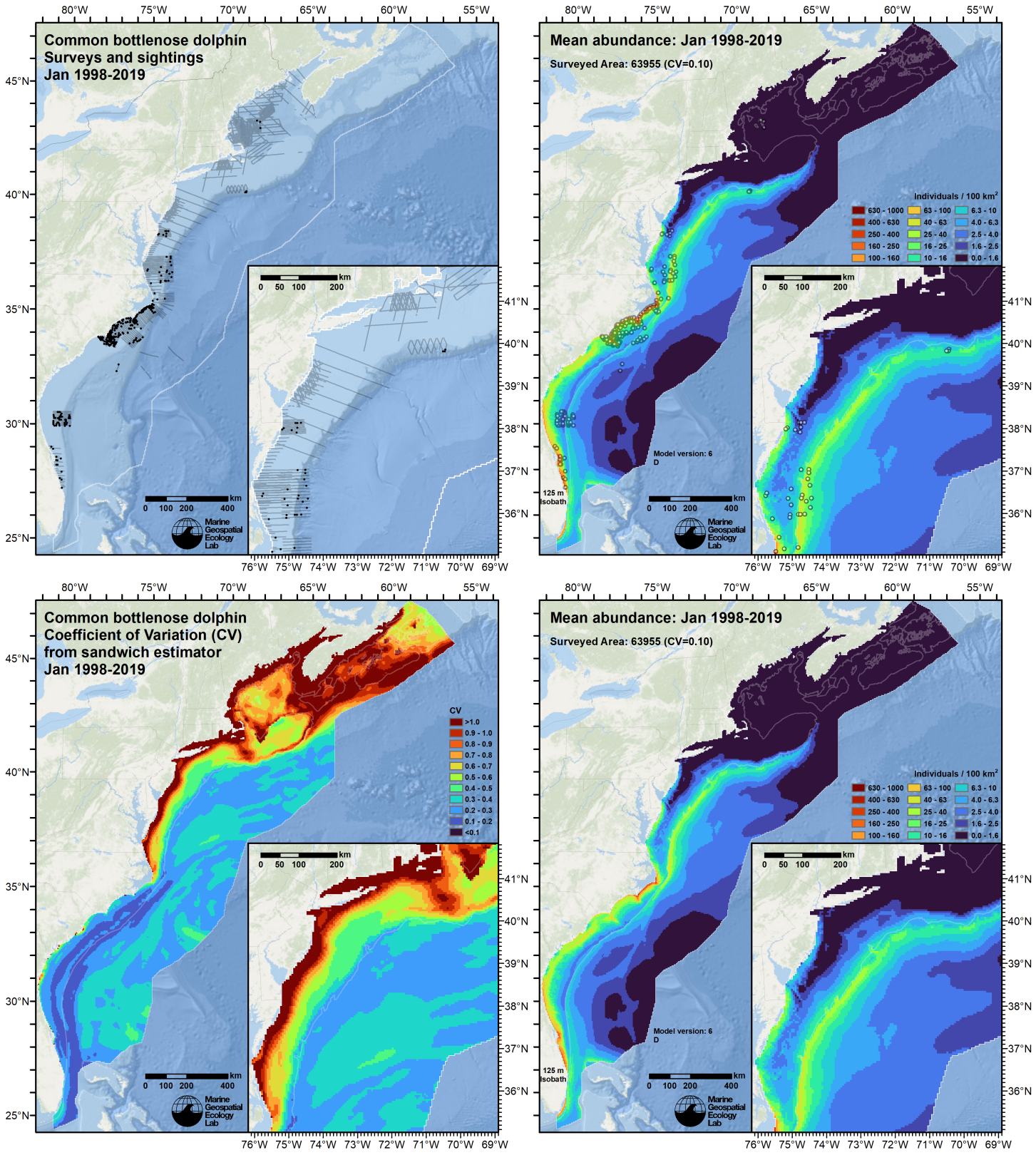

Figure 78: Survey effort and observations (top left), predicted density with observations (top right), predicted density without observations (bottom right), and coefficient of variation of predicted density (bottom left), for the month of January for the given era. Variance was estimated with the analytic approach given by Miller et al. (2022), Appendix S1, and accounts both for uncertainty in model parameter estimates and for temporal variability in dynamic covariates.

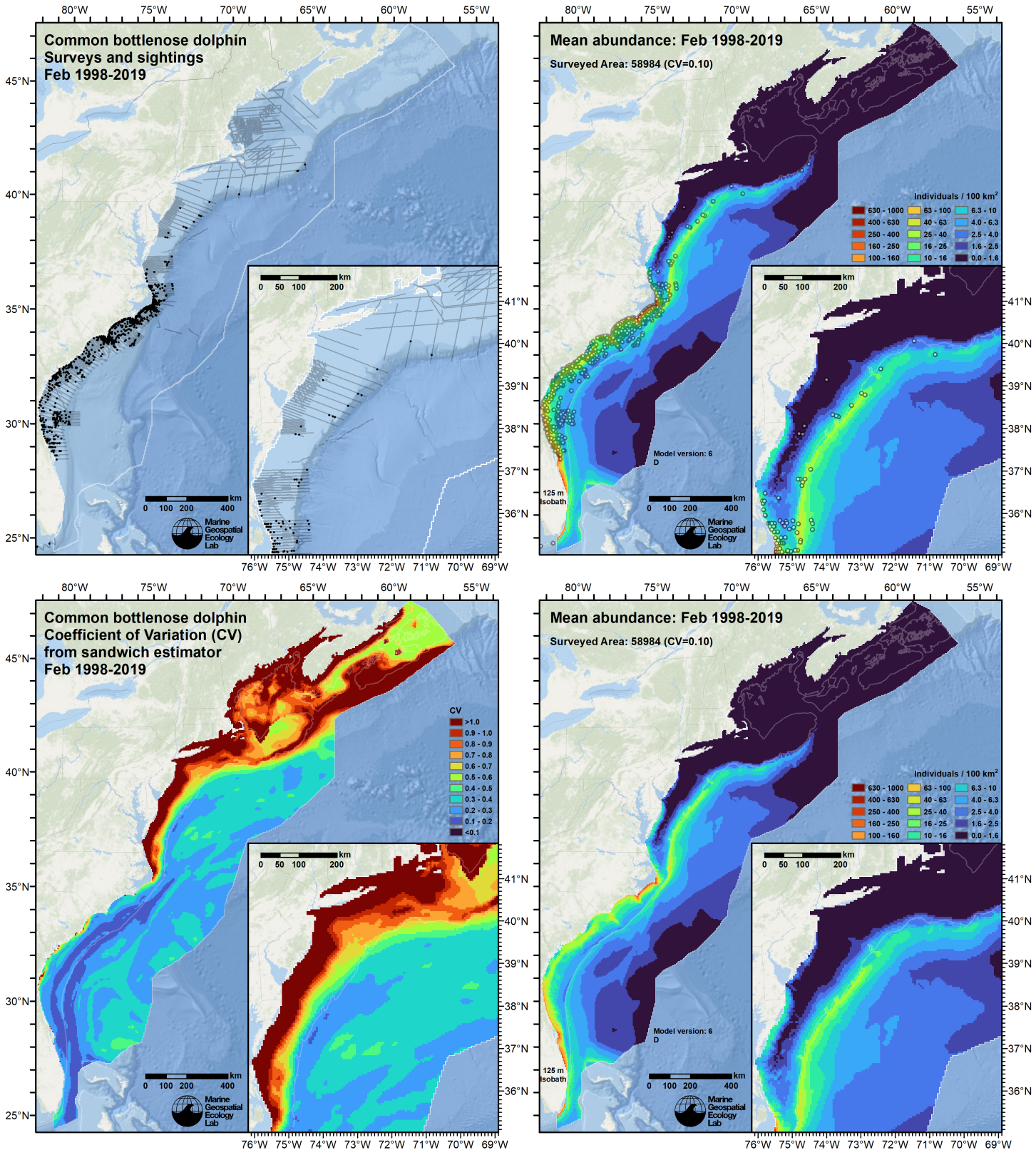

Figure 79: Survey effort and observations (top left), predicted density with observations (top right), predicted density without observations (bottom right), and coefficient of variation of predicted density (bottom left), for the month of February for the given era. Variance was estimated with the analytic approach given by Miller et al. (2022), Appendix S1, and accounts both for uncertainty in model parameter estimates and for temporal variability in dynamic covariates.

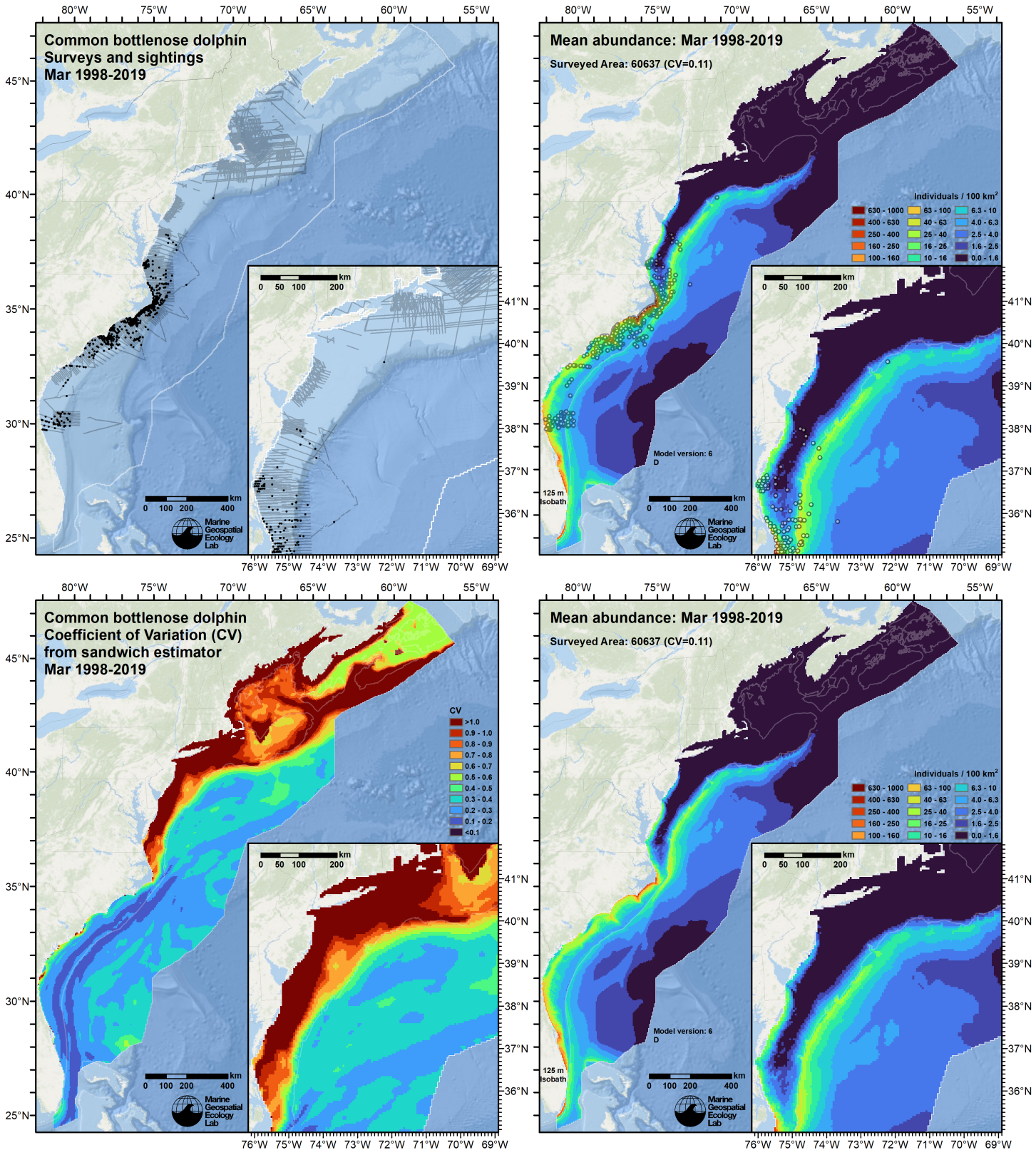

Figure 80: Survey effort and observations (top left), predicted density with observations (top right), predicted density without observations (bottom right), and coefficient of variation of predicted density (bottom left), for the month of March for the given era. Variance was estimated with the analytic approach given by Miller et al. (2022), Appendix S1, and accounts both for uncertainty in model parameter estimates and for temporal variability in dynamic covariates.

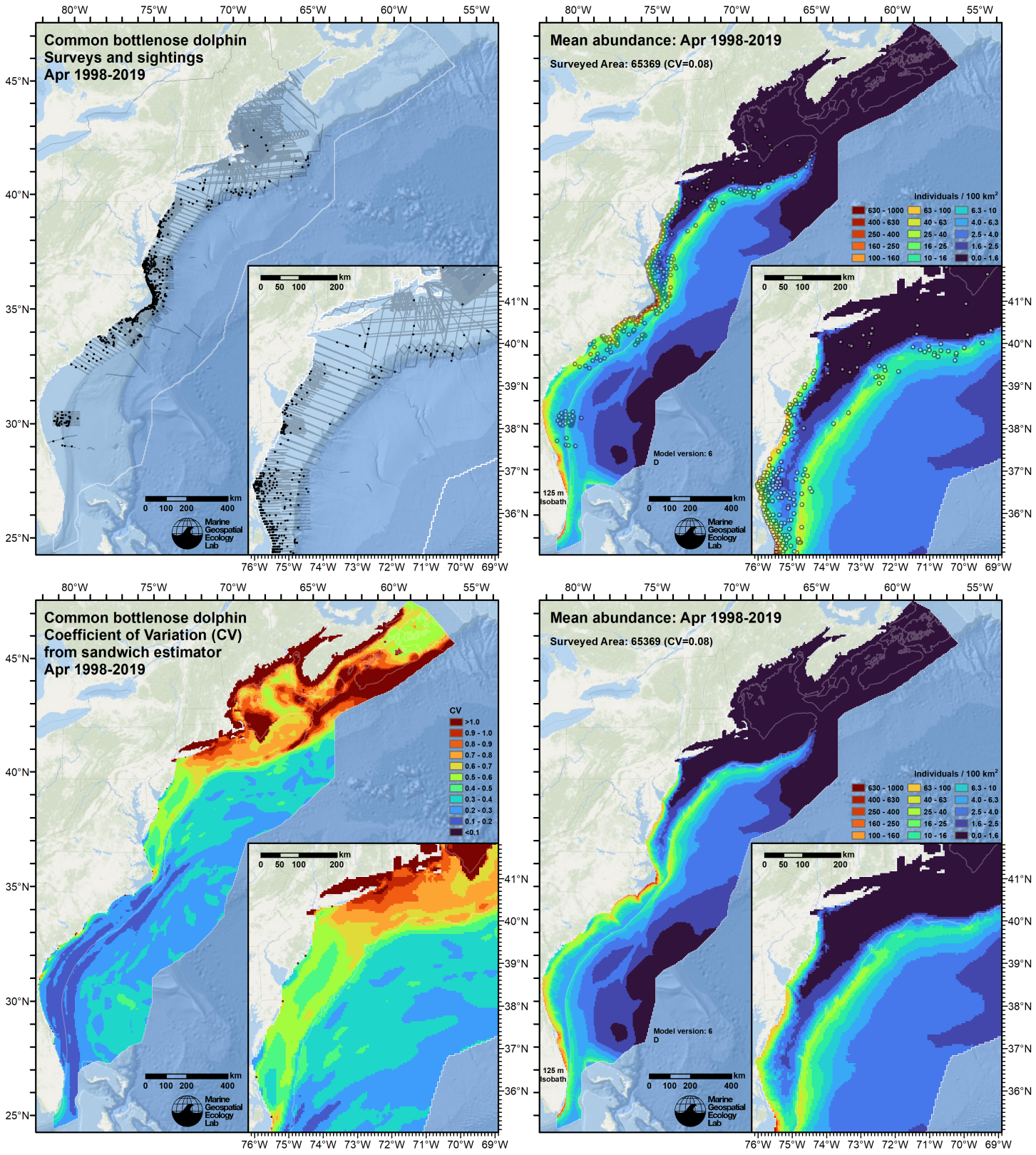

Figure 81: Survey effort and observations (top left), predicted density with observations (top right), predicted density without observations (bottom right), and coefficient of variation of predicted density (bottom left), for the month of April for the given era. Variance was estimated with the analytic approach given by Miller et al. (2022), Appendix S1, and accounts both for uncertainty in model parameter estimates and for temporal variability in dynamic covariates.

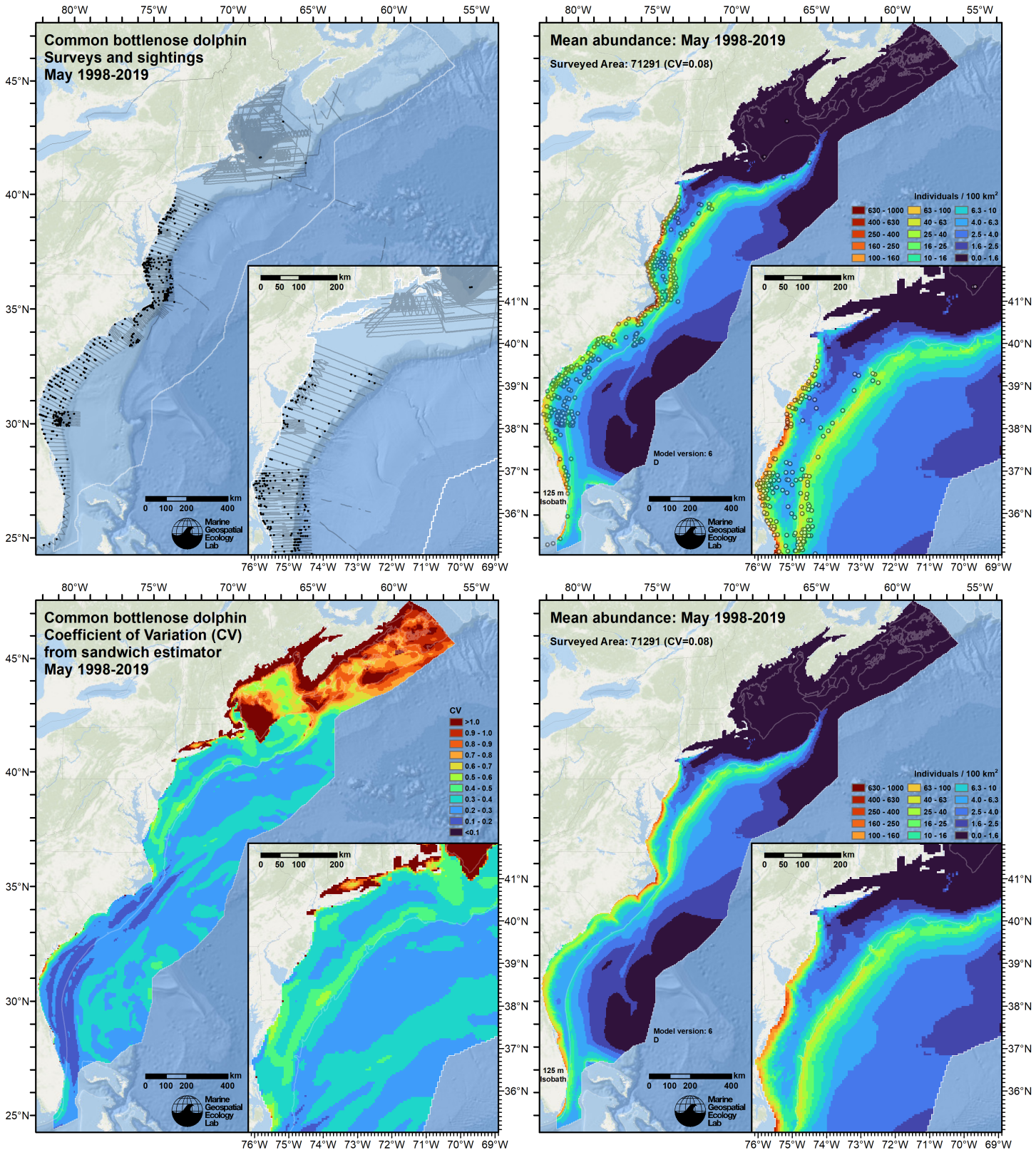

Figure 82: Survey effort and observations (top left), predicted density with observations (top right), predicted density without observations (bottom right), and coefficient of variation of predicted density (bottom left), for the month of May for the given era. Variance was estimated with the analytic approach given by Miller et al. (2022), Appendix S1, and accounts both for uncertainty in model parameter estimates and for temporal variability in dynamic covariates.

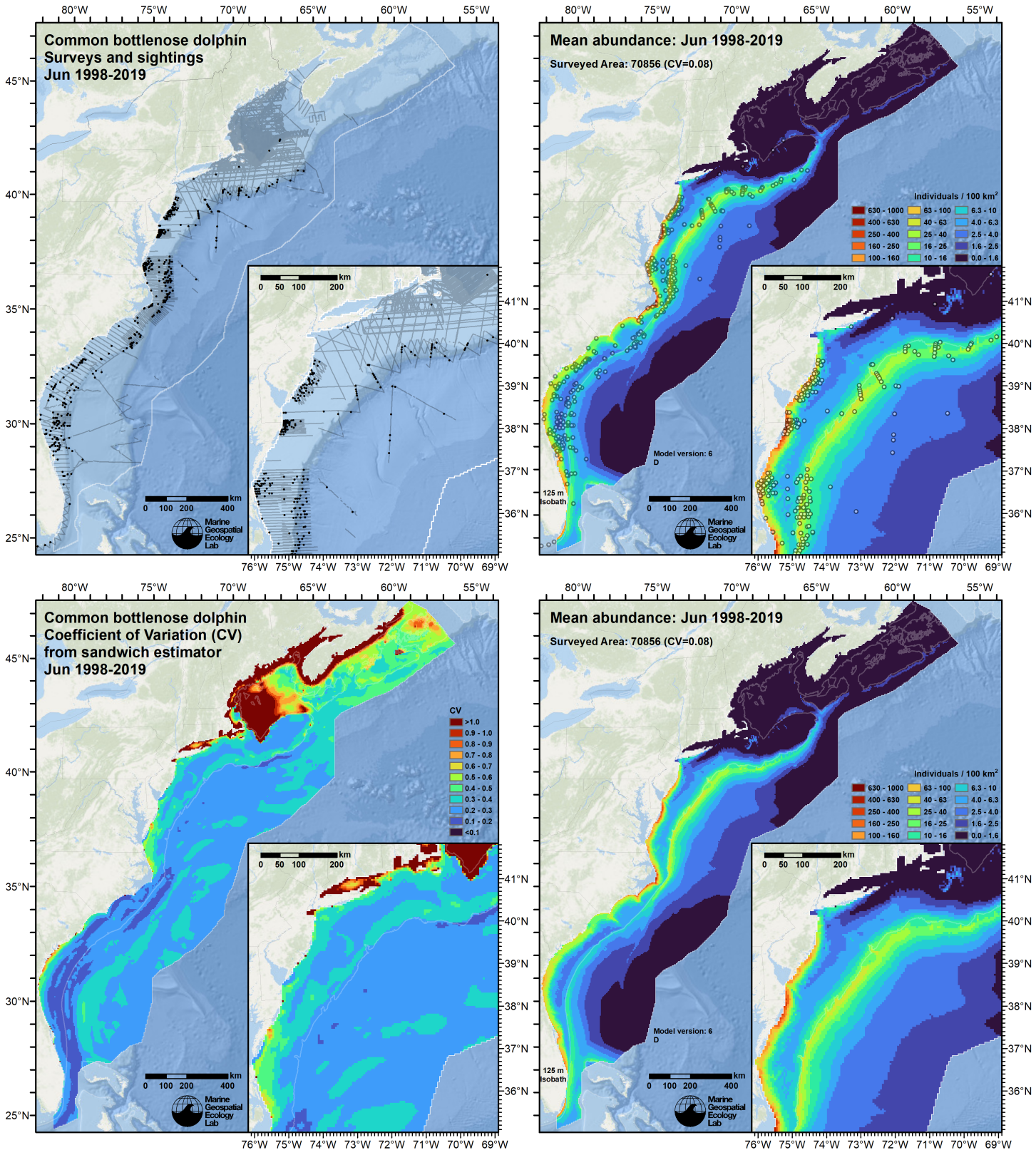

Figure 83: Survey effort and observations (top left), predicted density with observations (top right), predicted density without observations (bottom right), and coefficient of variation of predicted density (bottom left), for the month of June for the given era. Variance was estimated with the analytic approach given by Miller et al. (2022), Appendix S1, and accounts both for uncertainty in model parameter estimates and for temporal variability in dynamic covariates.

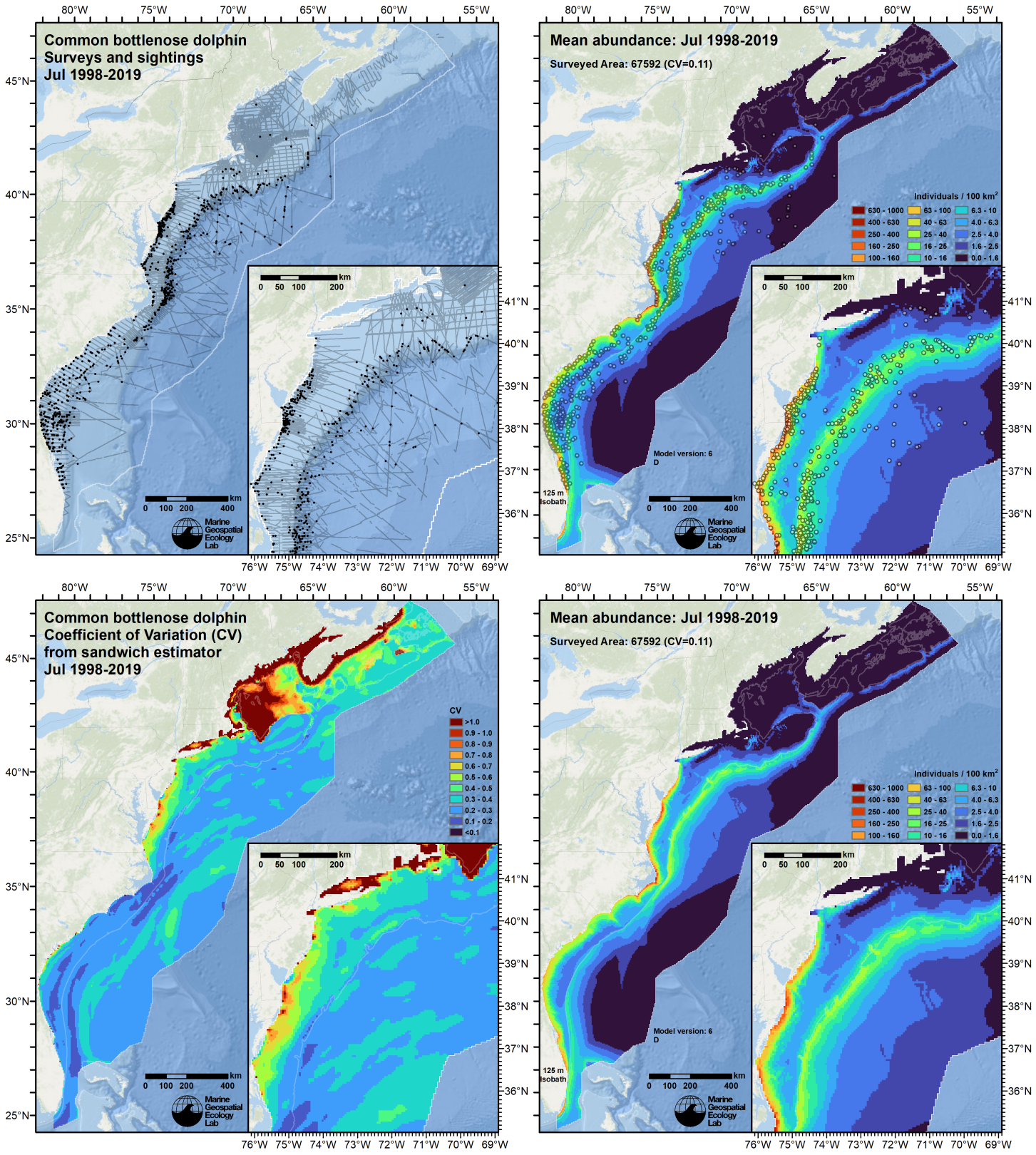

Figure 84: Survey effort and observations (top left), predicted density with observations (top right), predicted density without observations (bottom right), and coefficient of variation of predicted density (bottom left), for the month of July for the given era. Variance was estimated with the analytic approach given by Miller et al. (2022), Appendix S1, and accounts both for uncertainty in model parameter estimates and for temporal variability in dynamic covariates.

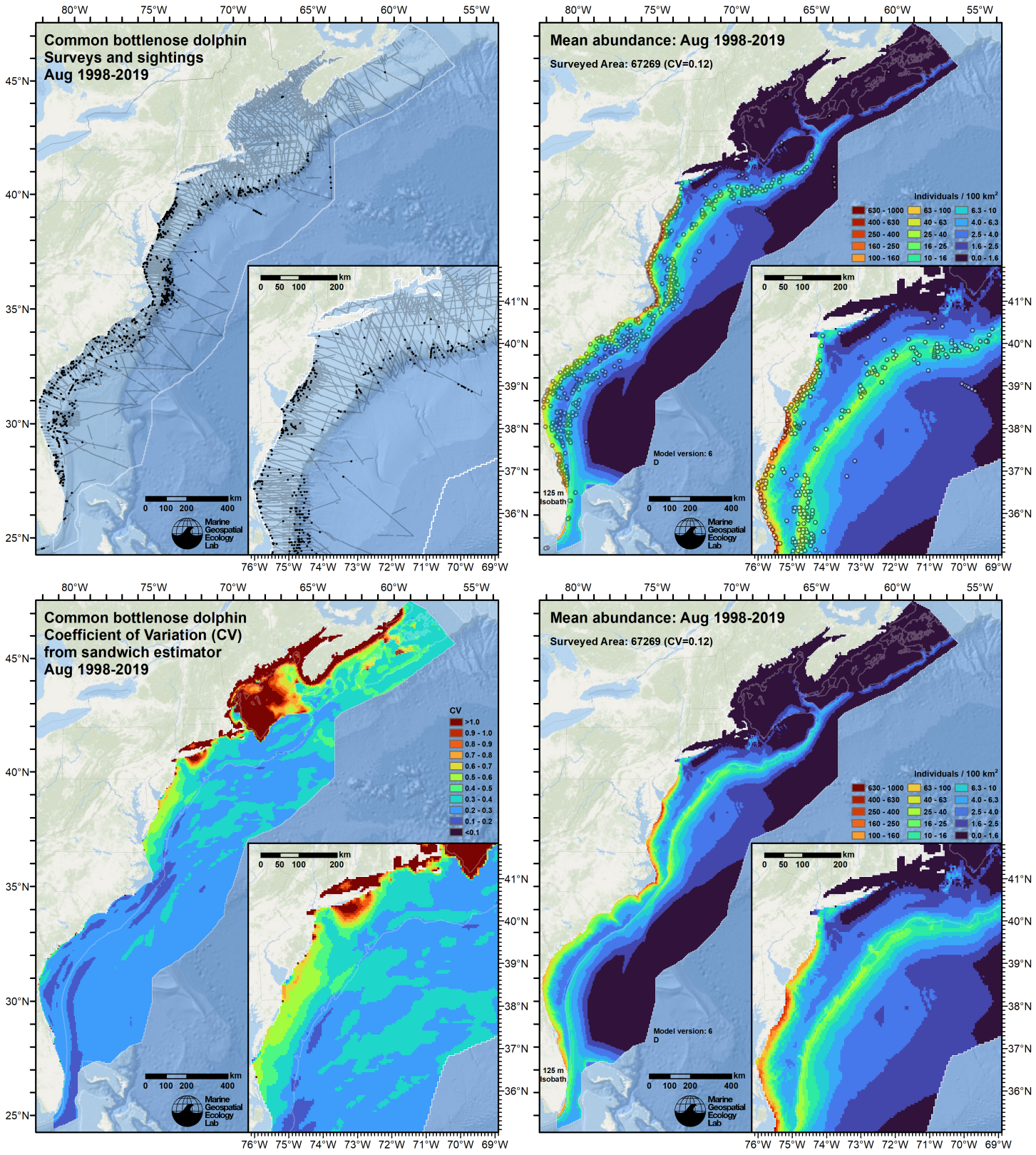

Figure 85: Survey effort and observations (top left), predicted density with observations (top right), predicted density without observations (bottom right), and coefficient of variation of predicted density (bottom left), for the month of August for the given era. Variance was estimated with the analytic approach given by Miller et al. (2022), Appendix S1, and accounts both for uncertainty in model parameter estimates and for temporal variability in dynamic covariates.

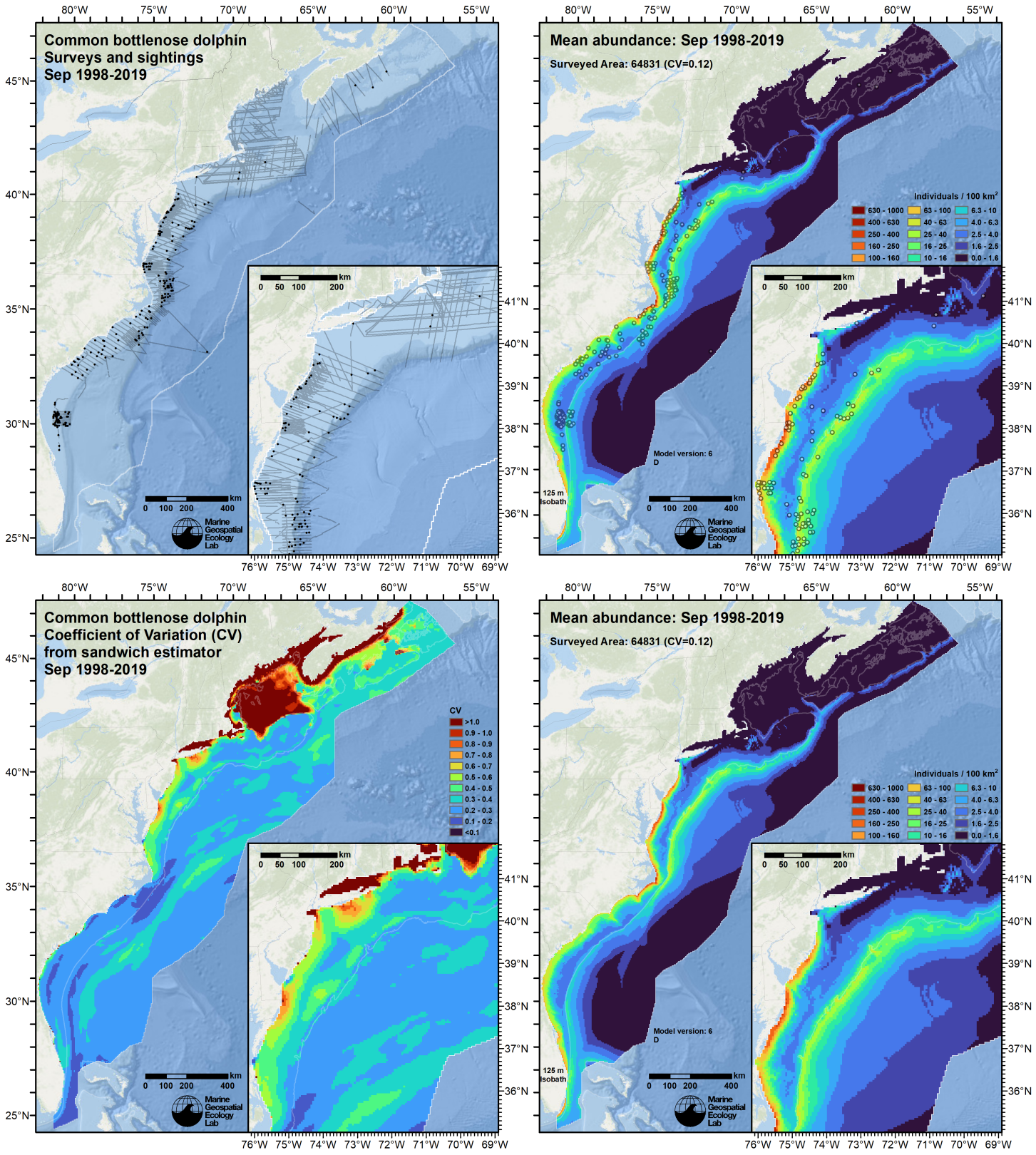

Figure 86: Survey effort and observations (top left), predicted density with observations (top right), predicted density without observations (bottom right), and coefficient of variation of predicted density (bottom left), for the month of September for the given era. Variance was estimated with the analytic approach given by Miller et al. (2022), Appendix S1, and accounts both for uncertainty in model parameter estimates and for temporal variability in dynamic covariates.

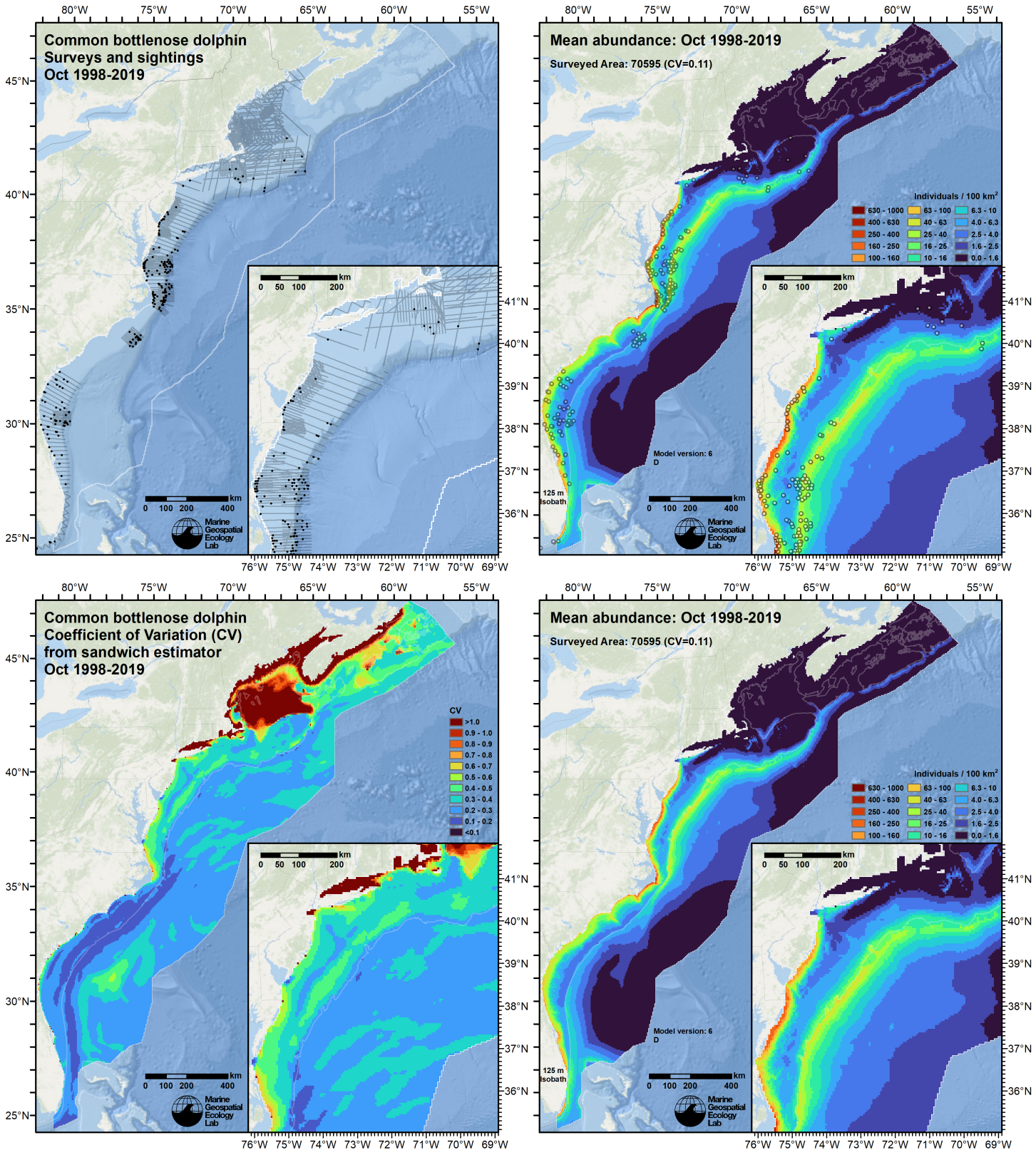

Figure 87: Survey effort and observations (top left), predicted density with observations (top right), predicted density without observations (bottom right), and coefficient of variation of predicted density (bottom left), for the month of October for the given era. Variance was estimated with the analytic approach given by Miller et al. (2022), Appendix S1, and accounts both for uncertainty in model parameter estimates and for temporal variability in dynamic covariates.

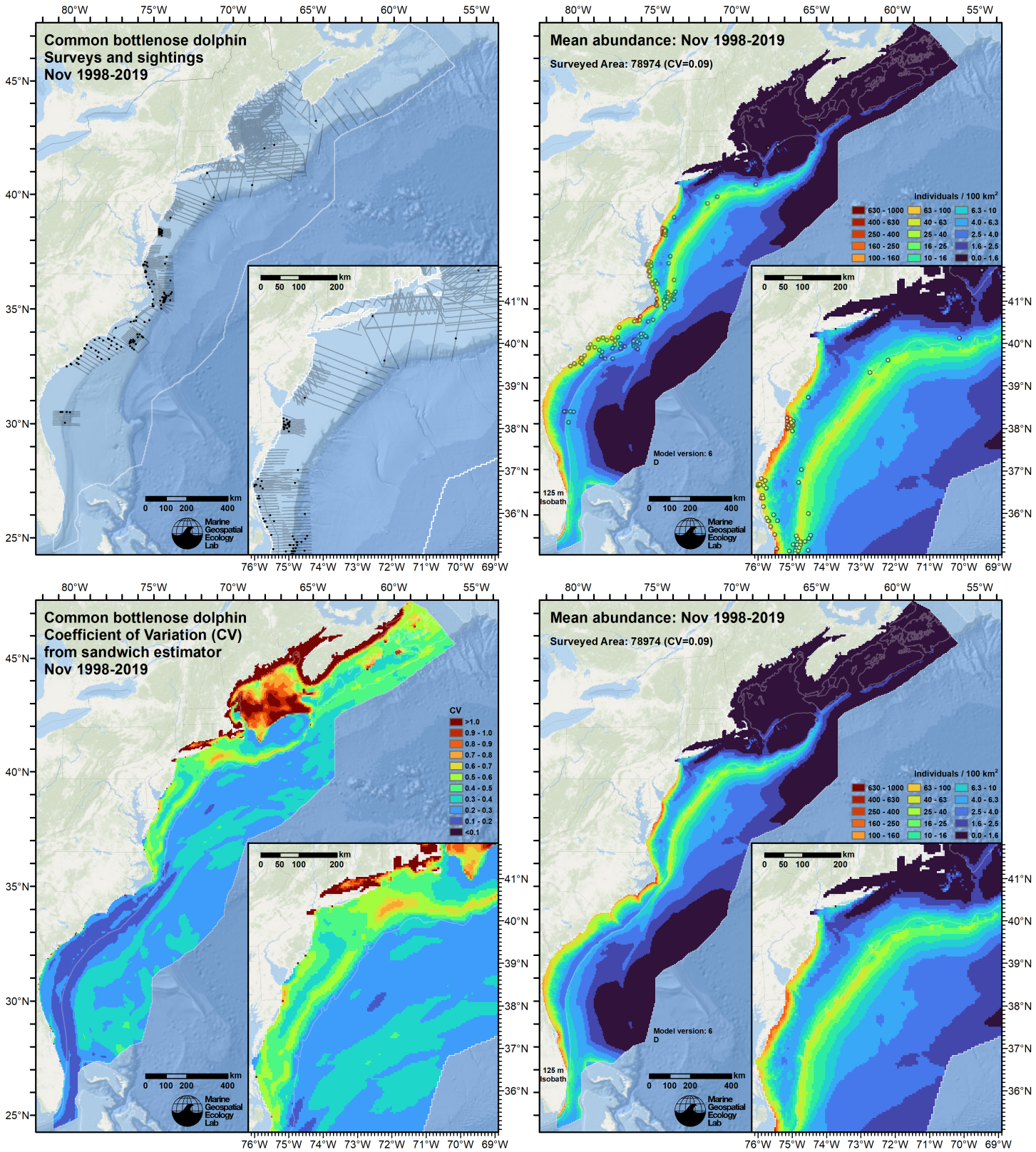

Figure 88: Survey effort and observations (top left), predicted density with observations (top right), predicted density without observations (bottom right), and coefficient of variation of predicted density (bottom left), for the month of November for the given era. Variance was estimated with the analytic approach given by Miller et al. (2022), Appendix S1, and accounts both for uncertainty in model parameter estimates and for temporal variability in dynamic covariates.

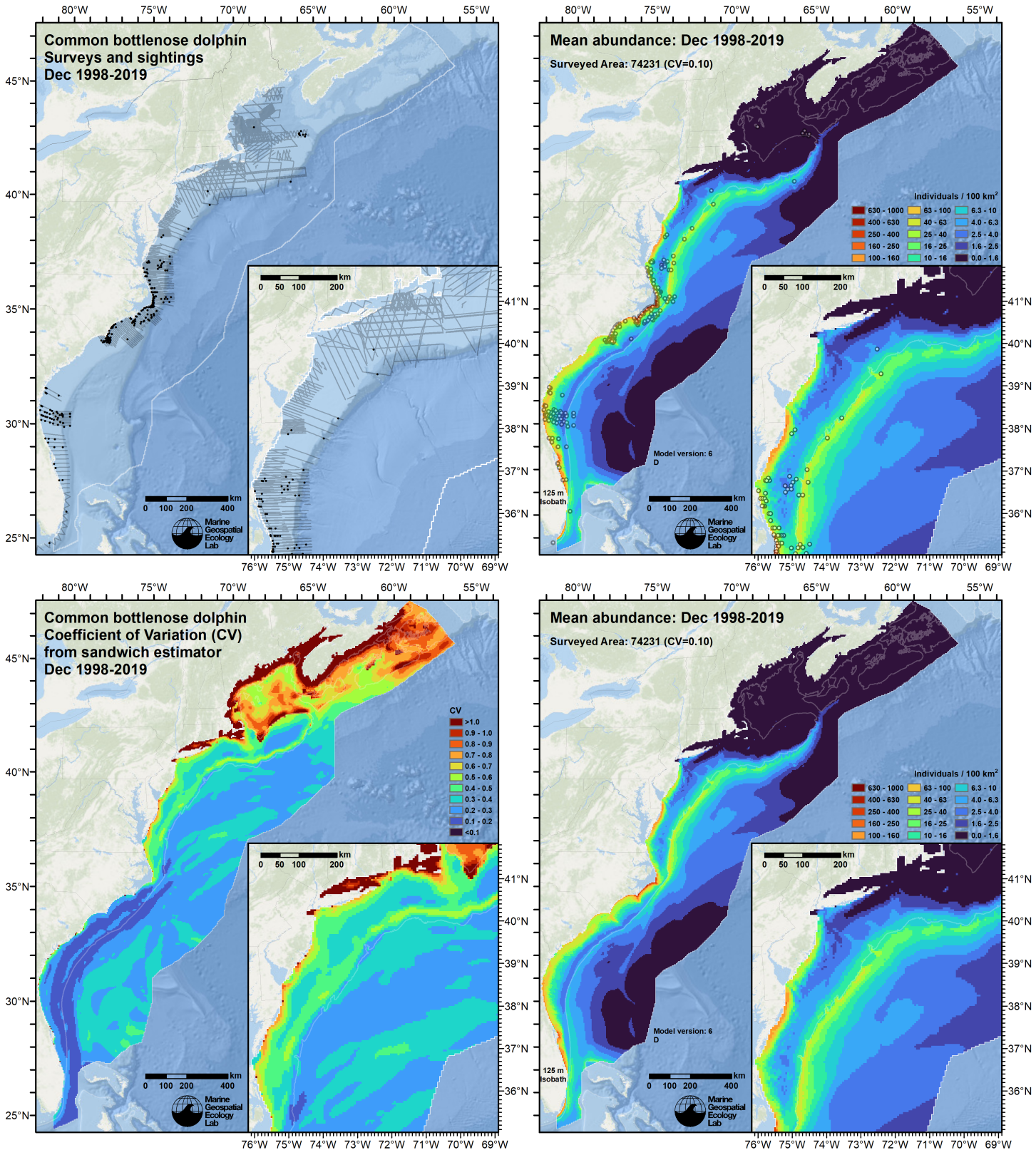

Figure 89: Survey effort and observations (top left), predicted density with observations (top right), predicted density without observations (bottom right), and coefficient of variation of predicted density (bottom left), for the month of December for the given era. Variance was estimated with the analytic approach given by Miller et al. (2022), Appendix S1, and accounts both for uncertainty in model parameter estimates and for temporal variability in dynamic covariates.

6.2 Abundance Comparisons

6.2.1 NOAA Stock Assessment Reports

Table 29: Comparison of regional abundance estimates from NOAA Stock Assessment Reports (SARs) to estimates from this density model extracted from roughly comparable zones (Figure 90 below). The SAR estimates were based on a single year of surveying, while the model estimates were taken from the multi-year mean density surfaces we provide to model users (Section 6.1).

Stock Assessment Report				Density Model		
Month/Year	Stock Area	N_{est}	SAR	Period	Zone	Abundance
Jun-Aug 2016	WNA Offshore, Central FL to NJ[a]	44,893	2019			
Jul-Aug 2016	WNA Northern Migratory Coastal[b]	6,639	2020			
Jul-Aug 2016	WNA Southern Migratory Coastal[b]	3,751	2020			
Jul-Aug 2016	WNA SC/GA Coastal[b]	6,027	2017			
Jul-Aug 2016	WNA Northern FL Coastal[b]	877	2017			
Jul-Aug 2016	WNA Central FL Coastal[b]	1,218	2017			
Jul-Aug 2016	Total, Offshore+Coastal, Central FL to NJ	63,405		Jun-Aug 1998-2019	SEFSC	54,014
Jun-Aug 2016	WNA Offshore, NJ to Lower Bay of Fundy[c]	17,958	2019	Jun-Aug 1998-2019	NEFSC	12,969
Jun-Aug 2016	Bay of Fundy/Scotian Shelf[d]			Jun-Aug 1998-2019	Canada	1,510
Jun-Aug 2016	Grand Total	81,363		Jun-Aug 1998-2019	Total	68,493

[a] Estimate originally from Garrison (2020).
[b] Estimates originally from Garrison et al. (2017).
[c] Estimate originally from Palka (2020).
[d] The SAR did not provide an estimate for this area. DFO's 2016 survey of the Scotian Shelf reported 7 sightings totalling 29 individuals but did not estimate abundance (Lawson and Gosselin (2018)).

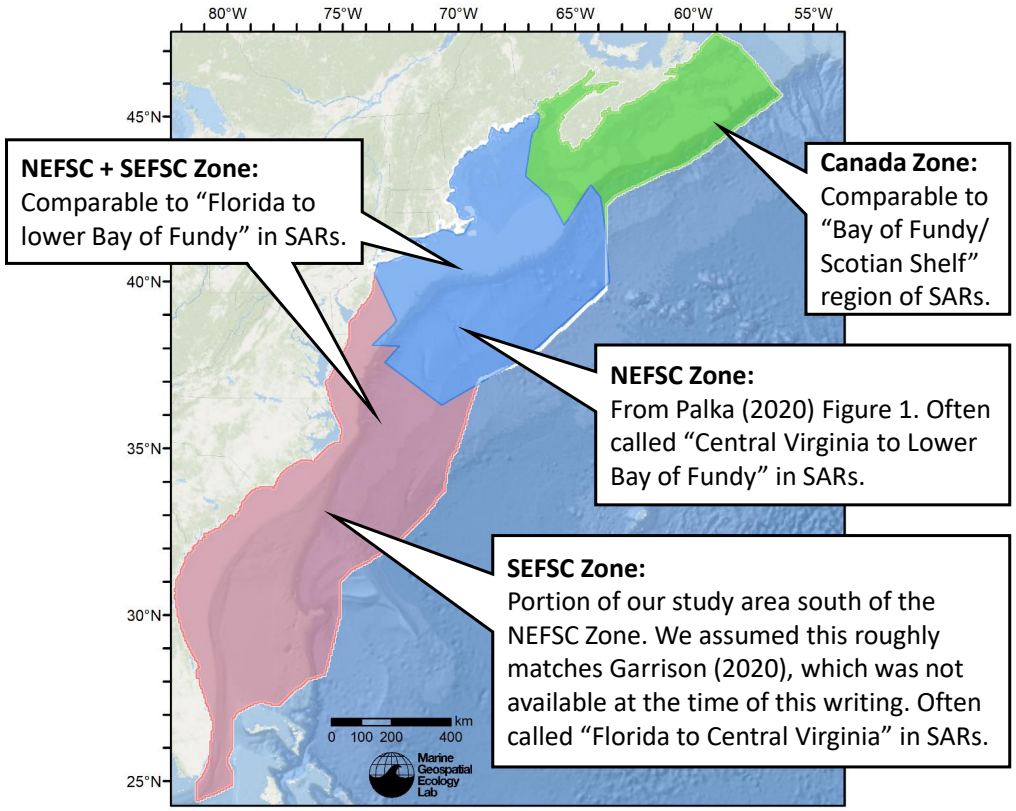

Figure 90: Zones for which we extracted abundance estimates from the density model for comparison to estimates from the NOAA Stock Assessment Report.

6.2.2 Previous Density Model

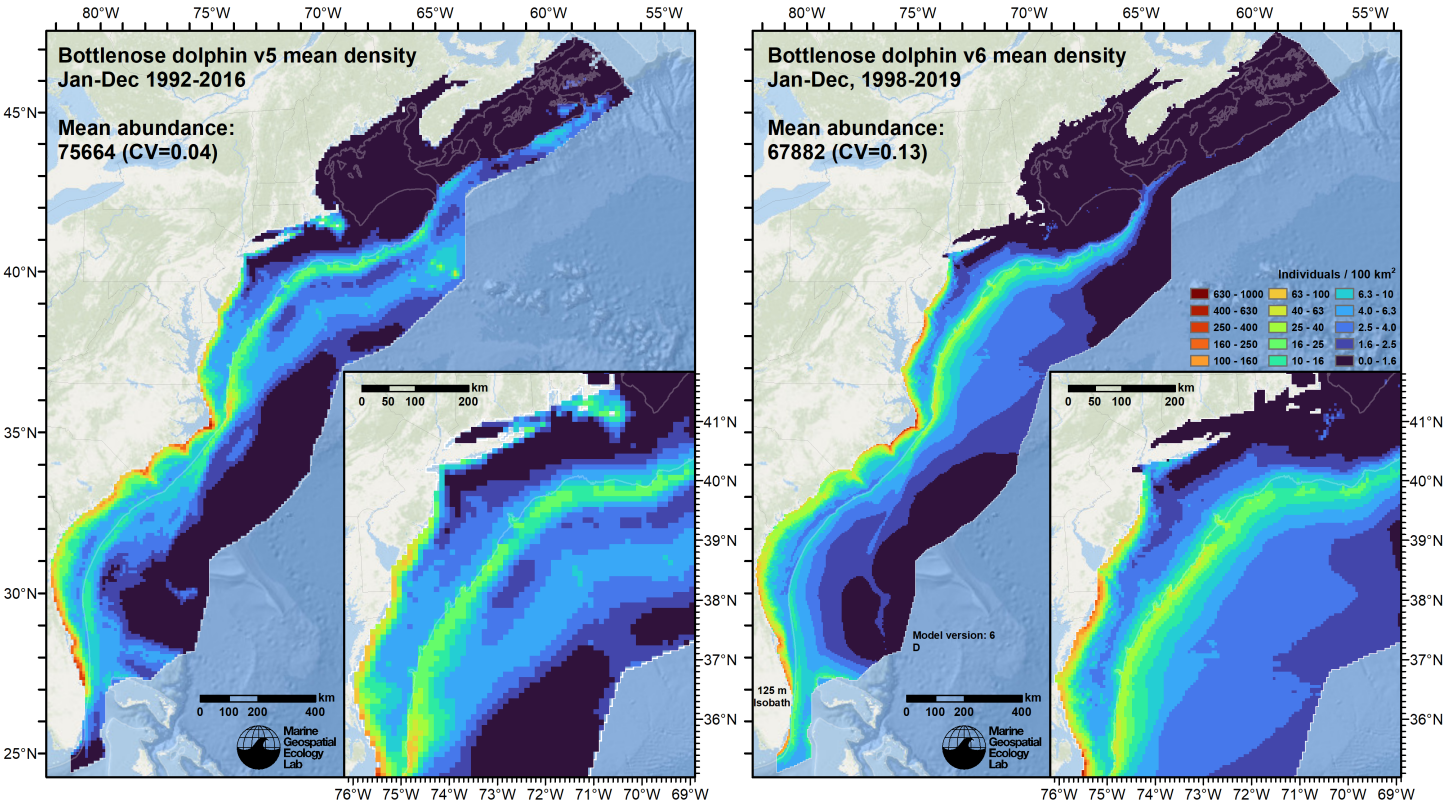

Figure 91: Comparison of the mean density predictions from the previous model (left) released by Roberts et al. (2018) to those from this model (right).

7 Discussion

When summarized across the modeled period (1998-2019), mean monthly density maps (Figures 78-89) broadly agreed with the overall distribution and seasonal pattern described in the literature. The model predicted highest densities close to shore, concentrated in the southeast and mid-Atlantic (Figure 62), where the coastal morphotype predominates. On the shelf, density remained high south of Cape Hatteras in all seasons. Monthly predictions showed density moving up the coast as spring progressed, reaching southern New England in summer, persisting through fall, and retreating south in early winter (Figures 78-89). Another band of elevated density, presumably of the offshore morphotype, occurred over the upper continental slope and spanned the study area (Figure 62), with a peak at Cape Hatteras, and diminishing at the northeast Scotian Shelf, where bottlenose dolphins have been sighted occasionally (Baird et al. 1993; Gowans and Whitehead 1995; Lawson and Gosselin 2009, 2018). This band persisted in all seasons as far north as the Northeast Channel of the Gulf of Maine. While sightings of bottlenose dolphins were reported around Georges Bank or in the Gulf of Maine in all seasons, most surveys of the continental slope occurred in summer, and we urge caution with model predictions in colder months.

Given the general match between the model's predictions and what has been reported in the literature, we elected to offer density predictions for this species at monthly temporal resolution.

Mean monthly abundance predicted by our model for the prediction region ranged from a low of 58,984 in February to a high of 78,974 in November (Figure 77; Table 28). NOAA gives population estimates for summer months (June-August) on a per-stock basis, which must be summed in order to obtain a total estimate for the species. Our model encompassed the entire coast between Florida and the Gulf. of St. Lawrence but excluded estuarine regions that bottlenose dolphins are known to inhabit. We therefore believe our model roughly comprises the five coastal and one offshore stock defined by NOAA for the western North Atlantic. Our model's mean summer (June-August) abundance (68,493) was 16% lower than the total abundance (81,363) of those stocks reported in the most recent NOAA SARs (Table 29). Regionally, our model predicted lower abundance in both the region covered by SEFSC, known in the SARs as "Central Florida to New Jersey" and presumed to encompass all five coastal stocks plus the offshore stock south of New Jersey (Figure 90), and in the region covered by NEFSC, known in the SARs as "New Jersey to lower Bay of Fundy" and presumed to comprise only the offshore stock north of New Jersey.

East coast bottlenose dolphins are known to suffer recurrent cetacean morbillivirus epizootics (Duignan et al. 2006) that can kill large fractions of affected stocks. During one such event in 1987-88, more than half of the inshore population between Florida and New Jersey may have died (Taubenberger et al. 1996). A similar event occurred from July 1, 2013 through March 1, 2015. As far as we know, mortality estimates for this event have not been published in the peer-reviewed literature yet, and analysis by NOAA is ongoing, but the total number of known strandings (over 1600) more than doubled that of the 1987-88 event (about 740) (https://www.fisheries.noaa.gov/national/marine-life-distress/2013-2015-bottlenose-dolphin-unusual-mortality-event-mid-atlantic). Populations are believed to have recovered somewhat in the years after such events (L. Garrison, pers. comm.). Given these wide fluctuations in the population, we do not find it surprising that our multi-decade estimate differed from NOAA's single-year estimate. However, because NOAA's estimate occurred in 2016, soon after the 2013-2015 event, we might expect their estimate to be lower than ours, not higher. We therefore urge caution and will continue to investigate possible reasons for this difference in our next modeling cycle.

References

Baird RW, Walters EL, Stacey PJ (1993) Status of the bottlenose dolphin, Tursiops truncatus, with special reference to Canada. Canadian Field-Naturalist 107:466–480.

Barco SG, Burt L, DePerte A, Digiovanni R Jr. (2015) Marine Mammal and Sea Turtle Sightings in the Vicinity of the Maryland Wind Energy Area July 2013-June 2015, VAQF Scientific Report #2015-06. Virginia Aquarium & Marine Science Center Foundation, Virginia Beach, VA

Barlow J, Forney KA (2007) Abundance and population density of cetaceans in the California Current ecosystem. Fishery Bulletin 105:509–526.

Becker JJ, Sandwell DT, Smith WHF, Braud J, Binder B, Depner J, Fabre D, Factor J, Ingalls S, Kim S-H, Ladner R, Marks K, Nelson S, Pharaoh A, Trimmer R, Von Rosenberg J, Wallace G, Weatherall P (2009) Global Bathymetry and Elevation Data at 30 Arc Seconds Resolution: SRTM30_PLUS. Marine Geodesy 32:355–371. doi: 10.1080/01490410903297766

Brasnett B (2008) The impact of satellite retrievals in a global sea-surface-temperature analysis. Quarterly Journal of the Royal Meteorological Society 134:1745–1760. doi: 10.1002/qj.319

Breiman L (2001) Random Forests. Machine Learning 45:5–32. doi: 10.1023/A:1010933404324

Buckland ST, Anderson DR, Burnham KP, Laake JL, Borchers DL, Thomas L (2001) Introduction to Distance Sampling: Estimating Abundance of Biological Populations. Oxford University Press, Oxford, UK

Burt ML, Borchers DL, Jenkins KJ, Marques TA (2014) Using mark-recapture distance sampling methods on line transect surveys. Methods in Ecology and Evolution 5:1180–1191. doi: 10.1111/2041-210X.12294

Canada Meteorological Center (2012) GHRSST Level 4 CMC0.2deg Global Foundation Sea Surface Temperature Analysis Version 2.0. PODAAC, CA, USA. doi: 10.5067/GHCMC-4FM02

Canada Meteorological Center (2016) GHRSST Level 4 CMC0.1deg Global Foundation Sea Surface Temperature Analysis Version 3.0. PODAAC, CA, USA. doi: 10.5067/GHCMC-4FM03

Canny JF (1986) A computational approach to edge detection. IEEE Transactions on Pattern Analysis and Machine Intelligence 8:679–698. doi: 10.1016/B978-0-08-051581-6.50024-6

Carretta JV, Lowry MS, Stinchcomb CE, Lynn MS, E. CR (2000) Distribution and abundance of marine mammals at San Clemente Island and surrounding offshore waters: Results from aerial and ground surveys in 1998 and 1999. NOAA Administrative Report LJ-00-02. NOAA National Marine Fisheries Service, Southwest Fisheries Center, La Jolla, CA

Chassignet E, Hurlburt H, Metzger EJ, Smedstad O, Cummings J, Halliwell G, Bleck R, Baraille R, Wallcraft A, Lozano C, Tolman H, Srinivasan A, Hankin S, Cornillon P, Weisberg R, Barth A, He R, Werner F, Wilkin J (2009) US GODAE: Global Ocean Prediction with the HYbrid Coordinate Ocean Model (HYCOM). Oceanog 22:64–75. doi: 10.5670/oceanog.2009.39

Chelton DB, Schlax MG, Samelson RM (2011) Global observations of nonlinear mesoscale eddies. Progress in Oceanography 91:167–216. doi: 10.1016/j.pocean.2011.01.002

Cole T, Gerrior P, Merrick RL (2007) Methodologies of the NOAA National Marine Fisheries Service Aerial Survey Program for Right Whales (Eubalaena glacialis) in the Northeast U.S., 1998-2006. U.S. Department of Commerce, Woods Hole, MA

Costa APB, Mcfee W, Wilcox LA, Archer FI, Rosel PE (2022) The common bottlenose dolphin (*Tursiops Truncatus*) ecotypes of the western North Atlantic revisited: An integrative taxonomic investigation supports the presence of distinct species. Zoological Journal of the Linnean Society zlac025. doi: 10.1093/zoolinnean/zlac025

Cotter MP (2019) Aerial Surveys for Protected Marine Species in the Norfolk Canyon Region: 2018–2019 Final Report. HDR, Inc., Virginia Beach, VA

Duignan PJ, House C, Odell DK, Wells RS, Hansen LJ, Walsh MT, Aubin DJSt, Rima BK, Geraci JR (2006) Morbillivirus Infection in Bottlenose Dolphins: Evidence for Recurrent Epizootics in the Western Atlantic and Gulf of Mexico. Marine Mammal Science 12:499–515. doi: 10.1111/j.1748-7692.1996.tb00063.x

Foley HJ, Paxton CGM, McAlarney RJ, Pabst DA, Read AJ (2019) Occurrence, Distribution, and Density of Protected Species in the Jacksonville, Florida, Atlantic Fleet Training and Testing (AFTT) Study Area. Duke University Marine Lab, Beaufort, NC

Garnesson P, Mangin A, Fanton d'Andon O, Demaria J, Bretagnon M (2019) The CMEMS GlobColour chlorophyll *a* product based on satellite observation: Multi-sensor merging and flagging strategies. Ocean Science 15:819–830. doi: 10.5194/os-15-819-2019

Garrison LP (2020) Abundance of cetaceans along the southeast U.S. East coast from a summer 2016 vessel survey. PRD Contribution # PRD-2020-04. NOAA National Marine Fisheries Service, Southeast Fisheries Science Center, Miami, FL

Garrison LP, Martinez A, Maze-Foley K (2010) Habitat and abundance of cetaceans in Atlantic Ocean continental slope waters off the eastern USA. Journal of Cetacean Research and Management 11:267–277.

Garrison LP, Barry K, Hoggard W (2017) The abundance of coastal morphotype bottlenose dolphins on the U.S. East coast: 2002-2016. NOAA National Marine Fisheries Service, Southeast Fisheries Science Center, Miami, FL

Geo-Marine, Inc. (2010) New Jersey Department of Environmental Protection Baseline Studies Final Report Volume III: Marine Mammal and Sea Turtle Studies. Geo-Marine, Inc., Plano, TX

Gowans S, Whitehead H (1995) Distribution and habitat partitioning by small odontocetes in the Gully, a submarine canyon on the Scotian Shelf. Can J Zool 73:1599–1608. doi: 10.1139/z95-190

Hayes SA, Josephson E, Maze-Foley K, Rosel PE, Byrd B, Chavez-Rosales S, Cole TVN, Engleby L, Garrison LP, Hatch J, Henry A, Horstman SC, Litz J, Lyssikatos MC, Mullin KD, Orphanides C, Pace RM, Palka DL, Soldevilla M, Wenzel FW (2018) US Atlantic and Gulf of Mexico Marine Mammal Stock Assessments - 2017: (Second edition). NOAA National Marine Fisheries Service, Northeast Fisheries Science Center, Woods Hole, MA

Hayes SA, Josephson E, Maze-Foley K, Rosel PE, Byrd B, Chavez-Rosales S, Cole TV, Garrison LP, Hatch J, Henry A, Horstman SC, Litz J, Lyssikatos MC, Mullin KD, Orphanides C, Pace RM, Palka DL, Powell J, Wenzel FW (2020) US Atlantic and Gulf of Mexico Marine Mammal Stock Assessments - 2019. NOAA National Marine Fisheries Service, Northeast Fisheries Science Center, Woods Hole, MA

Hayes SA, Josephson E, Maze-Foley K, Rosel PE, Wallace J, Brossard A, Chavez-Rosales S, Cole TVN, Garrison LP, Hatch J, Henry A, Horstman SC, Litz J, Lyssikatos MC, Mullin KD, Murray K, Orphanides C, Ortega-Ortiz J, Pace RM, Palka DL, Powell J, Rappucci G, Soldevilla M, Wenzel FW (2022) US Atlantic and Gulf of Mexico Marine Mammal Stock Assessments 2021. NOAA National Marine Fisheries Service, Northeast Fisheries Science Center, Woods Hole, MA

Hothorn T, Hornik K, Zeileis A (2006) Unbiased Recursive Partitioning: A Conditional Inference Framework. Journal of Computational and Graphical Statistics 15:651–674. doi: 10.1198/106186006X133933

Laake JL, Calambokidis J, Osmek SD, Rugh DJ (1997) Probability of Detecting Harbor Porpoise From Aerial Surveys: Estimating g(0). Journal of Wildlife Management 61:63–75. doi: 10.2307/3802415

Lawson JW, Gosselin J-F (2009) Distribution and preliminary abundance estimates for cetaceans seen during Canada's Marine Megafauna Survey-A component of the 2007 TNASS. Department of Fisheries and Oceans, St. John's, NL, Canada

Lawson JW, Gosselin J-F (2018) Estimates of cetacean abundance from the 2016 NAISS aerial surveys of eastern Canadian waters, with a comparison to estimates from the 2007 TNASS. NAMMCO SC/25/AE/09. In: Proceedings of the NAMMCO 25th Scientific Committee (SC). North Atlantic Marine Mammal Commission, Bergen-Tromsø, Norway,

Lehodey P, Senina I, Murtugudde R (2008) A spatial ecosystem and populations dynamics model (SEAPODYM)–Modeling of tuna and tuna-like populations. Progress in Oceanography 78:304–318. doi: 10.1016/j.pocean.2008.06.004

Lehodey P, Conchon A, Senina I, Domokos R, Calmettes B, Jouanno J, Hernandez O, Kloser R (2015) Optimization of a micronekton model with acoustic data. ICES Journal of Marine Science 72:1399–1412. doi: 10.1093/icesjms/fsu233

Mallette SD, Lockhart GG, McAlarney RJ, Cummings EW, McLellan WA, Pabst DA, Barco SG (2014) Documenting Whale Migration off Virginia's Coast for Use in Marine Spatial Planning: Aerial and Vessel Surveys in the Proximity of the Virginia Wind Energy Area (VA WEA), VAQF Scientific Report 2014-08. Virginia Aquarium & Marine Science Center Foundation, Virginia Beach, VA

Mallette SD, Lockhart GG, McAlarney RJ, Cummings EW, McLellan WA, Pabst DA, Barco SG (2015) Documenting Whale Migration off Virginia's Coast for Use in Marine Spatial Planning: Aerial Surveys in the Proximity of the Virginia Wind Energy Area (VA WEA) Survey/Reporting Period: May 2014 - December 2014, VAQF Scientific Report 2015-02. Virginia Aquarium & Marine Science Center Foundation, Virginia Beach, VA

Mallette SD, McAlarney RJ, Lockhart GG, Cummings EW, Pabst DA, McLellan WA, Barco SG (2017) Aerial Survey Baseline Monitoring in the Continental Shelf Region of the VACAPES OPAREA: 2016 Annual Progress Report. Virginia Aquarium & Marine Science Center Foundation, Virginia Beach, VA

Marsh H, Sinclair DF (1989) Correcting for Visibility Bias in Strip Transect Aerial Surveys of Aquatic Fauna. The Journal of Wildlife Management 53:1017. doi: 10.2307/3809604

McAlarney R, Cummings E, McLellan W, Pabst A (2018) Aerial Surveys for Protected Marine Species in the Norfolk Canyon Region: 2017 Annual Progress Report. University of North Carolina Wilmington, Wilmington, NC

McLellan WA, McAlarney RJ, Cummings EW, Read AJ, Paxton CGM, Bell JT, Pabst DA (2018) Distribution and abundance of beaked whales (Family Ziphiidae) Off Cape Hatteras, North Carolina, U.S.A. Marine Mammal Science. doi: 10.1111/mms.12500

Meissner T, Wentz FJ, Scott J, Vazquez-Cuervo J (2016) Sensitivity of Ocean Surface Salinity Measurements From Spaceborne L-Band Radiometers to Ancillary Sea Surface Temperature. IEEE Trans Geosci Remote Sensing 54:7105–7111. doi: 10.1109/TGRS.2016.2596100

Mesgaran MB, Cousens RD, Webber BL (2014) Here be dragons: A tool for quantifying novelty due to covariate range and correlation change when projecting species distribution models. Diversity Distrib 20:1147–1159. doi: 10.1111/ddi.12209

Miller DL, Becker EA, Forney KA, Roberts JJ, Cañadas A, Schick RS (2022) Estimating uncertainty in density surface models. PeerJ 10:e13950. doi: 10.7717/peerj.13950

Mullin KD, Fulling GL (2003) Abundance of cetaceans in the southern U.S. North Atlantic Ocean during summer 1998. Fishery Bulletin 101:603–613.

Palka D (2020) Cetacean Abundance in the US Northwestern Atlantic Ocean Summer 2016. Northeast Fish Sci Cent Ref Doc. 20-05. NOAA National Marine Fisheries Service, Northeast Fisheries Science Center, Woods Hole, MA

Palka D, Aichinger Dias L, Broughton E, Chavez-Rosales S, Cholewiak D, Davis G, DeAngelis A, Garrison L, Haas H, Hatch J, Hyde K, Jech M, Josephson E, Mueller-Brennan L, Orphanides C, Pegg N, Sasso C, Sigourney D, Soldevilla M, Walsh H (2021) Atlantic Marine Assessment Program for Protected Species: FY15 – FY19 (OCS Study BOEM 2021-051). U.S. Deptartment of the Interior, Bureau of Ocean Energy Management, Washington, DC

Palka DL (2006) Summer abundance estimates of cetaceans in US North Atlantic navy operating areas (NEFSC Reference Document 06-03). U.S. Department of Commerce, Northeast Fisheries Science Center, Woods Hole, MA

Palka DL, Chavez-Rosales S, Josephson E, Cholewiak D, Haas HL, Garrison L, Jones M, Sigourney D, Waring G, Jech M, Broughton E, Soldevilla M, Davis G, DeAngelis A, Sasso CR, Winton MV, Smolowitz RJ, Fay G, LaBrecque E, Leiness JB, Dettloff K, Warden M, Murray K, Orphanides C (2017) Atlantic Marine Assessment Program for Protected Species: 2010-2014 (OCS Study BOEM 2017-071). U.S. Deptartment of the Interior, Bureau of Ocean Energy Management, Washington, DC

Perkins NJ, Schisterman EF (2006) The Inconsistency of "Optimal" Cutpoints Obtained using Two Criteria based on the Receiver Operating Characteristic Curve. American Journal of Epidemiology 670–675.

Read AJ, Barco S, Bell J, Borchers DL, Burt ML, Cummings EW, Dunn J, Fougeres EM, Hazen L, Hodge LEW, Laura A-M, McAlarney RJ, Peter N, Pabst DA, Paxton CGM, Schneider SZ, Urian KW, Waples DM, McLellan WA (2014) Occurrence, distribution and abundance of cetaceans in Onslow Bay, North Carolina, USA. Journal of Cetacean Research and Management 14:23–35.

Roberts JJ, Best BD, Dunn DC, Treml EA, Halpin PN (2010) Marine Geospatial Ecology Tools: An integrated framework for ecological geoprocessing with ArcGIS, Python, R, MATLAB, and C++. Environmental Modelling & Software 25:1197–1207. doi: 10.1016/j.envsoft.2010.03.029

Roberts JJ, Best BD, Mannocci L, Fujioka E, Halpin PN, Palka DL, Garrison LP, Mullin KD, Cole TVN, Khan CB, McLellan WA, Pabst DA, Lockhart GG (2016) Habitat-based cetacean density models for the U.S. Atlantic and Gulf of Mexico. Scientific Reports 6:22615. doi: 10.1038/srep22615

Roberts JJ, Mannocci L, Schick RS, Halpin PN (2018) Final Project Report: Marine Species Density Data Gap Assessments and Update for the AFTT Study Area, 2017-2018 (Opt. Year 2), Document Version 1.2. Duke University Marine Geospatial Ecology Lab, Durham, NC

Roberts JJ, Yack TM, Halpin PN (2023) Marine mammal density models for the U.S. Navy Atlantic Fleet Training and Testing (AFTT) study area for the Phase IV Navy Marine Species Density Database (NMSDD), Document Version 1.3. Duke University Marine Geospatial Ecology Lab, Durham, NC

Robertson FC, Koski WR, Brandon JR, Thomas TA, Trites AW (2015) Correction factors account for the availability of bowhead whales exposed to seismic operations in the Beaufort Sea. Journal of Cetacean Research and Management 15:35–44.

Ryan C, Boisseau O, Cucknell A, Romagosa M, Moscrop A, McLanaghan R (2013) Final report for trans-Atlantic research passages between the UK and USA via the Azores and Iceland, conducted from R/V Song of the Whale 26 March to 28 September 2012. Marine Conservation Research International, Essex, UK

Schlax MG, Chelton DB (2016) The "Growing Method" of Eddy Identification and Tracking in Two and Three Dimensions. College of Earth, Ocean and Atmospheric Sciences, Oregon State University, Corvallis, OR

Taubenberger JK, Tsai M, Krafft AE, Lichy JH, Reid AH, Schulman Y, Lipscomb TP (1996) Two Morbilliviruses Implicated in Bottlenose Dolphin Epizootics. Emerging Infectious Diseases 2:213–216. doi: 10.3201/eid0203.960308

Torres LG, Rosel PE, D'Agrosa C, Read AJ (2003) Improving management of overlapping bottlenose dolphin ecotypes through spatial analysis and genetics. Marine Mammal Science 19:502–514.

Torres LG, Mclellan WA, Meagher E, Pabst DA (2005) Seasonal distribution and relative abundance of bottlenose dolphins, Tursiops truncatus, along the US mid-Atlantic coast. Journal of Cetacean Research and Management 7:153.

Toth JL, Hohn AA, Able KW, Gorgone AM (2012) Defining bottlenose dolphin (Tursiops truncatus) stocks based on environmental, physical, and behavioral characteristics. Marine Mammal Science 28:461–478. doi: 10.1111/j.1748-7692.2011.00497.x

Whitt AD, Powell JA, Richardson AG, Bosyk JR (2015) Abundance and distribution of marine mammals in nearshore waters off New Jersey, USA. Journal of Cetacean Research and Management 15:45–59.

Wood SN (2011) Fast stable restricted maximum likelihood and marginal likelihood estimation of semiparametric generalized linear models. Journal of the Royal Statistical Society: Series B (Statistical Methodology) 73:3–36. doi: 10.1111/j.1467-9868.2010.00749.x